

AD-A090 138

REYNOLDS METALS CO RICHMOND VA METALLURGICAL RESEARCH DIV F/6 11/6
THE DEVELOPMENT OF ALUMINUM-LITHIUM ALLOYS. (U)
JUL 80 F W GAYLE

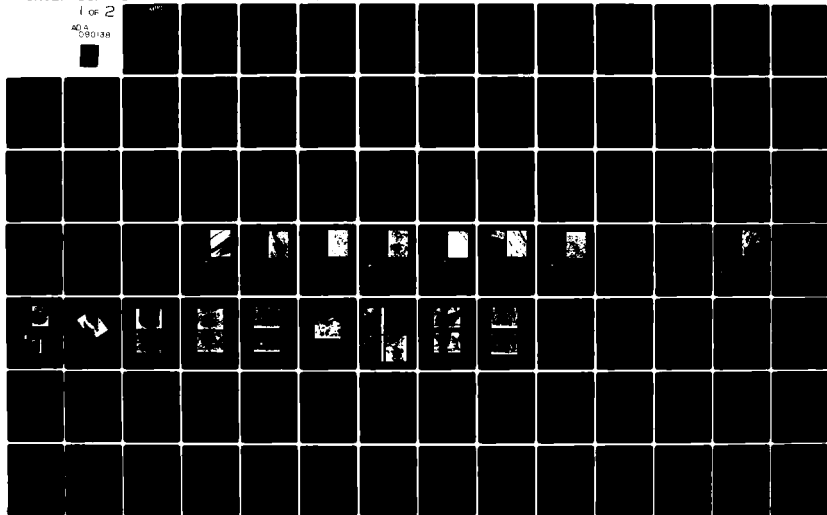
N00019-78-C-0485

NL

UNCLASSIFIED

1 of 2

AD-A
090138





AD A090138

REYNOLDS ALUMINUM
REYNOLDS METALS COMPANY • RICHMOND, VIRGINIA 23261
RESEARCH AND DEVELOPMENT

1980 July 31

TO: Department of the Navy
Naval Air Systems Command
Washington, D. C. 20361

FROM: Reynolds Metals Company
Metallurgical Research Division
Fourth and Canal Streets
Richmond, Virginia 23261

SUBJECT: FINAL REPORT

CONTRACT NO.: N00019-78-C-0485

TITLE: THE DEVELOPMENT OF ALUMINUM-LITHIUM ALLOYS

REYNOLDS PROJECT NOS.: 38-833-8Z02, 39-848-8Z02,
and 30-846-8Z02

APPROVED FOR PUBLIC RELEASE; DISTRIBUTION UNLIMITED

Frank W. Gayle
Frank W. Gayle, Research Scientist

R. F. Ashton
Richard F. Ashton, Director
Alloy Development Section

David S. Thompson
David S. Thompson, Director
Department of Metallurgy

Sander A. Levy
Sander A. Levy, Director
Department of Metallurgical Services
and Ingot Casting Technology

Grant E. Spangler
Grant E. Spangler, General Director
Metallurgical Research Division

DTIC
ELECTE
OCT 9 1980
S
C

DDC FILE COPY
bd

REYNOLDS METALS COMPANY METALLURGICAL RESEARCH DIVISION
4TH AND CANAL STREETS • RICHMOND, VIRGINIA 23261 • 804/788-7400

80 10 9 134

UNCLASSIFIED

SECURITY CLASSIFICATION OF THIS PAGE (When Data Entered)

REPORT DOCUMENTATION PAGE		READ INSTRUCTIONS BEFORE COMPLETING FORM
1. REPORT NUMBER	2. GOVT ACCESSION NO.	3. RECIPIENT'S CATALOG NUMBER
	AD-A090138	
4. TITLE (and Subtitle)	5. TYPE OF REPORT & PERIOD COVERED	
THE DEVELOPMENT OF ALUMINUM-LITHIUM ALLOYS	FINAL	
	6. PERFORMING ORG. REPORT NUMBER	
7. AUTHOR(s)	8. CONTRACT OR GRANT NUMBER(s)	
Frank W. / Gayle	N00019-78-C-0485	
9. PERFORMING ORGANIZATION NAME AND ADDRESS		10. PROGRAM ELEMENT, PROJECT, TASK AREA & WORK UNIT NUMBERS
Reynolds Metals Company Metallurgical Research Division P. O. Box 27003 Richmond, Virginia 23261		
11. CONTROLLING OFFICE NAME AND ADDRESS		12. REPORT DATE
		1980 July 31
		13. NUMBER OF PAGES
		176
14. MONITORING AGENCY NAME & ADDRESS (if different from Controlling Office)		15. SECURITY CLASS. (of this report)
		UNCLASSIFIED
		15a. DECLASSIFICATION/DOWNGRADING SCHEDULE
16. DISTRIBUTION STATEMENT (of this Report)		
Approved for public release; distribution unlimited		
17. DISTRIBUTION STATEMENT (of the abstract entered in Block 20, if different from Report)		
18. SUPPLEMENTARY NOTES		
19. KEY WORDS (Continue on reverse side if necessary and identify by block number)		
Al-Li Fracture Toughness		
Al-Li-Cu Fractography		
Al-Li-Zr Mechanical Properties		
Al-Li-Mn-(Fe) Microstructure		
Al-Li-Mg-Si Alloy Development		
20. ABSTRACT (Continue on reverse side if necessary and identify by block number)		
Aluminum-lithium based alloys have shown promise as high strength, high modulus, low density alloys, but suffer from low toughness levels currently unacceptable in aerospace design. The present study was directed toward increasing the fracture toughness of such alloys in sheet form, primarily through alloying. Attempts to increase fracture toughness were made through modification of the fracture-controlling Al ₃ Li precipitate, addition of dispersoid-forming elements and the use of coprecipitation of other phases.		

DD FORM 1 JAN 73 1473

EDITION OF 1 NOV 65 IS OBSOLETE

UNCLASSIFIED

SECURITY CLASSIFICATION OF THIS PAGE (When Data Entered)

UNCLASSIFIED

SECURITY CLASSIFICATION OF THIS PAGE (When Date Entered)

Alloying additions investigated include copper, magnesium, silicon, manganese, iron, scandium, gallium, and silver. Tensile test results and fracture behavior of these alloys as a function of temper are reported.

The copper-containing alloy showed the best fracture behavior with moderate strength. Other additions generally resulted in increased strength but no improvement in ductility or crack propagation energy over that of the binary alloys. Analysis indicated that the brittle fracture behavior is associated with grain boundary or subgrain boundary failure. High hydrogen levels, inherent planar slip, and (sub-)grain boundary precipitate-free-zones which grow with aging appear to be factors in the grain boundary or subgrain boundary weakness.

Accession For	
THIS COM&I	<input checked="" type="checkbox"/>
DTIC TAB	<input type="checkbox"/>
Unannounced	<input type="checkbox"/>
Justification	<input type="checkbox"/>
By	
Distribution/	
Availability Codes	
Dist	Avail and/or Special
A	

UNCLASSIFIED

SECURITY CLASSIFICATION OF THIS PAGE (When Date Entered)

TABLE OF CONTENTS

	<u>Page No.</u>
ABSTRACT -----	
<u>SECTION 1</u> -----	1
INTRODUCTION -----	2
<u>SECTION 2</u> -----	8
PHASE I: DEVELOPMENT OF CASTING PROCEDURES -----	9
<u>Experimental Procedure and Results</u> -----	9
<u>Discussion and Conclusion</u> -----	11
<u>SECTION 3</u> -----	13
PHASE II: PRELIMINARY SURVEY OF ALLOY SYSTEMS -----	14
<u>Introduction</u> -----	14
<u>Experimental Procedure</u> -----	15
<u>Production of Extrusions</u> -----	15
<u>Chemical Analysis</u> -----	16
<u>Aging Curves</u> -----	16
<u>Mechanical Tests</u> -----	16
<u>Metallography</u> -----	16
<u>Results and Discussion</u> -----	17
<u>Fabrication</u> -----	17
<u>Chemical Analysis</u> -----	17
<u>Aging Curves</u> -----	17
<u>Mechanical Test Results</u> -----	18
<u>Metallography</u> -----	20
<u>Microstructure</u> -----	20
<u>Fractography</u> -----	21
<u>Conclusions of Phase II</u> -----	22
<u>SECTION 4</u> -----	52
PHASE III: SHEET -----	53
<u>Introduction</u> -----	53
<u>Experimental Procedure</u> -----	54
<u>Fabrication of Sheet</u> -----	54
<u>Hot Isostatic Pressing (HIP)</u> -----	55
<u>Chemical Analysis and Hydrogen Content</u> -----	55
<u>Heat Treatment</u> -----	55
<u>Aging Studies</u> -----	55
<u>Mechanical Testing</u> -----	56
<u>Metallography</u> -----	56
<u>Results</u> -----	56
<u>Chemical Analysis</u> -----	56
<u>Microstructure</u> -----	57
<u>Aging Study</u> -----	58
<u>Tensile Test Results</u> -----	59
<u>Fracture Characteristics</u> -----	59
<u>Kahn Tear Tests</u> -----	61
<u>Transmission Electron Microscopy (TEM)</u> -----	62

TABLE OF CONTENTS Continued

	<u>Page No.</u>
<u>Discussion and Conclusions of Phase III</u> -----	64
<u>Casting and Fabrication of Sheet</u> -----	64
<u>Grain Structure</u> -----	65
<u>Precipitation and Aging Response</u> -----	65
<u>Tensile and Yield Strengths and Elongation</u> -----	66
<u>Tensile Fracture Characteristics</u> -----	67
<u>Fracture Toughness--Kahn Tear Tests</u> -----	67
<u>SECTION 5</u> -----	151
<u>CONCLUSIONS AND RECOMMENDATIONS</u> -----	152
<u>Process Development</u> -----	152
<u>Alloy Development</u> -----	152
<u>Recommendations for Future Work</u> -----	154
<u>Casting and Fabrication</u> -----	154
<u>Alloy Development</u> -----	154
<u>ACKNOWLEDGMENT</u> -----	156
<u>REFERENCES</u> -----	157
<u>NAVY DISTRIBUTION LIST</u> -----	162

LIST OF TABLES

	<u>Page No.</u>
<u>TABLE 1-1.</u> ALLOY SYSTEMS INVESTIGATED IN PHASE II (EXTRUSIONS) -----	6
<u>TABLE 1-2.</u> ALLOY SYSTEMS INVESTIGATED IN PHASE III (SHEET) -----	7
<u>TABLE 2-1.</u> INGOTS PRODUCED IN PHASE I -----	12
<u>TABLE 3-1.</u> CHEMICAL ANALYSIS OF PHASE II EXTRUSIONS NSWC Produced Material -----	23
<u>TABLE 3-2.</u> MECHANICAL PROPERTIES OF PHASE II EXTRUSIONS AGED AT 375°F (191°C) TO PEAK HARDNESS -----	24
<u>TABLE 3-3.</u> MECHANICAL PROPERTIES OF PHASE II EXTRUSIONS AGED AT 300°F (149°C) FOR 24 HOURS OR 300°F (149°C) FOR 24 HOURS + 350°F (177°C) FOR 4 HOURS -----	25
<u>TABLE 4-1.</u> CHEMICAL ANALYSES OF ALLOYS PRODUCED IN PHASE III -----	69
<u>TABLE 4-2.</u> HYDROGEN LEVELS IN PHASE III INGOTS -----	70
<u>TABLE 4-3.</u> MICROSTRUCTURAL DETAILS OF PHASE III SHEET -----	71
<u>TABLE 4-4.</u> LONGITUDINAL AND TRANSVERSE TENSILE PROPERTIES OF Al-Li (#10-HIP) SHEET SHT 975°F/30 MINUTES -----	72
<u>TABLE 4-5.</u> LONGITUDINAL AND TRANSVERSE TENSILE PROPERTIES OF Al-Li-Zr (#22) SHEET SHT 975°F/30 MINUTES -----	73
<u>TABLE 4-6.</u> LONGITUDINAL AND TRANSVERSE TENSILE PROPERTIES OF Al-Li-Zr (#26A--AR) SHEET SHT 975°F/30 MINUTES -----	74
<u>TABLE 4-7.</u> LONGITUDINAL AND TRANSVERSE TENSILE PROPERTIES OF Al-Li-Zr (#26B) SHEET SHT 975°F/30 MINUTES -----	75
<u>TABLE 4-8.</u> LONGITUDINAL AND TRANSVERSE TENSILE PROPERTIES OF Al-Li-Cu (#19--AR) SHEET SHT 975°F/30 MINUTES -----	76
<u>TABLE 4-9.</u> LONGITUDINAL AND TRANSVERSE TENSILE PROPERTIES OF Al-Li-Mq-Si (#20) SHEET SHT 975°F/30 MINUTES -----	77

LIST OF TABLES Continued

	<u>Page No.</u>
<u>TABLE 4-10.</u> LONGITUDINAL AND TRANSVERSE TENSILE PROPERTIES OF Al-Li-Mg-Si (#21--AR) SHEET SHT 975°F/30 MINUTES -----	78
<u>TABLE 4-11.</u> LONGITUDINAL AND TRANSVERSE TENSILE PROPERTIES OF Al-Li-Mn-Fe (#23) SHEET SHT 975°F/30 MINUTES -----	79
<u>TABLE 4-12.</u> LONGITUDINAL AND TRANSVERSE TENSILE PROPERTIES OF Al-Li-Mn-Fe (#24) SHEET SHT 975°F/30 MINUTES -----	80
<u>TABLE 4-13.</u> LONGITUDINAL AND TRANSVERSE TENSILE PROPERTIES OF Al-Li-Mn (#25) SHEET SHT 975°F/30 MINUTES -----	81
<u>TABLE 4-14.</u> TENSILE TEST FRACTURE SURFACE CHARACTERISTICS OF PHASE III SHEET -----	82
<u>TABLE 4-15.</u> KAHN TEAR TEST RESULTS--#10 -----	83
<u>TABLE 4-16.</u> KAHN TEAR TEST RESULTS--#22 -----	84
<u>TABLE 4-17.</u> KAHN TEAR TEST RESULTS--#26A -----	85
<u>TABLE 4-18.</u> KAHN TEAR TEST RESULTS--#19 -----	86
<u>TABLE 4-19.</u> KAHN TEAR TEST RESULTS--#21 -----	87
<u>TABLE 4-20.</u> KAHN TEAR TEST RESULTS--#25 -----	88
<u>TABLE 4-21.</u> TYPICAL TENSILE AND TEAR PROPERTIES OF SOME COMMERCIAL ALLOYS -----	89

LIST OF FIGURES

	<u>Page No.</u>
<u>FIGURE 3-1.</u> HARDNESS AGING CURVES AT 375°F (191°C) FOR PHASE II EXTRUSIONS 1-3, 3-0, 3-1, 11-1 (BINARY ALLOYS) -----	26
<u>FIGURE 3-2.</u> HARDNESS AGING CURVES AT 375°F (191°C) FOR PHASE II EXTRUSIONS 4-1, 5-1, 8-1, 9-0 (CONTAINING Sc OR Ga) -----	27
<u>FIGURE 3-3.</u> HARDNESS AGING CURVES AT 375°F (191°C) FOR PHASE II EXTRUSIONS 10-2A, 13-1, 15-1 (CONTAINING Mn OR Mg) -----	28
<u>FIGURE 3-4.</u> HARDNESS AGING CURVE AT 375°F (191°C) FOR PHASE II EXTRUSION 14-1 (CONTAINING Ag) -----	29
<u>FIGURE 3-5.</u> HARDNESS AGING CURVES AT 300°F (149°C) FOR PHASE II EXTRUSIONS -----	30
<u>FIGURE 3-6.</u> HARDNESS AGING CURVES FOR PHASE II EXTRUSIONS, TWO-STEP AGE 300°F (149°C)/24 HOURS + 350°F (177°C)/X HOURS -----	31
<u>FIGURE 3-7.</u> OPTICAL MICROGRAPHS OF EXTRUSION #1-3, SHT 932°F (500°C)/20 MIN., WATER QUENCHED -----	32
<u>FIGURE 3-8.</u> OPTICAL MICROGRAPHS OF EXTRUSION #11-1, SHT 932°F (500°C)/20 MIN., WATER QUENCHED, SHOWING LARGE METALLIC IRON INCLUSION -----	33
<u>FIGURE 3-9.</u> OPTICAL MICROGRAPHS OF EXTRUSION #4-1, SHT 932°F (500°C)/20 MIN., WATER QUENCHED -----	34
<u>FIGURE 3-10.</u> OPTICAL MICROGRAPHS OF EXTRUSION #8-1, SHT 932°F (500°C)/20 MIN., WATER QUENCHED -----	35
<u>FIGURE 3-11.</u> OPTICAL MICROGRAPHS OF EXTRUSION #10-2A, SHT 932°F (500°C)/20 MIN., WATER QUENCHED -----	36
<u>FIGURE 3-12.</u> OPTICAL MICROGRAPHS OF EXTRUSION #10-1, SHT 932°F (500°C)/20 MIN., WATER QUENCHED -----	37
<u>FIGURE 3-13.</u> OPTICAL MICROGRAPHS OF EXTRUSION #13-1, SHT 932°F (500°C)/20 MIN., WATER QUENCHED -----	38
<u>FIGURE 3-14.</u> OPTICAL MICROGRAPHS OF EXTRUSION #15-1, SHT 932°F (500°C)/20 MIN., WATER QUENCHED, AS-POLISHED -----	39
<u>FIGURE 3-15.</u> OPTICAL MICROGRAPHS OF EXTRUSION #15-2, SHT 932°F (500°C)/20 MIN., WATER QUENCHED, AS-POLISHED -----	40
<u>FIGURE 3-16.</u> OPTICAL MICROGRAPHS OF EXTRUSION #14-1, SHT 932°F (500°C)/20 MIN., WATER QUENCHED -----	41

	<u>Page</u> <u>No.</u>
<u>FIGURE 3-17.</u> SCANNING ELECTRON MICROGRAPH OF EXTRUSION #4-1, WITH LARGE INSOLUBLES IDENTIFIED AS Al-Sc COMPOUND, INTERDENDRITIC PARTICLES INCLUDE IRON-RICH PARTICLES -----	42
<u>FIGURE 3-18.</u> EXTRUSION #10-2A PEAK HARDNESS, BROKEN TENSILE FRACTURE SURFACE -----	43
<u>FIGURE 3-19.</u> EXTRUSION #3-1 PEAK HARDNESS, BROKEN TENSILE FRACTURE SURFACE, SHOWING 45° SHEAR FAILURE --	43
<u>FIGURE 3-20.</u> OPTICAL MICROGRAPH OF EXTRUSION #1-3, SHT 932°F (500°C)/30 MIN. AND AGED 300°F (149°C)/24 HOURS + 350°F (177°C)/4 HOURS, SHOWING TRANSGRANULAR FRACTURE (45° SHEAR) -----	44
<u>FIGURE 3-21.</u> SEM OF EXTRUSION #3-1, PEAK HARDNESS, FRACTURE SURFACE -----	45
<u>FIGURE 3-22.</u> SEM OF EXTRUSION #10-2A, PEAK HARDNESS (EXCEPT WHERE NOTED), FRACTURE SURFACE -----	46
<u>FIGURE 3-23.</u> SEM OF EXTRUSION #4-1, PEAK HARDNESS, FRACTURE SURFACE -----	48
<u>FIGURE 3-24.</u> SEM OF EXTRUSION #8-1, PEAK HARDNESS, FRACTURE SURFACE -----	49
<u>FIGURE 3-25.</u> SEM OF EXTRUSION #14-1, PEAK HARDNESS, FRACTURE SURFACE -----	50
<u>FIGURE 3-26.</u> SEM OF EXTRUSION #15-1, PEAK HARDNESS, FRACTURE SURFACE -----	51
<u>FIGURE 4-1.</u> LONGITUDINAL CROSS-SECTION OF Al-Li (#10) ----	90
<u>FIGURE 4-2.</u> LONGITUDINAL CROSS-SECTIONS OF Al-Li-Zr (#22) -----	91
<u>FIGURE 4-3.</u> LONGITUDINAL CROSS-SECTION OF Al-Li-Zr (#26A--AR) -----	92
<u>FIGURE 4-4.</u> LONGITUDINAL CROSS-SECTION OF Al-Li-Zr (#26B) -----	92
<u>FIGURE 4-5.</u> LONGITUDINAL CROSS-SECTION OF Al-Li-Cu (#19--AR) -----	93
<u>FIGURE 4-6.</u> LONGITUDINAL CROSS-SECTION OF Al-Li-Mg-Si (#20--AR) -----	93
<u>FIGURE 4-7.</u> LONGITUDINAL CROSS-SECTION OF Al-Li-Mg-Si (#21--AR) -----	94
<u>FIGURE 4-8.</u> LONGITUDINAL CROSS-SECTIONS OF Al-Li-Mn-Fe (#23) -----	95

	<u>Page No.</u>
<u>FIGURE 4-9.</u> LONGITUDINAL CROSS-SECTIONS OF Al-Li-Mn-Fe (#24) -----	96
<u>FIGURE 4-10.</u> LONGITUDINAL CROSS-SECTIONS OF Al-Li-Mn (#25) -----	97
<u>FIGURE 4-11.</u> LONGITUDINAL CROSS-SECTION OF Al-Li-Zr (#22-AR) -----	98
<u>FIGURE 4-12.</u> LONGITUDINAL CROSS-SECTION OF Al-Li-Cu (#19--AR) -----	98
<u>FIGURE 4-13.</u> LONGITUDINAL CROSS-SECTION OF Al-Li-Mg-Si (#20) -----	99
<u>FIGURE 4-14.</u> LONGITUDINAL CROSS-SECTION OF Al-Li-Mn-Fe (#24--AR) -----	99
<u>FIGURE 4-15.</u> LONGITUDINAL CROSS-SECTION OF Al-Li-Mn (#25--AR) -----	100
<u>FIGURE 4-16.</u> TRANSVERSE CROSS-SECTION OF Al-Li-Zr (#26A--AR) -----	101
<u>FIGURE 4-17.</u> LONGITUDINAL CROSS-SECTION OF Al-Li-Cu (#19--AR) -----	101
<u>FIGURE 4-18.</u> LONGITUDINAL CROSS-SECTION OF Al-Li-Mg-Si (#20) -----	102
<u>FIGURE 4-19.</u> LONGITUDINAL CROSS-SECTION OF Al-Li-Mn-Fe (#24-h) -----	102
<u>FIGURE 4-20.</u> HARDNESS AGING CURVES FOR Al-Li (#10) -----	103
<u>FIGURE 4-21.</u> HARDNESS AGING CURVES FOR Al-Li-Zr (#22) -----	104
<u>FIGURE 4-22.</u> HARDNESS AGING CURVES FOR Al-Li-Zr (#22--AR) --	105
<u>FIGURE 4-23.</u> HARDNESS AGING CURVES FOR Al-Li-Zr (#26A--AR) --	106
<u>FIGURE 4-24.</u> HARDNESS AGING CURVES FOR Al-Li-Zr (#26B) -----	107
<u>FIGURE 4-25.</u> HARDNESS AGING CURVES FOR Al-Li-Cu (#19--AR) --	108
<u>FIGURE 4-26.</u> HARDNESS AGING CURVES FOR Al-Li-Mg-Si (#20) --	109
<u>FIGURE 4-27.</u> HARDNESS AGING CURVES FOR Al-Li-Mg-Si (#21--AR) -----	110
<u>FIGURE 4-28.</u> HARDNESS AGING CURVES FOR Al-Li-Mn-Fe (#23) --	111
<u>FIGURE 4-29.</u> HARDNESS AGING CURVES FOR Al-Li-Mn-Fe (#23-h) --	112
<u>FIGURE 4-30.</u> HARDNESS AGING CURVES FOR Al-Li-Mn-Fe (#24--AR) -----	113
<u>FIGURE 4-31.</u> HARDNESS AGING CURVES FOR Al-Li-Mn-Fe (#24-h) --	114
<u>FIGURE 4-32.</u> HARDNESS AGING CURVES FOR Al-Li-Mn (#25) -----	115
<u>FIGURE 4-33.</u> HARDNESS AGING CURVES FOR Al-Li-Mn (#25--AR) --	116

	<u>Page</u> <u>No.</u>
<u>FIGURE 4-34.</u> HARDNESS AGING CURVES FOR Al-Li-Mn (#25-h) ---	117
<u>FIGURE 4-35.</u> SEM OF Al-Li (#10--AR) -----	118
<u>FIGURE 4-36.</u> SEM OF Al-Li (#10) -----	119
<u>FIGURE 4-37.</u> SEM OF Al-Li (#10) -----	120
<u>FIGURE 4-38.</u> SEM OF Al-Li-Zr (#22--AR) -----	121
<u>FIGURE 4-39.</u> Al-Li-Cu (#19--AR) TENSILE TEST ELONGATION VERSUS AGING TIME -----	122
<u>FIGURE 4-40.</u> SEM OF Al-Li-Cu (#19--AR) -----	123
<u>FIGURE 4-41.</u> SEM OF Al-Li-Cu (#19--AR) -----	124
<u>FIGURE 4-42.</u> SEM OF Al-Li-Cu (#19--AR) -----	125
<u>FIGURE 4-43.</u> SEM OF Al-Li-Mg-Si (#20--AR) -----	126
<u>FIGURE 4-44.</u> SEM OF Al-Li-Mn-Fe (#23--AR) -----	127
<u>FIGURE 4-45.</u> TEM OF Al-Li-Zr (#26A) SHEET -----	128
<u>FIGURE 4-46.</u> TEM OF Al-Li-Zr (#26A) SHEET -----	129
<u>FIGURE 4-47.</u> TEM OF Al-Li-Zr (#26A) SHEET -----	130
<u>FIGURE 4-48.</u> TEM OF Al-Li-Zr (#26A) SHEET -----	131
<u>FIGURE 4-49.</u> TEM OF Al-Li-Mn (#25--AR) SHEET -----	132
<u>FIGURE 4-50.</u> TEM OF Al-Li-Mn (#25--AR) SHEET -----	133
<u>FIGURE 4-51.</u> TEM OF Al-Li-Mn (#25-h) SHEET -----	134
<u>FIGURE 4-52.</u> TEM OF Al-Li-Cu (#19--AR) SHEET -----	135
<u>FIGURE 4-53.</u> TEM OF Al-Li-Cu (#19--AR) SHEET -----	136
<u>FIGURE 4-54.</u> TEM OF Al-Li-Cu (#19--AR) SHEET -----	137
<u>FIGURE 4-55.</u> TEM OF Al-Li-Cu (#19--AR) SHEET -----	138
<u>FIGURE 4-56.</u> TEM OF Al-Li-Cu (#19--AR) SHEET -----	139
<u>FIGURE 4-57.</u> TEM OF Al-Li-Cu (#19--AR) SHEET -----	140
<u>FIGURE 4-58.</u> TEM OF Al-Li-Cu (#19--AR) SHEET -----	141
<u>FIGURE 4-59.</u> TEM OF Al-Li-Cu (#19--AR) SHEET -----	142
<u>FIGURE 4-60.</u> TEM OF Al-Li-Cu (#19--AR) SHEET -----	143
<u>FIGURE 4-61.</u> TEM OF Al-Li-Cu (#19--AR) SHEET -----	144
<u>FIGURE 4-62.</u> TEM OF Al-Li-Cu (#19--AR) SHEET -----	145
<u>FIGURE 4-63.</u> TEM OF Al-Li-Cu (#19--AR) SHEET -----	146
<u>FIGURE 4-64.</u> TEM OF Al-Li-Cu (#19--AR) SHEET -----	147
<u>FIGURE 4-65.</u> TEM OF Al-Li-Cu (#19--AR) SHEET -----	148
<u>FIGURE 4-66.</u> TEM OF Al-Li-Cu (#19--AR) SHEET -----	149
<u>FIGURE 4-67.</u> TEM OF Al-Li-Cu (#19--AR) SHEET -----	150

ABSTRACT

Aluminum-lithium based alloys have shown promise as high strength, high modulus, low density alloys, but suffer from low toughness levels currently unacceptable in aerospace design. The present study was directed toward increasing the fracture toughness of such alloys in sheet form, primarily through alloying. Attempts to increase fracture toughness were made through modification of the fracture-controlling Al_3Li precipitate, addition of dispersoid forming elements, and the use of co-precipitation of other phases. Alloying additions investigated include copper, magnesium, silicon, manganese, iron, scandium, gallium, and silver. Tensile test results and fracture behavior of these alloys as a function of temper are reported.

The copper-containing alloy showed the best fracture behavior with moderate strength. Other additions generally resulted in increased strength but no improvement in ductility or crack propagation energy over that of the binary alloys. Analysis indicated that the brittle fracture behavior is associated with grain boundary or subgrain boundary failure. High hydrogen levels, inherent planar slip, and (sub-)grain boundary precipitate-free-zones which grow with aging appear to be factors in the grain boundary or subgrain boundary weakness.

SECTION 1

INTRODUCTION

The addition of 2-3 wt. % lithium to aluminum results in lower density, increased modulus of elasticity, and a potential for high strength through precipitation hardening. [1-4] These properties make the development of such alloys highly desirable for airframe and other uses where weight is a critical factor. However, fracture toughness for these high lithium alloys is low compared with commercial high strength aircraft alloys. [3-5] The present work is directed toward investigation of mechanisms for increasing the toughness of alloys in this system, with emphasis on ternary or higher-order alloying additions.

The basic strengthening mechanism of aluminum-lithium binary alloys is the formation of the metastable precipitate δ' (Al_3Li). This precipitate has an ordered, face-centered cubic crystal structure of the Cu_3Au type (Ll_2). [6,7] δ' forms spherical precipitates, which are fully coherent with the α -Al matrix with a very small lattice mismatch. [8] This particular precipitation mechanism is not seen in other aluminum-based systems, but is analogous to the equilibrium γ - γ' (Ni-Ni₃Al) system, which gives nickel-based superalloys high temperature strength and ductility.

However, the aluminum-lithium precipitate system, with its small lattice mismatch and low matrix-precipitate interfacial energy, is responsible for the low ductility and fracture toughness observed in these alloys. In an ordered structure (superlattice) such as δ' , the passage of a single dislocation through the lattice creates a disturbance in the order, resulting in an antiphase boundary (APB). The extra energy associated with the APB is an impediment to dislocation movement and is increasingly important as a strengthening mechanism when coherency strains are small. [9] The passage of a second dislocation recreates the order disturbed by the

first, and, thus, dislocations in such an alloy tend to move in pairs (or superdislocations).

After the passage of a superdislocation, the cross-section area of the precipitate on the slip plane is reduced by an amount proportional to the Burgers vector and the precipitate radius. The precipitate size is then effectively reduced on that slip plane, and the APB required for subsequent dislocation movement is smaller. Thus once slip occurs on a particular plane, further slip on that plane is encouraged. Consequently, intense planar slip occurs during deformation, leading to dislocation pileups at grain boundaries and subsequent grain boundary failure. Severe planar slip and intergranular fracture, with associated low ductility and toughness, are therefore an inherent characteristic of aluminum-lithium binary alloys.

Lithium has seen limited use in commercial alloys. AA2020, developed by Alcoa, contained approximately 1% lithium. The alloy is no longer produced, primarily due to casting difficulties and problems with toughness. The Soviets have developed VAD 23 and alloy 01420. VAD 23 is an Al-Li-Cu alloy with 1.2% lithium; 01420 is an Al-Li-Mg alloy with nominally 2% lithium. Both alloys have fairly low ductility.

The current program has investigated alloys of higher lithium content in order to take full advantage of the beneficial effects of lithium on density and elastic modulus. The initial phase of this program involved the development of methods for producing sheet. The casting and rolling of highly alloyed aluminum-lithium ingots present some difficulty. [10,11] The casting of a sound ingot is a problem which first must be solved. Loss of lithium, porosity, and high hydrogen content are the primary problems. This is due to the high reactivity of lithium with oxygen and hydrogen. Oxidation of the melt results in a loss of lithium and the formation of a surface oxide layer including $\text{LiO}_2 \cdot \text{Al}_2\text{O}_3$, which does not inhibit the

reaction of aluminum with water vapor in the furnace atmosphere. [12,13] This factor and the affinity of lithium for hydrogen result in an immediate increase of hydrogen level when lithium is introduced into the melt. [10,13-15] We have approached this problem of ingot quality by casting under vacuum or argon atmosphere. The development of casting techniques to produce a sound ingot is presented as Phase I in Section 2.

Approaches that have been taken for improving toughness involve encouraging dislocation cross-slip or precipitate bypassing in the alloys. This includes modification of the Al-Al₃Li system lattice parameters to increase mismatch, introduction of other precipitation systems, and use of a dispersion hardening system in addition to the precipitation hardening system.

Phase II involved a preliminary survey of several Al-Li-X systems. Several small extrusions produced at the Naval Surface Weapons Center (Silver Spring, Maryland) were used for this investigation. Systems examined included the aluminum-lithium binary system and aluminum-lithium alloys containing scandium, gallium, magnesium, manganese, or silver. Additions of zirconium and bismuth were also investigated.

The basic systems investigated are presented in Table 1-1, along with the primary strengthening mechanisms involved. The various mechanisms are described in more detail in Section 3, along with the complete analyses of the extrusions produced in Phase II.

Based in part on the results of Phase II, we selected for Phase III compositions to be cast as 10-lb bookmold ingots and rolled to sheet. The compositions included aluminum and lithium alloyed with magnesium and silicon, copper, and manganese with and without iron. The systems investigated and corresponding

strengthening mechanism are listed in Table 1-2. The analysis of sheet produced in Phase III is presented in Section 4.

Aging studies at various temperatures were conducted on both extruded and sheet material. Mechanical testing included the testing of tensile and yield strength and percent elongation. In addition Kahn tear tests were used to obtain comparative toughness levels of the sheet product.

Section 5 includes a summary of conclusions drawn from this work and recommendations for future work.

TABLE 1-1

ALLOY SYSTEMS INVESTIGATED IN PHASE II (EXTRUSIONS)

<i>Alloy No.</i>	<i>Aim Composition</i>	<i>Primary Mechanisms Involved</i>
1,2,3,11	Al-3.0Li	Base properties of binary system.
4 7	Al-2.6Li-2.5Sc (2.1Li-2.0Sc)	Substitution of scandium for lithium in Al ₃ Li to alter lattice parameter.
5 9	Al-3.0Li-5.0Ga (2.5Ga)	Substitution of gallium for aluminum in Al ₃ Li to alter lattice parameter.
8	Al-2.1Li-2.0Sc-2.5Ga	As above for scandium and gallium.
10	Al-3.0Li-1.5Mn	Dispersion strengthening by MnAl ₆ encouraging cross-slip.
12 13	Al-3.0Li-2.5Mg (1.5Mg)	Solid solution strengthening.
15	Al-3.0Li-1.5Mg-1.5Mn	Dispersion (MnAl ₆) and solid solution strengthening.
14	Al-3.0Li-3.0Ag	Modification of Al ₃ Li

Cast and extruded by Naval Surface Weapons Center (NSWC).

TABLE 1-2

ALLOY SYSTEMS INVESTIGATED IN PHASE III (SHEET)

<i>Alloy No.</i>	<i>Aim Composition</i>	<i>Primary Mechanisms Involved</i>
22	Al-3.0Li-0.1Zr	Base properties of binary system.
26	Al-3.0Li-0.1Zr-0.005Bi	Tie up sodium with bismuth.
10	Al-3.0Li	Binary system (HIP).
19	Al-2.2Li-2.0Cu	$\theta'' + \delta'$ precipitation.
20	6063 type + 3.0% Li	$Mg_2Si + \delta'$ precipitation.
21	6061 type + 3.0% Li	$Mg_2Si + \delta'$ precipitation.
23, 24	Al-3.0Li-1.5Mn-1.5Fe	Dispersion [(Mn,Fe)Al ₆] strengthening to encourage cross-slip.
25	Al-3.0Li-1.5Mn	Dispersion (MnAl ₆) strengthening to encourage cross-slip.

SECTION 2

PHASE I: DEVELOPMENT OF CASTING PROCEDURES

The casting of a sound ingot is the first requirement for production of aluminum-lithium wrought products. As discussed earlier, the high reactivity of lithium with oxygen and hydrogen leads to poor lithium recovery, porosity, and high hydrogen content. Our approach to this problem was to melt and cast under argon atmosphere or vacuum.

Experimental Procedure and Results

A summary of the various casting conditions that were tried during this period and the resultant ingot chemical analyses are presented in Table 2-1.

The first four trials involved solidification within the crucible used for melting. A trial melt of 7050 in vacuum (melted and solidified three times) resulted in almost total loss of magnesium and zinc. The three subsequent trials involved the addition of elemental lithium sealed in AA3003 alloy tubes to 99.99% (superpurity) aluminum. Very high hydrogen levels were recorded, and lithium recovery was low. Much porosity was evident. There was a reaction of the melt with the crucible walls, using both clay-graphite crucibles and clay-graphite crucibles with a refractory "terra paint" coating. The crucibles had to be destroyed to remove the ingots. The high hydrogen levels were most likely due to the use of elemental lithium and the lack of fluxing.

Subsequent trials were conducted by melting under vacuum, fluxing with argon, and casting as bookmold ingots under an argon atmosphere. The use of an 18.5% lithium hardener (Foote Mineral Company) resulted in fairly high hydrogen levels. Use of a 9.5% lithium hardener (KBI*) resulted in lower hydrogen readings and significantly better lithium recovery.

*Kawecki Berylco Inc.

Lithium recovery in the later castings was typically 0.5 wt. % less than the level in the charge. To obtain a 3.0% lithium recovery, it was necessary to add 3.5% lithium to the charge. A remelt casting (#9) showed a better lithium recovery but higher hydrogen content.

A beryllium addition (0.005%), #12 and #14, failed to significantly enhance the lithium recovery. Beryllium was added in an attempt to produce an oxide layer on the melt to inhibit the oxidation of lithium. Though beryllium improves oxidation resistance of some alloy melts, these results are supported by Soviet research, which indicates that lithium negates the effect of beryllium. [12]

In general our hydrogen values have improved with refinement of casting procedure. The later castings show typically 0.11 to 0.86 ml/100 g hydrogen, with the lowest readings near the bottom of the ingot. This compares favorably with other studies of casting of aluminum-lithium alloys. Values obtained by British Aluminium are given for reference in the table below. Note that British Aluminium obtained lower hydrogen readings in castings containing beryllium.

<i>Producer</i>	<i>Lithium (%)</i>	<i>Beryllium (%)</i>	<i>Hydrogen (ml/100 g)</i>
British Aluminium [10]	2.33	0	2.43
	2.63	0	1.97
	1.95	0	1.63
	2.50	0.005	1.26
	1.64	0.01	0.86

Some hydrogen porosity is expected, however, since porosity generally is associated with hydrogen levels above approximately 0.12 ml/100 g.

Sodium levels have been excellent (<0.0004%) for all castings, and the potassium level in the one ingot analyzed appeared to be good (<0.0005%). In contrast calcium levels

were 100 times greater. It is expected that any effect of high calcium would be negative due to possible segregation to grain boundaries. The use of a new lithium hardener in Phase III reduced the calcium level to 0.001%.

Radiographs of the ingots showed gross porosity in the early ingots. The later ingots showed much less porosity, though generally the top 20%-50% of each ingot had to be scrapped to avoid porosity.

Discussion and Conclusion

The final casting procedure developed for casting 10-lb bookmold ingots is as follows. The charge is made up from alloy hardeners and 99.99% aluminum (superpurity) ingot. The charge is melted under vacuum in an induction-heated, machined graphite crucible. Thermocouples in the crucible and flux wand, and attached to the load, are used to prevent overheating. No cover flux is used.

A 45-minute argon flux is used to remove hydrogen and promote thorough mixing of the melt. The furnace is backfilled with argon to atmospheric pressure, and the melt is poured at approximately 1280°-1290°F (693°-698°C) into a steel bookmold. The resulting ingots are approximately 2 5/8" x 7" x 6".

Chemistry and hydrogen levels of the ingots have been shown to be controllable, though hydrogen levels are above the limits for commercial aircraft alloys. Porosity remains a problem and was handled in this work only by removing that part of the ingot which shows significant porosity.

TABLE 2-1: INGOTS PRODUCED IN PHASE I

Alloy No.	% Li Charge	Hardener	Melt Cond.	Pour Cond.	H ₂ Surface		H ₂ Volume		% Li Recovery	Be (%)	Na (%)	Ca (%)	K (%)
					Top	Bottom	Top	Bottom					
1	(AA7050)	--	Vac.	--	.912	.069	.890	.206					
2	.3	Elemental	Vac.	--	.093	.088	.262	.227	.08				
3	7.5	Elemental	Vac.	--	3.363	8.184	3.613	.867	2.06				
4	3.0	Elemental	Ar.	--	9.545	2.957	14.711	4.224	1.29				
5	3.0	18.5% Foote	Vac.	Ar.	.493	.629	.698	.805	1.14	<.0001	.005		
6	3.0	9.5 KBI	Vac.	Ar.	.299	.157	.542	.459	2.37	<.0001	.018		
7	3.0	9.5 KBI	Vac.	Ar.	.110	.088	.660	.297	2.55	.0003	.017		
8	3.0	9.5 KBI	Vac.	Ar.	.105	.259	.265	.287	2.59	.0003	.017		
9	--	(Remelt of -7,-8)	Vac.	Ar.	.272	.368	.951	1.084	2.37	<.0001	.017		
10	3.5	9.5 KBI	Vac.	Ar.									
11	3.5	9.5 KBI	Vac.	Ar.	.208	.189	.675	.195	2.94	.0002	.019		
12	3.5 (.005 Be)	9.5 KBI	Vac.	Ar.	.189	0	.276	.231	2.71	.005	.017	<.0005 Center .0001 (est.)	
13	--	--	Vac.	Ar.	0	0	.155	.109					
14	3.5 (.005 Be)	9.5 KBI	Vac.	Ar.		.136		.170	3.06	.004	.021		
15	--	--	Vac.	Ar.									

Filter test only

SECTION 3

PHASE II: PRELIMINARY SURVEY OF ALLOY SYSTEMS

Introduction

A preliminary survey of several alloy systems was conducted using a series of small extrusions produced at the Naval Surface Weapons Center, Silver Spring, Maryland. Methods of encouraging cross-slip included alloying with manganese, magnesium, gallium, scandium, or silver. The alloy compositions and corresponding hardening mechanisms are listed in Table 1-1 and are discussed further below.

The Al-3.0Li binary system was included to obtain base properties of the alloy system. Zirconium was used to inhibit recrystallization. (All manganese-free castings contained a 0.12% zirconium addition.) Zirconium in the amount of 0.1%-0.2% has been shown to effectively inhibit recrystallization in the Al-Mg-Li system and Soviet alloy 01420.^[3,16-17] Two castings also contained bismuth in an attempt to tie up sodium, which is reported to cause grain boundary embrittlement.^[4,18]

The Al-Li-Sc system involves an attempt to modify the δ' (Al_3Li) precipitate. Scandium forms an equilibrium precipitate, Al_3Sc , of the same crystal structure (Ll_2) as δ' . A substitution of scandium for lithium in δ' may significantly change the lattice parameter and the Al- δ' interfacial energy. This, in turn, could encourage dislocation cross-slip or precipitate bypassing rather than precipitate cutting, and possibly decrease the planar slip responsible for the low ductility of aluminum-lithium systems. However, it is possible that the very low solubility of scandium in aluminum may preclude obtaining the desired fine precipitation of $\text{Al}_3(\text{Sc},\text{Li})$.

In a similar manner the substitution of gallium for aluminum in Al_3Li may result in a beneficial lattice parameter change. Both ternary Al-Li-Ga and quaternary Al-Li-Ga-Sc castings were included in this survey.

Manganese has been added to the binary aluminum-lithium system and in combination with magnesium. These alloys should exhibit dispersion strengthening as well as precipitation hardening. A fine dispersion should encourage cross-slip, thereby increasing ductility. In addition manganese decreases the solubility of lithium in aluminum^[19,20], thereby encouraging more complete precipitation of Al_3Li .

Alloys incorporating magnesium, both with and without manganese, are included. Under equilibrium conditions, Al-Mg-Li alloys with a Mg/Li ratio of 2.5 to 1.5 form the S phase (Al_2MgLi)^[21], which is isomorphous with the S phase (Al_2MgCu) found in high strength copper-bearing 7XXX alloys. Soviet researchers report that alloy 01420 is based on precipitation hardening by Al_2MgLi .^[17,22] Other work^[4,23] reports, however, that strengthening in this system is due to the intermediate precipitate δ' and that magnesium contributes solid solution strengthening. However, it appears that magnesium also contributes to detrimental grain boundary precipitation of Al_2MgLi .^[4]

A limited investigation by Hardy^[24] of the Al-Li-Ag system has shown significant age hardening in an Al-1.0Li-2.0Ag alloy. The composition presently under study is Al-3.0Li-3.0Ag.

Experimental Procedure

Production of Extrusions

Casting and extrusion for this phase of the work were carried out at the Naval Surface Weapons Center (NSWC) in Silver Spring, Maryland. All melting, casting, and homogenization were done in an argon atmosphere dry-box. The lithium was melted and held at 1112°F (600°C) in an iron crucible. In some cases the lithium was fluxed by bubbling argon to remove sodium. The aluminum and other alloying elements were melted and held at 1742°F (950°C) in an alumina crucible. The molten aluminum was then added to the iron crucible, stirred with a stainless steel rod, and poured into a tapered 1.5"-1.75" dia. x 3" deep brass mold.

The ingots produced were homogenized at 850°F (455°C)/ 8 hours + 960°F (515°C)/16 hours in an argon atmosphere. The homogenized ingots were then scalped to 1.25" diameter.

Billets were heated to 752±18°F (400±10°C) and extruded to a 0.5" x 0.25" bar. This represents a 10:1 extrusion ratio. Breakthrough pressure was on the order of 50 tons.

Chemical Analysis

Chemical composition of the homogenized billets was determined by atomic emission spectroscopy.

Aging Curves

Hardness specimens were solution heat treated at 975°F (524°C) for 30 minutes in argon and water quenched. Hardness aging curves were established for samples aged at 375°F (191°C) in air.

In addition hardness aging curves for some alloys solution heat treated at 932°F (500°C) for 30 minutes, water quenched, and aged at 300° and 350°F (149° and 177°C) were established.

Mechanical Tests

Due to the small cross-sections (approximately 0.5" x 0.25"), longitudinal tension tests only were conducted. Tensile sample gauge sections were machined to a 0.25" width, full thickness (approximately 0.25"), with a 1" gauge length. Lack of material necessitated using subsize tension test samples (0.160" rounds) for sample #10-2A and #3-0 aged at 375°F (191°C).

Metallography

Samples of the solution heat treated extrusions were examined optically and by scanning electron microscopy (SEM). In some cases qualitative chemical identification of insolubles and inclusions could be made by electron microprobe.

Low power binocular and SEM examination of fracture surfaces was conducted.

Results and Discussion

Fabrication

The extruded rods produced by NSWC exhibited some tearing and bending. Those alloys containing gallium showed a white powder on the surface as-homogenized, as-scalped, and as-extruded.

Chemical Analysis

The chemical analyses of the homogenized billets are given in Table 3-1. There was some variation in elemental levels from the aimed for compositions, aside from the expected difficulty in controlling the lithium level. There was apparent difficulty in getting bismuth in solution. More surprising was the high iron level, which ranged from 0.59% to 2.37%. Some of the iron could have been due to the 1100 alloy used as aluminum stock. (The Aluminum Association limit for [Fe+Si] in 1100 is 1.0%.) A large part of the iron, however, apparently was introduced from the iron crucible used for melting the lithium and mixing the alloy prior to casting. Previous studies of the Al-Li-Mg system melted in iron or stainless steel crucibles have shown considerable iron contamination. [25]

Sodium levels were fairly low for the two billets analyzed. Alloy #11-1, made with lithium fluxed with bubbling argon, had no lower sodium than #3-1, made with unfluxed lithium.

Aging Curves

Hardness aging curves for extrusions solution heat treated at 975°F (524°C) for 30 minutes in argon, water quenched, and aged at 375°F (191°C) are presented in Figures 3-1 through 3-4. In addition aging curves for some alloys solution heat treated at 932°F (500°C) for 30 minutes in argon, water quenched, and aged at 300°F (149°C) or two-step aged at 300° and 350°F (149° and 177°C) are presented in Figures 3-5 and 3-6 respectively.

Those samples aged at 300° and 350°F (149° and 177°C) did not reach peak hardness for the aging times studied (up to 142 hours). Aging at 375°F (191°C) enabled peak hardness to be reached within 100 hours for all compositions.

The aluminum-lithium binary (some with high iron) compositions (Figure 3-1) showed an aging response similar to that reported for Al-2.8Li-0.12Zr^[23], reaching peak hardness at approximately 10 hours at 375°F (191°C).

Compositions containing gallium and scandium reached peak hardness with the least aging at 375°F (191°C)--4-8 hours (Figure 3-2). The peak hardness reached for the gallium-containing extrusions was lower than that reached by aluminum-lithium binary alloys of similar lithium content.

The magnesium-containing extrusions (Figure 3-3) exhibited a higher hardness value than the binary alloys at slightly longer aging times (16-32 hours). The Al-Li-Mn alloy #10-2A (Figure 3-3) showed the slowest aging response, reaching peak hardness after 64 hours at 375°F (191°C). Hardness readings on extrusion #10-1 showed large variations in different locations, presumably due to chemical inhomogeneity. An aging curve could not be determined for this extrusion.

Mechanical Test Results

Tables 3-2 and 3-3 present longitudinal tensile strength, yield strength, and elongation data for the extrusions aged to peak hardness at 375°F (191°C) and those aged at 300°F (149°C) or 350°F (177°C).

In general the percent elongation was very low for all aging practices. This low ductility was very likely encouraged by the high lithium and high iron content. In addition several of the fracture surfaces showed large inclusions of metallic zirconium, iron, or scandium. (This is discussed further under Metallography.) Such inclusions and

associated stress concentrations normally contribute to early failure and low ductility.

At peak hardness the Al-Li-Mg-Mn alloy (#15-1) showed the greatest tensile strength (70.1 ksi), and the Al-Li-(Fe) alloy (#3-1) showed the greatest yield strength (62.0 ksi). Each exhibited very low elongation (2%). Extrusions #8-1, Al-Li-(Fe), and #10-2A, Al-Li-Mn-(Fe) showed the greatest elongation--8% and 14.8% respectively.

At peak hardness the tensile strengths ranged from 53.6 to 70.1 ksi, and yield strengths ranged from 37.6 to 62.0 ksi. For comparison, Soviet alloy 01420 (Al-2.0Li-6.0Mg-0.25Mn) has the following properties:

65.2-71.0 ksi tensile strength
43.5-52.2 ksi yield strength
8%-10% elongation

The Fulmer Research Institute^[3] reports the following properties on a high lithium alloy (Al-2.7Li-5.2Mg-0.2Zr):

79.5 ksi tensile strength
61.4 ksi yield strength
5.5% elongation

Alcoa^[26] reports the following properties for a high lithium (Al-3.1Li-1.9Mg) extrusion at peak hardness:

<u>Longitudinal</u>	<u>Transverse</u>
70.0 ksi tensile strength	59.4 ksi tensile strength
61.4 ksi yield strength	48.0 ksi yield strength
1.4% elongation	4.0% elongation

For extrusion #10-2A the combination of tensile properties (57.1 ksi tensile strength, 41.5 ksi yield strength) and elongation (14.8%) is encouraging. For comparison, a Soviet alloy of similar composition (2.7-3.0Li, 1.25-5.0Mn) had the following reported properties^[27]:

64-71 ksi tensile strength
42.5-57.0 ksi yield strength
4-8% elongation

However, the ductility seen in the test of #10-2A is in contrast to the 5.0% elongation seen in the underaged samples in Table 3-3. Due to lack of material, #10-2A could not be retested at peak hardness.

The peak hardness #10-2A tensile specimen was a subsize round sample, 0.1599" dia. x 0.640" gauge length. The elongation seen in this test includes significant uniform elongation. A reduction in area was seen along the gauge length, with little necking at the fracture. The gauge section after test had an elliptical cross-section (presumably due to texturing caused by extrusion of a rectangular section) with axes measuring 0.1565" and 0.1585", compared to the circular pre-test cross-section with a diameter of 0.1599". This is similar to Soviet alloy 01420, where elongation is primarily uniform with little contribution by necking.

The very high level of dispersoid-forming elements of #10-2A (2.9% Mn+Fe) may be enough to require cross-slip for significant dislocation movement. This could prevent the planar slip encouraged by the coherent Al_3Li precipitate, which leads to low ductility. The addition of iron also increases the amount of MnAl_6 or $(\text{Mn,Fe})\text{Al}_6$ phase present. [28] Also of possible significance is that the #10-2A composition is probably in the primary FeAl_3 phase field for equilibrium cooling based on the Al-Mn-Fe ternary phase diagram. [28] This can be detrimental due to the precipitation of large crystals of FeAl_3 during solidification.

Metallography

Microstructure. Figures 3-7 through 3-16 show optical micrographs of extrusions solution heat treated at 932°F (500°C) for 30 minutes and water quenched. These sections indicate a large amount of inhomogeneity. Large FeAl_3 or $(\text{Mn,Fe})\text{Al}_6$ particles (as determined by morphology and

qualitative probe analysis) are apparent in each of the alloys. As discussed under Chemical Analysis in this section, the significant iron contamination occurred during the casting procedure. Similar primary segregation of scandium-rich insolubles (by qualitative electron microprobe analysis) is apparent in the scandium-containing alloys.

Figures 3-7 through 3-10, 3-13, 3-14, and 3-16 show what appear to be remnants of a dendritic structure. This indicates the extrusion ratio, 10:1, was too low to break up the cast structure completely.

Figure 3-17 is a scanning electron micrograph (SEM) of a cross-section from extrusion #4-1, as-solution heat treated, showing the residual dendritic structure. The large insolubles have been identified as scandium-rich compounds by qualitative microprobe analysis. The interdendritic particles are iron-rich.

Fractography. Figures 3-18 and 3-19 give optical views of fracture surfaces with examples of intergranular cracking and transgranular failure. Figure 3-20 gives a longitudinal view of the fracture of extrusion #1-3, showing more clearly the transgranular nature of the fracture (45° shear).

SEMs of fracture surfaces are presented in Figures 3-21 through 3-26. Extrusion #3-1 (Figure 3-21) failed predominantly by 45° shear. Seen at the beginning of the shear face (in 50X photo) is a large metallic iron inclusion that possibly initiated the fracture. Inclusions found in other fracture surfaces were identified as elemental scandium and elemental zirconium. The iron, scandium, and zirconium particles are each located near a surface where the failure is likely to initiate.

Dimpling of the fracture surface is apparent in each of the ternary or high-order alloys in Figures 3-21 through 3-26.

Samples of #10-2A (Figure 3-22) and #15-1 (Figure 3-26) also exhibited intergranular cracking.

While showing a dimpled "matrix," some of the samples exhibit brittle fracture of intermetallic phases. Brittle fracture of $(\text{Fe},\text{Mn})\text{Al}_3$ insolubles is apparent in #10-2A (Figure 3-22). Microprobe analysis determined approximately equal amounts of iron and manganese in these particles. Scandium-rich insolubles in #8-1 (Figure 3-24) and silver-rich particles in #14-1 (Figure 3-25) also exhibited brittle fracture.

Despite the dimpled appearance of the fracture surfaces, the samples in general showed little elongation and very little necking. Phase III includes a further investigation which associates the micro-dimples with possible subgrain boundary failure.

Conclusions of Phase II

The extrusions produced in this phase generally showed very low ductility. This was due, at least in part, to the severe iron contamination which occurred during casting. The iron contamination causes any conclusions from this study to be limited.

The addition of 5.0% gallium produced corrosion under ambient conditions, resulting in a white, powdery oxide on all surfaces. At this level gallium is likely to be impractical from this standpoint. Scandium and manganese, at least when in combination with 1.0%-1.5% iron, appear to be at levels too high to achieve a homogeneous structure using conventional casting methods. Application of rapid solidification technology may be beneficial. The other alloying elements, silver (which formed coarse particles) and magnesium, did not show any benefit, but again the detrimental effects of excessive iron must be considered.

TABLE 3-1
 CHEMICAL ANALYSIS OF PHASE II EXTRUSIONS
 NSWC * Produced Material

Ident.	Weight Percent															
	Si	Fe	Cu	Mn	Mg	Cr	Ni	Zn	Ti	Li	Sc	Ga	Bi	Ag	Ca	Na
1-3**	--	.93	--	--	--	--	--	--	--	3.19	--	--	--	--	--	--
3-0	--	2.10	--	--	--	--	--	--	--	3.33	--	--	.032	--	--	--
3-1	.03	2.37	.14	<.01	.01	<.01	.01	.03	<.01	3.51	--	--	<.005	--	.02	.0006
4-1	--	1.07	--	--	--	--	--	--	--	2.80	2.02	--	--	--	--	--
5-1	--	.79	--	--	--	--	--	--	--	3.12	--	5.56	--	--	--	--
8-1	--	.93	--	--	--	--	--	--	--	3.09	<.01	<.01	--	--	--	--
9-0	--	.85	--	--	--	--	--	--	--	2.89	--	5.01	--	--	--	--
10-1	.04	.70	.14	<.01	.01	<.01	.01	.04	.22	2.17	--	--	<.005	--	--	--
10-2A	.05	1.33	.13	1.55	.01	<.01	.01	.02	<.01	2.98	--	--	.009	--	--	--
11-1	.03	1.51	.14	<.01	.01	<.01	.01	.03	<.01	3.54	--	--	.024	--	.02	.001
13-1	.05	1.67	.12	<.01	1.44	<.01	.01	.04	<.01	3.14	--	--	<.005	--	--	--
14-1	--	.78	--	--	--	--	--	--	--	3.24	--	--	--	2.93	--	--
15-1	--	.59	--	1.21	1.67	--	--	--	--	3.14	--	--	--	--	--	--

*Cast and extruded at the Naval Surface Weapons Center, Silver Spring, Maryland.

** .12 Zr added to all except 10-1, 10-2A, and 15-1.

TABLE 3-2

MECHANICAL PROPERTIES OF PHASE II EXTRUSIONS
AGED AT 375°F (191°C) TO PEAK HARDNESS*

Ident.	Composition	Hours @ 375°F (191°C)	Longitudinal		
			UTS (ksi)	YS (ksi)	Elong. (%)
1-1	3.0 Li (Nominal)	8	66.8	57.6	4.0
1-3	3.2Li-.9Fe	8	67.5	56.6	4.0
3-0	3.3Li-2.1Fe	8	53.7	--	~1.0
3-1	3.5Li-2.4Fe	8	69.3	62.0	2.0
4-1	2.8Li-2.0Sc-1.1Fe	4	61.3	58.2	2.0
8-1	3.1Li-.9Fe	8	58.9	46.9	8.0
10-2A	3.0Li-1.6Mn-1.3Fe	64	57.1	41.5	14.8
13-1	3.1Li-1.4Mg-1.7Fe	4	66.2	60.8	2.0
14-1	3.2Li-2.9Ag-.8Fe	32	53.6	37.6	5.0
15-1	3.1Li-1.7Mg-1.2Mn-.6Fe	16	70.1	59.6	2.0

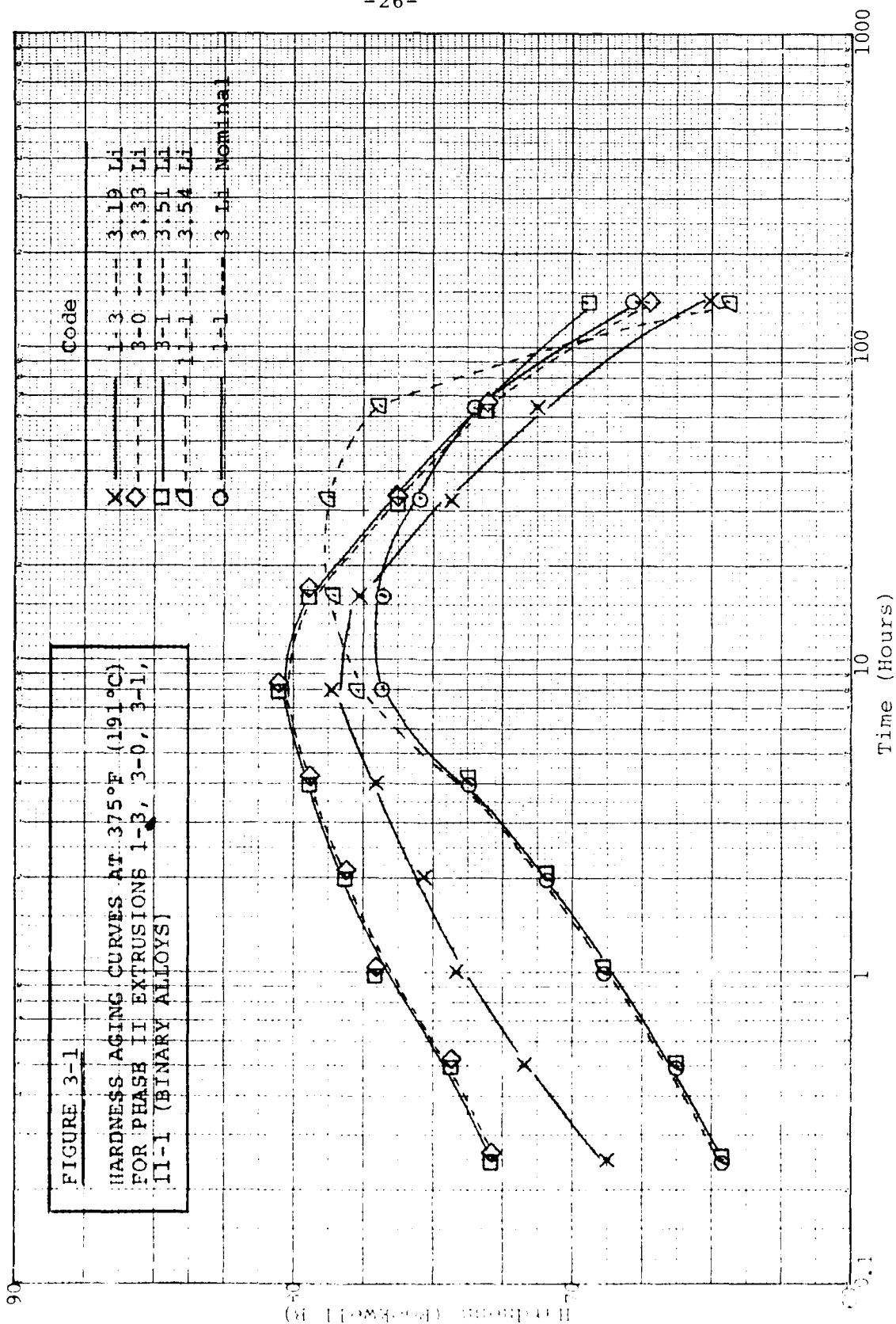
*SHT 975°F (524°C)/30 minutes + age 375°F (191°C)/peak hardness.

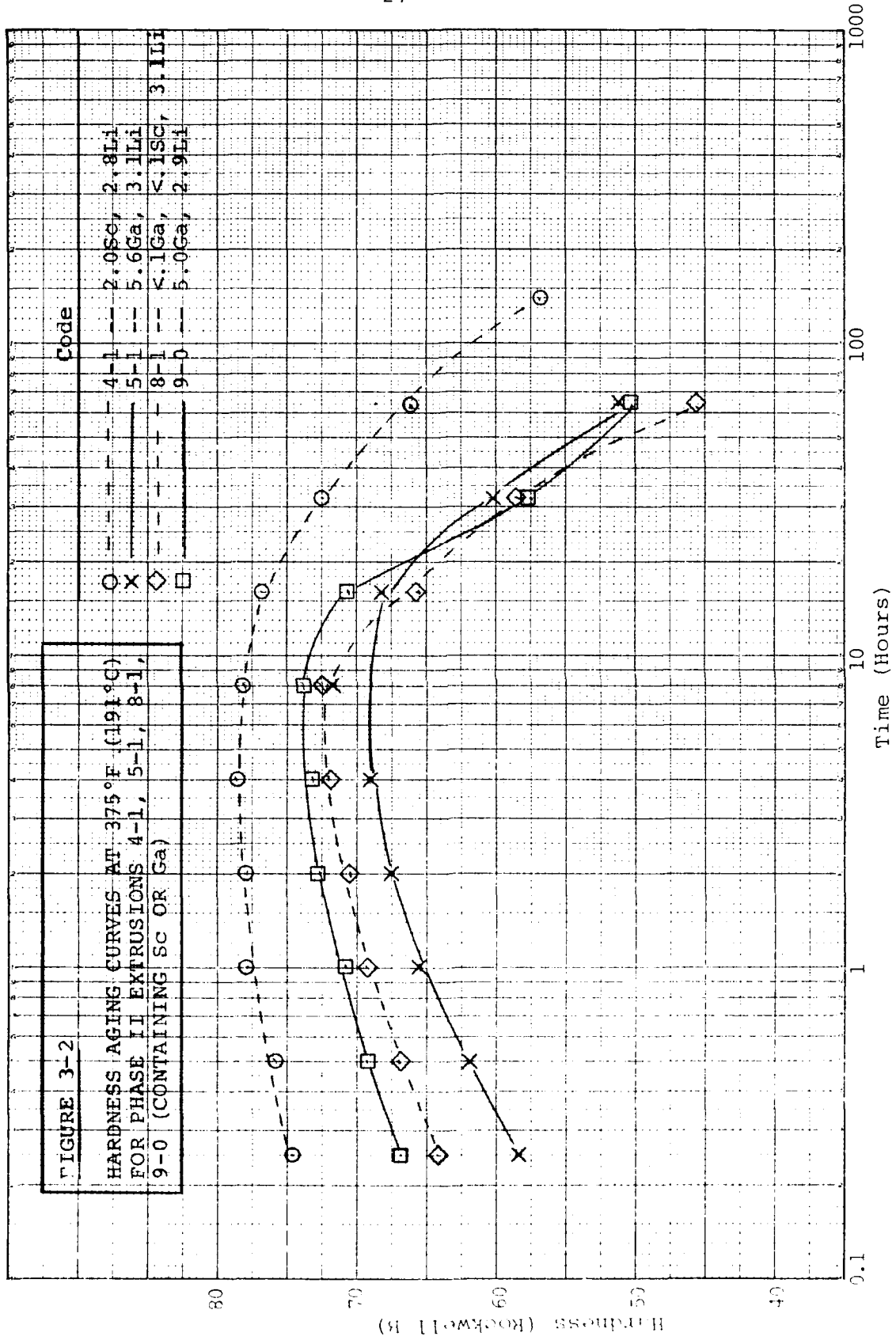
TABLE 3-3

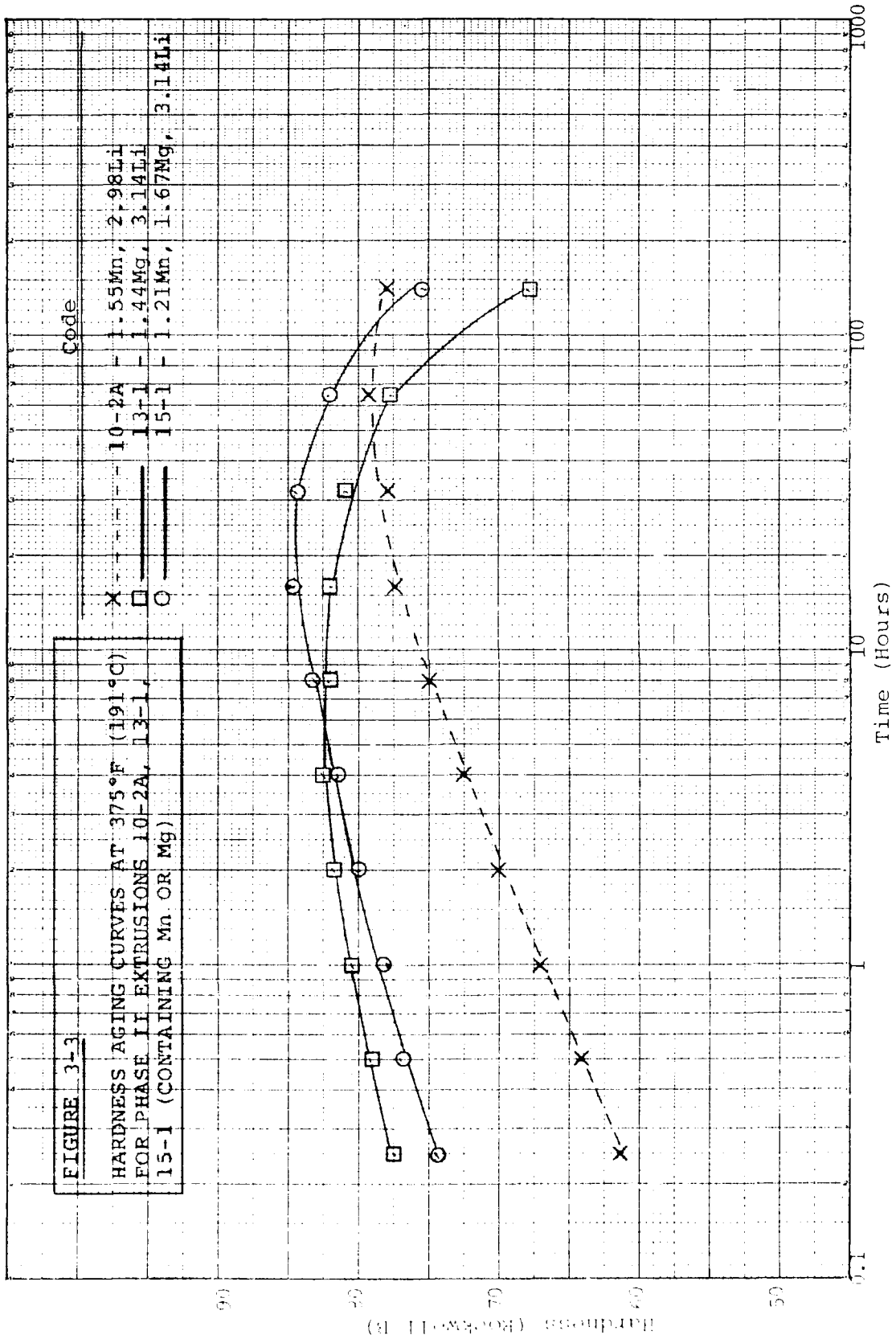
MECHANICAL PROPERTIES OF PHASE II EXTRUSIONS
 AGED @ 300°F (149°C) FOR 24 HOURS OR
 300°F (149°C) FOR 24 HOURS + 350°F (177°C) FOR 4 HOURS

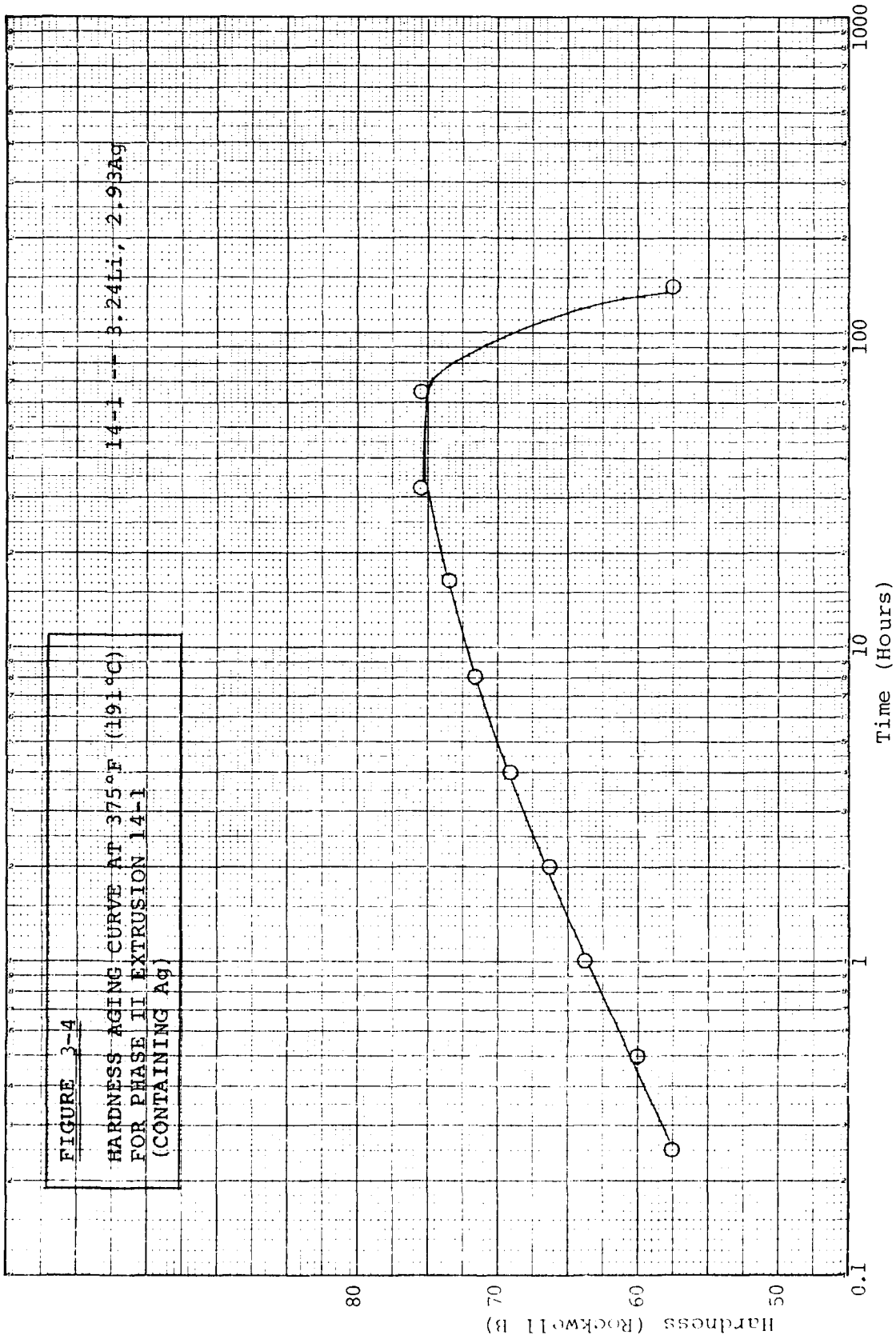
Ident.	Composition	300°F (149°C) / 24 Hours*			300°F (149°C) / 24 Hours + 350°F (177°C) / 4 Hours		
		UTS (ksi)	YS (ksi)	Elong. (%)	UTS (ksi)	YS (ksi)	Elong. (%)
1-3	3.2Li-.9Fe	66.7	50.9	4.0	67.0	58.3	4.0
9-0	2.9Li-5.0Ga-.85Fe	61.6	51.5	5.0	59.7	51.7	5.0
10-1	2.2Li-.7Fe	39.3	32.1	4.0	49.1	34.5	5.0
10-2A	3.0Li-1.6Mn-1.3Fe	51.1	34.2	5.0	51.7	36.5	5.0
11-1	3.54Li-1.5Fe	61.6	50.5	4.0	59.8	51.7	3.0

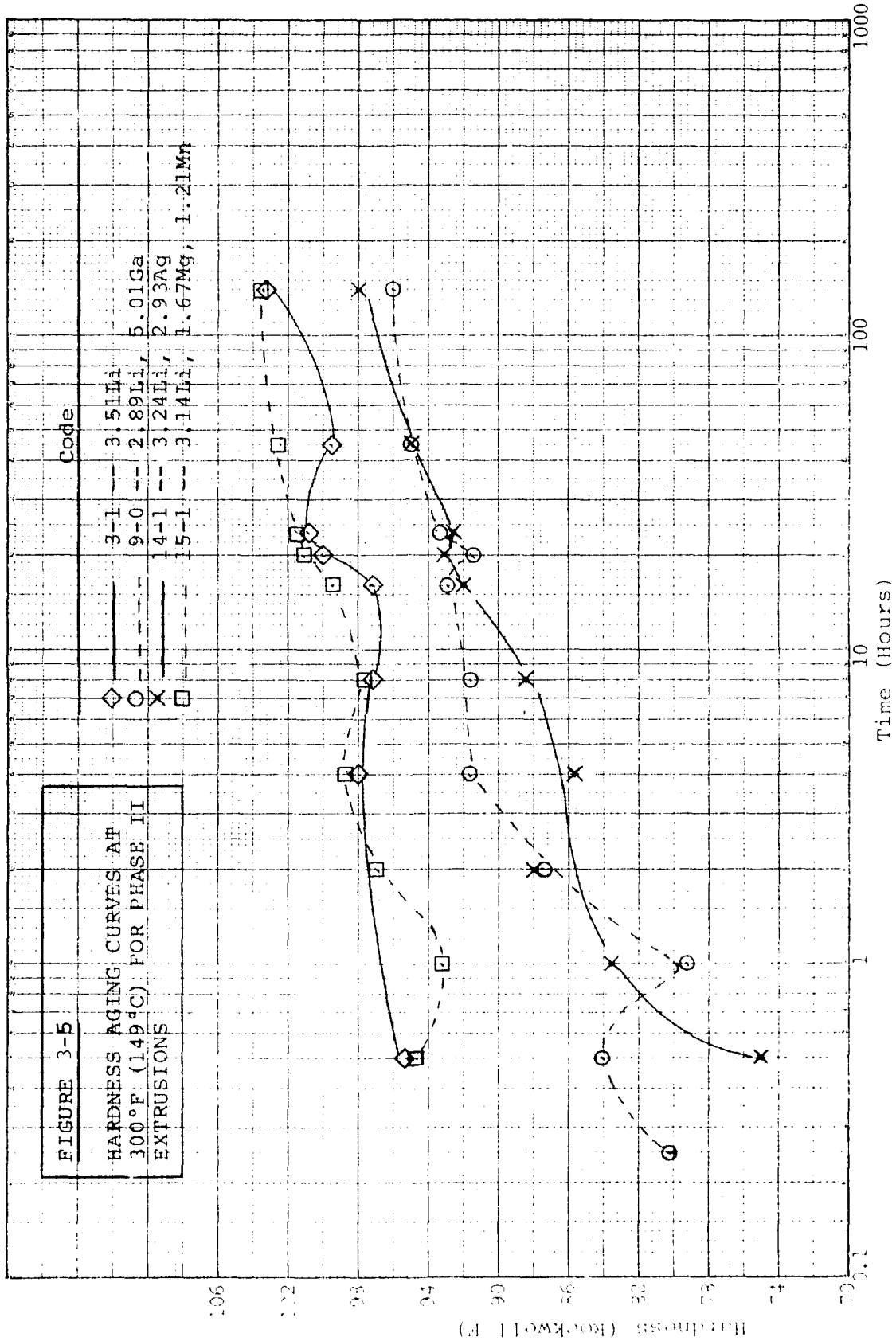
*SHT 932°F (500°C)/30 minutes in argon, water quench.

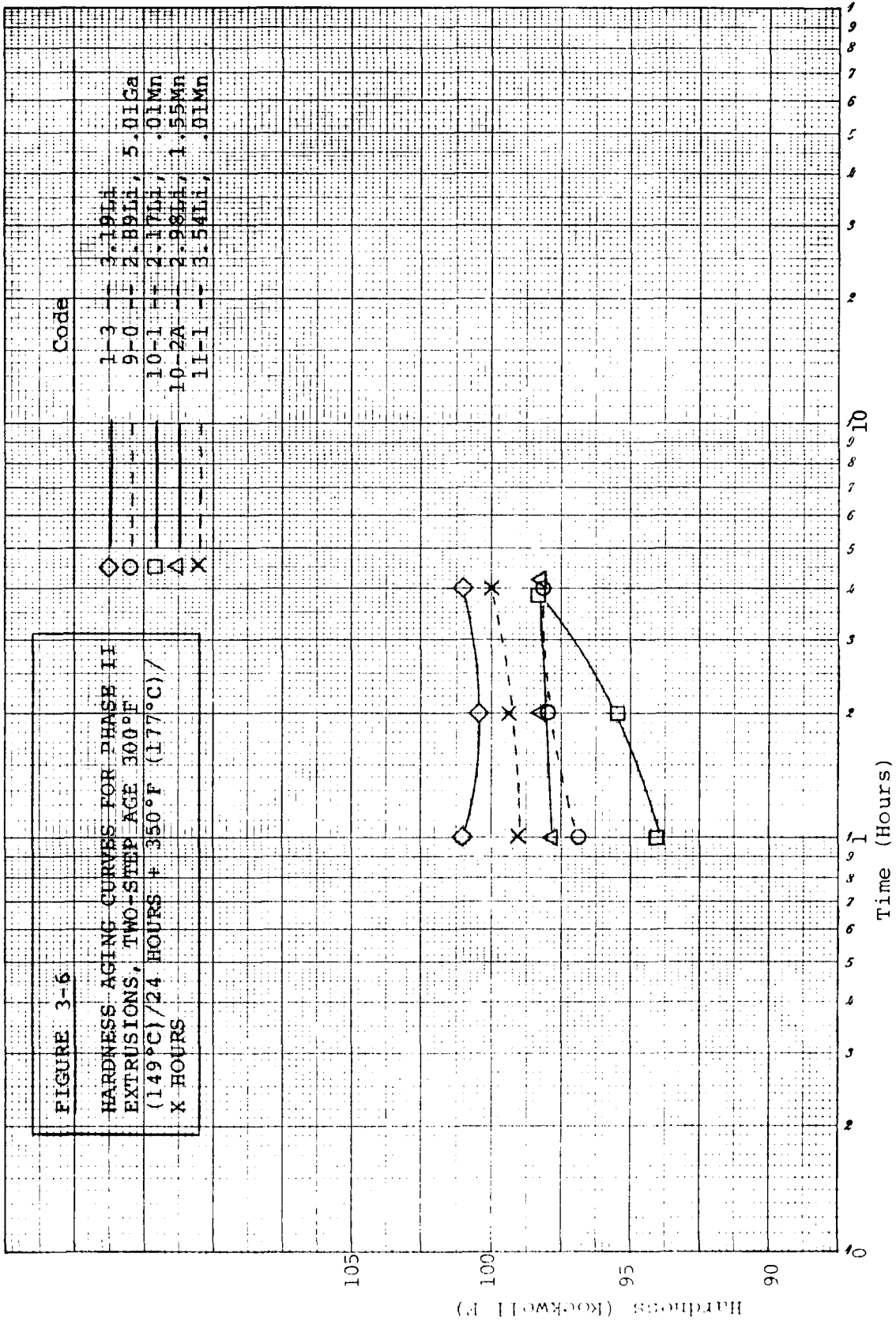














A. As-polished, 100X



C. Bakers etch, 100X

100μ



B. As-polished, 500X

20μ

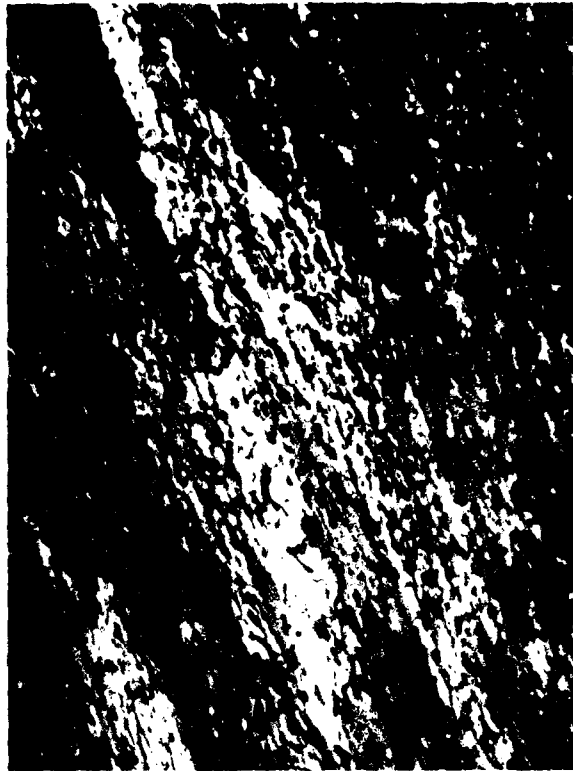
FIGURE 3-7

OPTICAL MICROGRAPHS OF EXTRUSION
#1-3, SHT 932°F (500°C)/20 MIN.,
WATER QUENCHED

Al-3.19Li-0.93Fe



A. As-polished, 100X



C. Barkers etch, 100X



B. As-polished, 500X

100 μ

20 μ

FIGURE 3-8

OPTICAL MICROGRAPHS OF EXTRUSION
#11-1 SHT 932°F (500°C)/20 MIN.,
WATER QUENCHED, SHOWING LARGE
METALLIC IRON INCLUSION

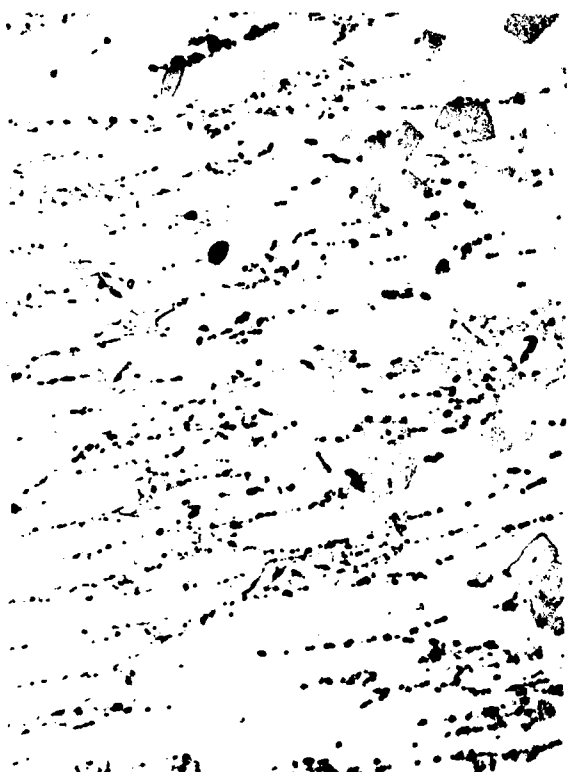
Al-3.54Li-1.51Fe



A. As-polished, 100X



C. Barkers etch, 100X



B. As-polished, 500X

100μ

FIGURE 3-9

OPTICAL MICROGRAPHS OF EXTRUSION
#4-1, SHT 932°F (500°C)/20 MIN.,
WATER QUENCHED

Al-2.8Li-2.02Sc-1.07Fe

← Interdendritic insolubles
include Fe-containing
particles.
← Large insolubles are
Sc-containing.

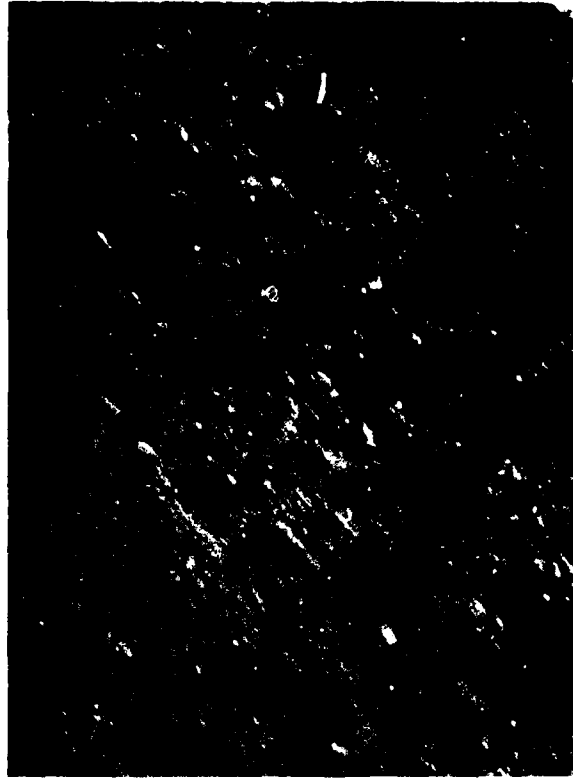
20μ



A. As-polished, 100X



B. As-polished, 500X



C. Bakers etch, 100X

FIGURE 3-10

OPTICAL MICROGRAPHS OF EXTRUSION
#3-1, SHT 932°F (500°C) 20 MIN.,
WATER QUENCHED

A1- 3.09L1-0.9038--0.0133--0.0161



B. As-polished, 500X

20 μ



C. Barkers etch, 100X

100 μ

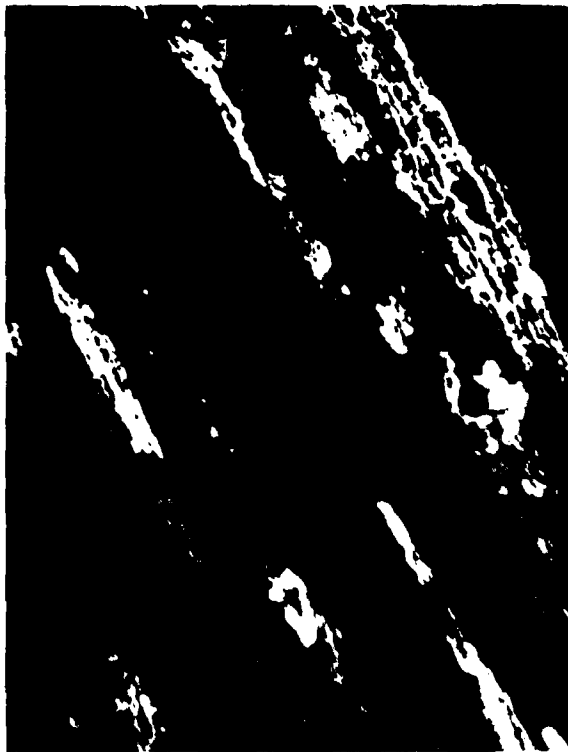
FIGURE 3-11

OPTICAL MICROGRAPHS OF EXTRUSION
#10-2A, SHT 932°F (500°C)/20 MIN.,
WATER QUENCHED, showing
(Mn,Fe)Al₆ insolubles.

Al-2.98Li-1.55Mn-1.33Fe-0.13Cu-
0.05Si-0.009Bi



A. As-polished, 100X



C. Barkers etch, 100X

100 μ



B. As-polished, 500X
showing $(\text{Mn Fe})\text{Al}_6$ insolubles.

20 μ

FIGURE 3-12

OPTICAL MICROGRAPHS OF EXTRUSION
#10-1, SHT 932°F (500°C)/20 MIN.,
WATER QUENCHED

Al-2.17Li-0.70Fe-0.22Ti



A. As-polished, 100X



B. As-polished, 500X

20 μ



C. Bakers etch, 100X

100 μ

FIGURE 3-13

OPTICAL MICROGRAPHS OF EXTRUSION
#13-1, SHT 932°F (500°C)/20 MIN.,
WATER QUENCHED

Al-3.14Li-1.67Fe-1.44Mg

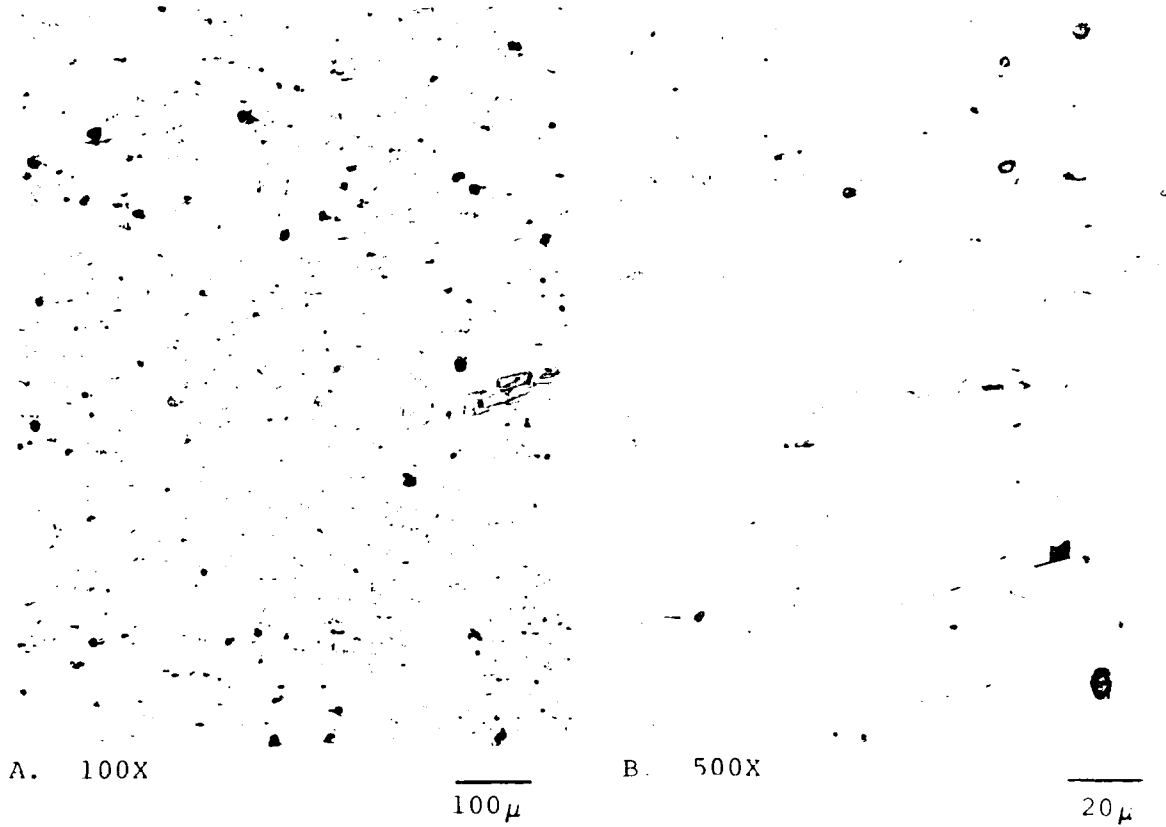


FIGURE 3-14. OPTICAL MICROGRAPHS OF EXTRUSION #15-1, SHT 932°F (500°C)/20 MIN., WATER QUENCHED, AS-POLISHED

Al-3.14Li-1.67Mg-1.21Mn-0.59Fe



A. 100X

100 μ



B. 500X

20 μ

FIGURE 3-15. OPTICAL MICROGRAPHS OF EXTRUSION #15-2, SHT 932°F (500°C)/20 MIN., WATER QUENCHED, AS-POLISHED



A. As-polished, 100X



C. Bakers etch, 100X



B. As-polished, 500X

100μ

20μ

FIGURE 3-16

OPTICAL MICROGRAPHS OF EXTRUSION
#14-1, SHT 932°F (500°C)/20 MIN.,
WATER QUENCHED

Al-3.24Li-2.93Ag-0.78Fe

Interdendritic
insolubles include
Fe-containing
particles. →



← Large insolubles
are Sc-containing.

FIGURE 3-17. SCANNING ELECTRON MICROGRAPH OF EXTRUSION #4-1,
WITH LARGE INSOLUBLES IDENTIFIED AS Al-Sc
COMPOUND, INTERDENDRITIC PARTICLES INCLUDE IRON-
RICH PARTICLES

As-polished.

1000X

Intergranular
cracking



FIGURE 3-18. EXTRUSION #10-2A PEAK HARDNESS, BROKEN TENSILE FRACTURE SURFACE

30X. Intergranular cracking in long transverse direction is visible.



FIGURE 3-19. EXTRUSION #3-1 PEAK HARDNESS, BROKEN TENSILE FRACTURE SURFACE, SHOWING 45° SHEAR FAILURE

10X.

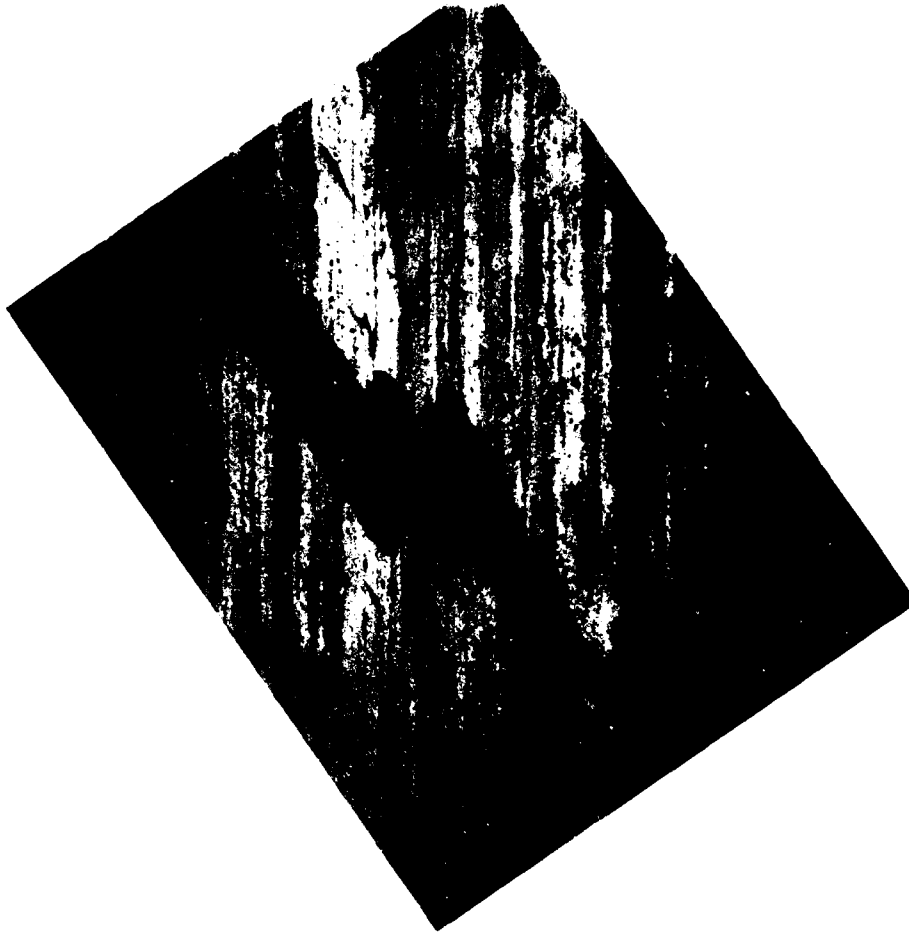
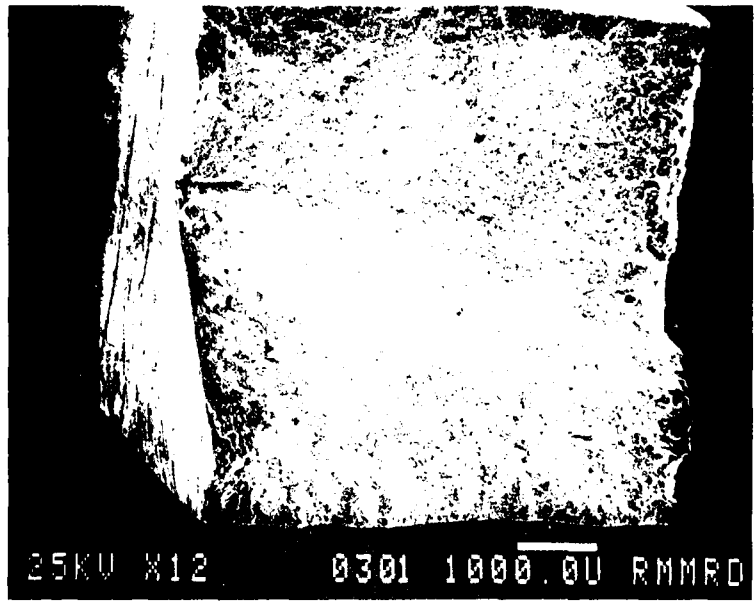
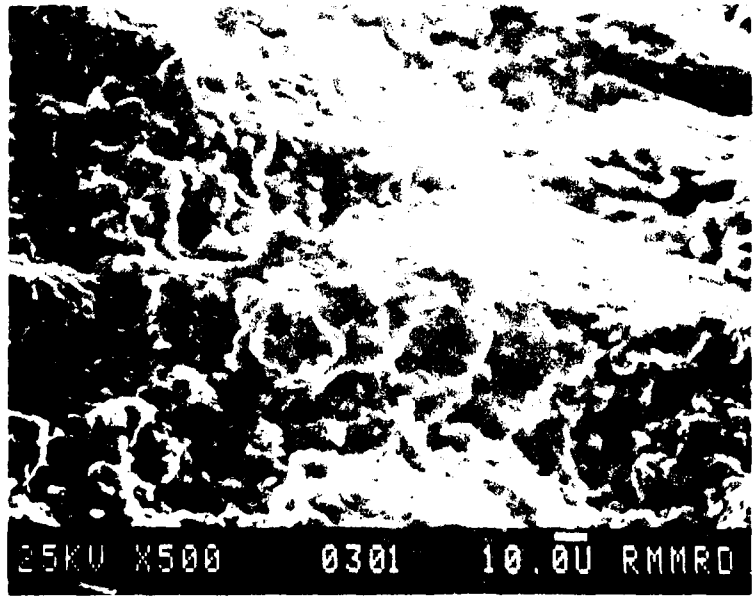


FIGURE 3-20. OPTICAL MICROGRAPH OF EXTRUSION #1-3, SHT 932°F (500°C)/30 MIN. AND AGED 300°F (149°C)/24 HOURS + 350°F (177°C)/4 HOURS, SHOWING TRANSGRANULAR FRACTURE (45° SHEAR)

Barkers etch, 200X.

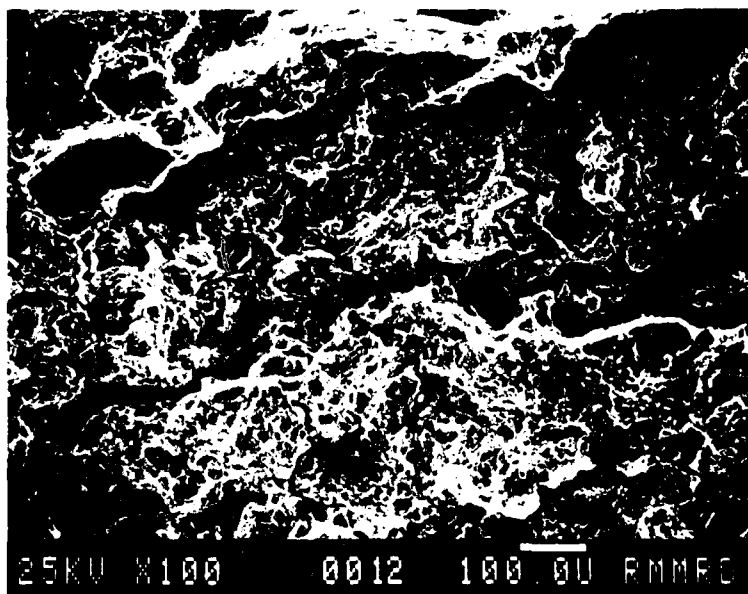


A. Showing Fe inclusion at left. 12X.

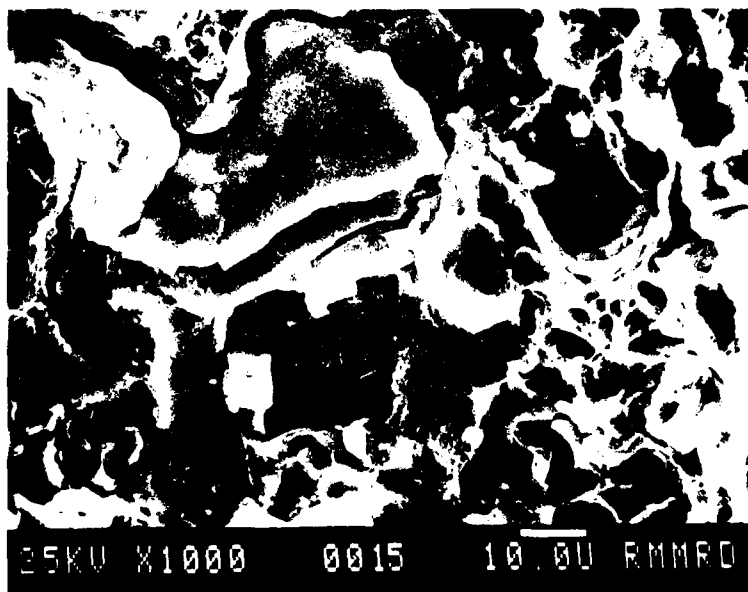


B. Detail of surface texture. 500X.

FIGURE 1-21. SEM of surface of 100% Fe powder, showing surface texture, and Fe inclusion.



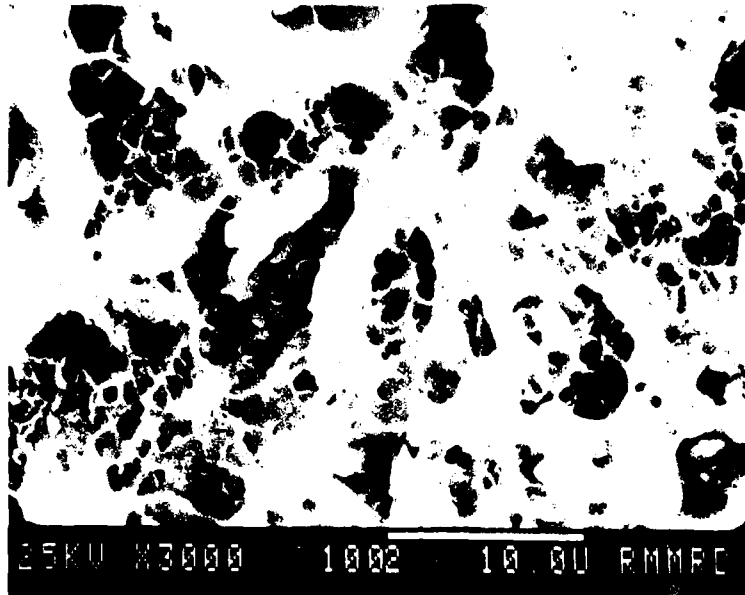
A. Showing interfacial cracking. 100X.



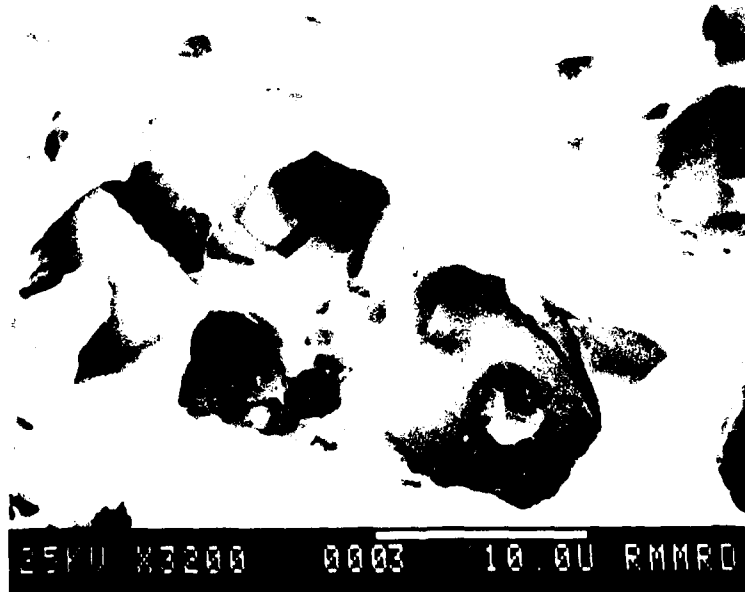
B. Aged 100°C in PEG (24 hours) + 150°C (1.7 hr) + aging, showing large cracks, etc. 1000X.

FIGURE 3-22. SEM OF FRACTURE SURFACE, LEAF HARDNESS (100X), SURFACE POROSITY, FRACTURE SURFACE

(1000X) AND SURFACE

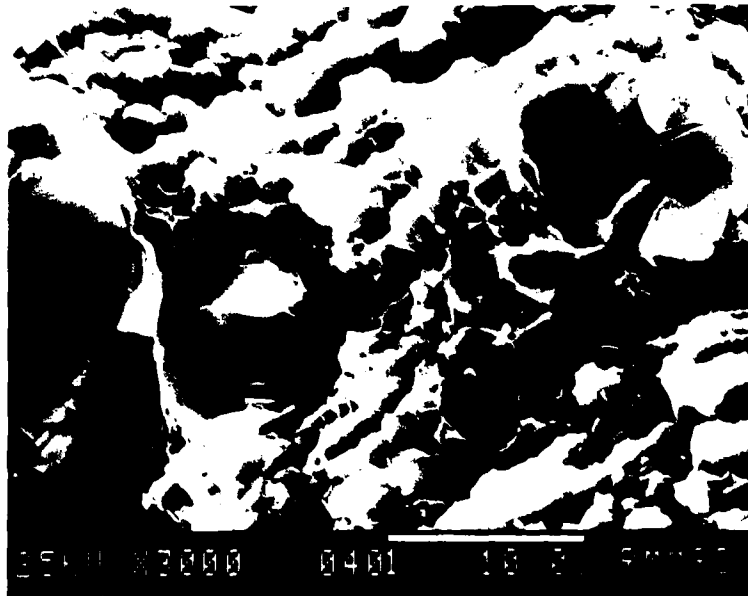


C. Dimpled appearance of aluminum matrix.
3000X.



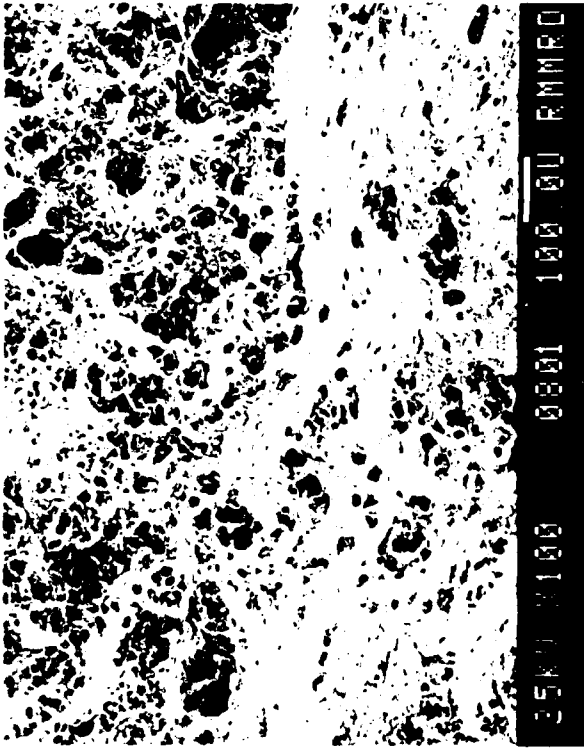
D. Dimpled (ductile) fracture of aluminum
matrix with brittle fracture of
(Mn,Fe)Al₇. 3200X.

FIGURE 3-22 End. SEM OF EXTENSION #10-2A, PEAK HARDNESS
(EXCEPT WHERE NOTED), FRACTURE SURFACE

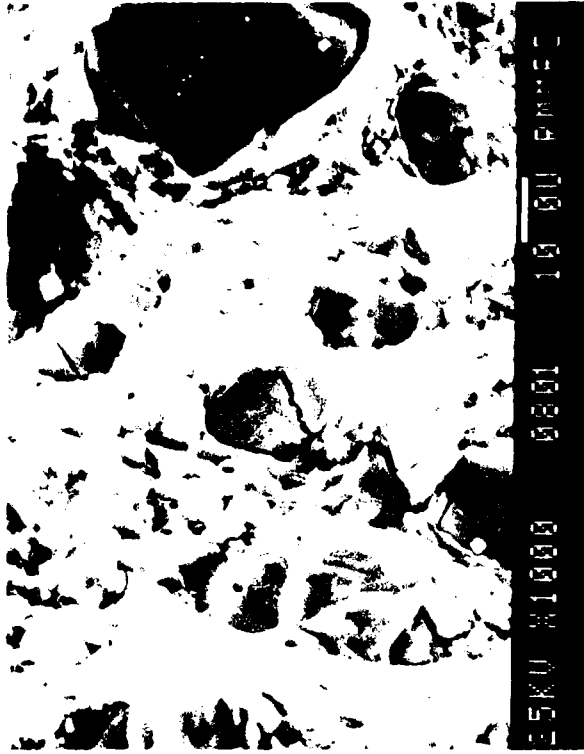


Dimpled appearance of matrix. Scandium-rich insolubles are visible. 3000X.

FIGURE 3-23. SEM OF EXTRUSION #4-1, PLAK HARDNESS, FRACTURE SURFACE



A. 100X.



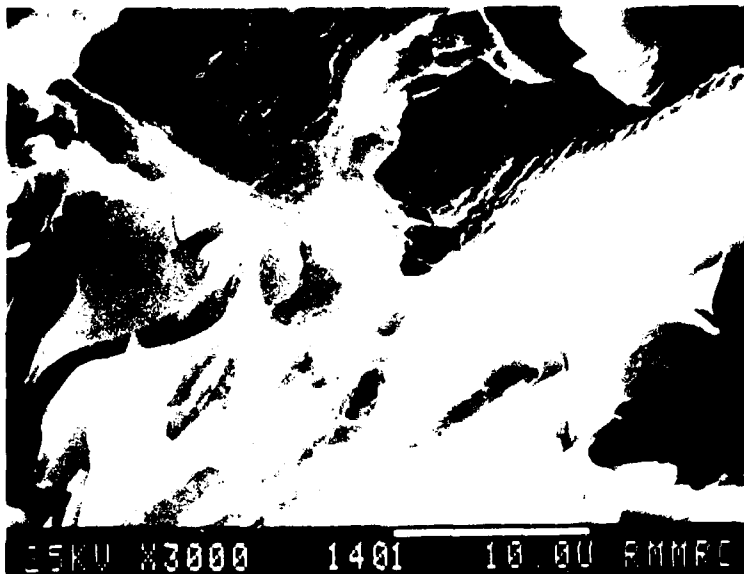
B. With particles exhibiting cleavage. Particle with brittle fracture in center is an Al-Sc compound. 1000X.



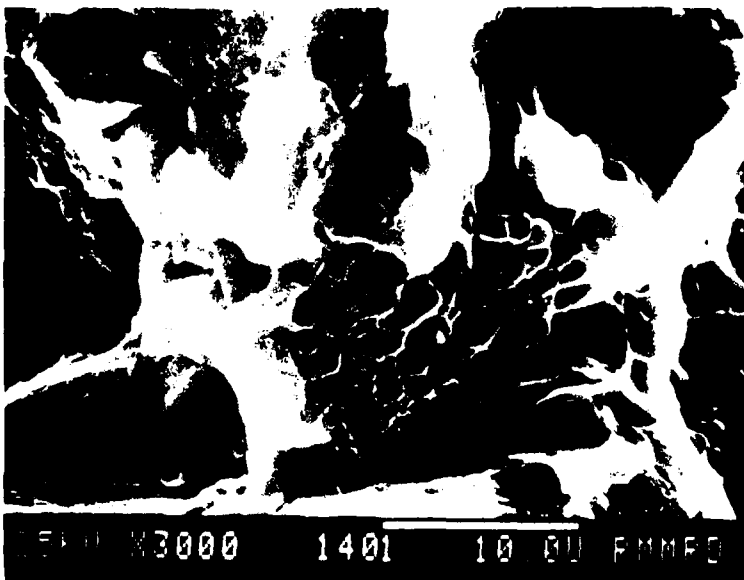
C. Showing dimpled appearance of matrix. 5000X.

FIGURE 3-24

SEM OF EXTRUSION #8-1, PEAK HARDNESS,
FRACTURE SURFACE

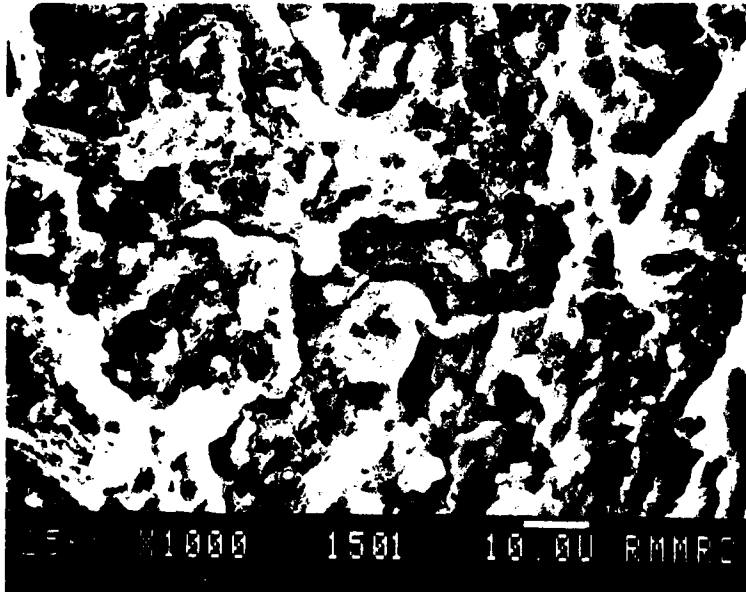


A. Area of surface showing
3000X.

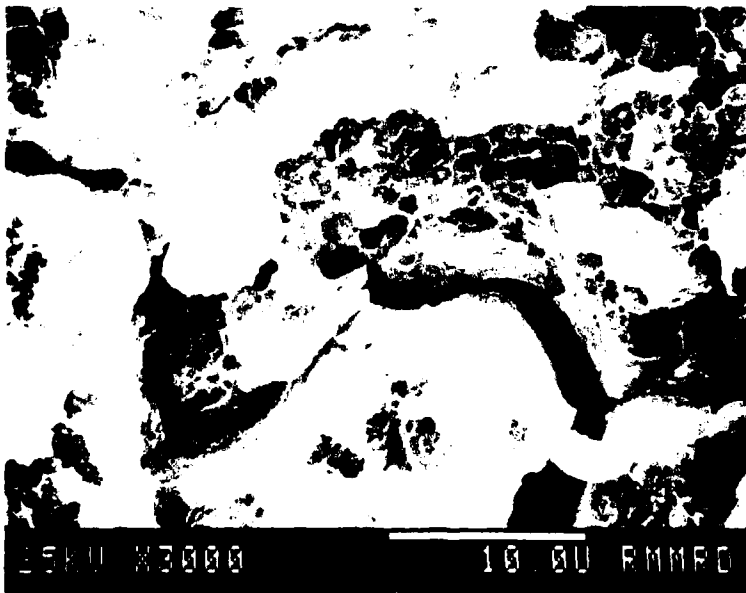


B. Area of surface showing
3000X.

FIGURE 1. SURFACE MORPHOLOGY, PLATE HARDNESS, AND PLATE STRENGTH.



A. Intergranular cracking. 100X.



B. Same area as A., showing dimpled aluminum matrix. 3000X.

FIGURE 3-26. SEM OF EXTRUSION #15-1, BEAK HARDNESS, FRACTURE SURFACE

SECTION 4

PHASE III: SHEET

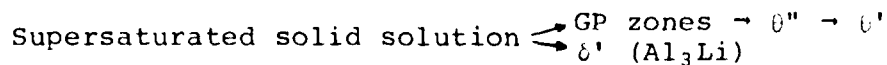
Introduction

This phase of the development program involved the analysis of fracture behavior of various aluminum-lithium based alloys in sheet form. The selection of particular compositions was based in part on the results of the preliminary study in Phase II. The systems examined include Al-Li, Al-Li-Cu, Al-Li-Mg-Si, Al-Li-Mn, and Al-Li-Mn-Fe. The systems and strengthening mechanisms, listed in Table 1-2, are discussed in detail below.

The Al-Li system was included to determine properties of the binary alloy sheet. Zirconium was used to inhibit recrystallization in all the manganese-free alloys. Ingots 23-26 were cast with bismuth additions, which is believed to help prevent grain boundary embrittlement by sodium. [4,18] In addition an early binary alloy casting (#10) was included to determine if HIPing (hot isostatic pressing) is useful in healing porosity created during casting.

Cast #19 was an Al-2.2Li-2.0Cu alloy. This composition was calculated to contain approximately the maximum level of lithium soluble in Al-2.0Cu at 932°F (500°C). [29]

Precipitation in the Al-Li-Cu system has been studied by several investigators and has been shown to follow the Al-Cu and Al-Li system precipitation sequences individually: [26,30]



With extended aging there is significant diffusion of lithium into θ' , which can lead to the formation of an equilibrium ternary phase T_B ($\text{Al}_{15}\text{Cu}_8\text{Li}_2$). [30,31] The phase T_B forms from θ' and retains the characteristic θ' plate morphology. In addition, with greater than approximately 2% lithium, the ternary equilibrium phase is T_1 . [30] T_1 has a hexagonal structure ($a = 4.97\text{\AA}$, $c = 9.34\text{\AA}$), and its basal plane (also

the habit plane) matches very closely the (111) matrix plane. (At the aging temperatures under consideration, T_1 forms platelets similar to δ' .)

Peak strength in a commercial Al-4.0Cu-1.0Li alloy (2020) has been attributed to the formation of θ'' and δ' . [26] The present alloy is expected to show significantly greater precipitation of δ' than 2020 and precipitation of T_B and T_1 in at least the overaged tempers.

Two ingots of Al-Li-Mg-Si type alloys were included. AA6063 and 6061-type alloys were cast with 3% lithium (#20, #21). These compositions are expected to show co-precipitation of Mg_2Si and δ' .

Three compositions represent an attempt at dispersion hardening in conjunction with δ' precipitation by adding manganese (#25) or manganese with iron (#23, #24) to an Al-3.0Li alloy. Dispersoids may have the effect of encouraging cross-slip, thereby decreasing the planar slip typical of Al-Al₃Li systems. A 15% elongation in an Al-3.0Li-1.55Mn-1.3Fe extrusion in Phase II prompted further investigation of this system, though that test could not be repeated due to lack of material.

Experimental Procedure

Fabrication of Sheet

The various alloys were cast as bookmold ingots by the procedure described under Phase I of this investigation. KBI 9.5% lithium hardener was used for casts #19-#21. A 20% lithium hardener (KBI) was used for casts #22-#26. Super-purity aluminum (99.99%) and commercial hardeners for the other alloying elements were used in all casts.

The ingots were homogenized for 8 hours at 850°F (454°C) plus 16 hours at 960°F (515°C) in a nitrogen atmosphere. Half of ingot #26 (#26B) received 850°F (454°C)/8 hours plus

900°F (482°C)/16 hours to determine if zirconium maintains a better dispersion with a low temperature homogenization, as is the case with 7XXX alloys.

The ingots were scalped until no porosity was evident. The material was then hot rolled at 750°F (400°C), 0.125" reduction/pass, to 0.125" sheet. Some of #22 was retained at this gauge, while the remainder of the material was cold rolled to 0.063" (1.60 mm). Severe edge cracking occurred in some alloys. These required an intermediate anneal of 932°F (500°C) for 1 hour with cold water quenching before cold rolling. Those alloys directly cold rolled are designated "AR"; those samples with no subscript received an intermediate anneal.

Hot Isostatic Pressing (HIP)

HIP treatment of ingot #10 was done by Kawecki-Berylco Inc. The ingot was heated to 900°F (482°C) for 2 hours at a pressure of 15,000 psi of argon.

Chemical Analysis and Hydrogen Content

Chemical analysis was done by atomic emission spectroscopy. Hydrogen analysis was performed for surface and volume hydrogen using an Ithac 02 Fast Hydrogen Determinator. This instrument uses the nitrogen carrier fusion method as described by Degreve. [32]

Heat Treatment

All material was solution heat treated at 975°F (524°C) for 30 minutes in argon, followed by a cold water quench. A limited number of Al-Li-Mn and Al-Li-Mn-Fe samples (designated "-h") were solution heat treated at 1050°F (565°C) for 1 hour and cold water quenched.

Aging Studies

Hardness-aging curves were established for 325°, 350°, 375°, and 400°F (163°, 177°, 191°, and 204°C respectively).

Hardness measurements were taken using the Rockwell B scale. Aging of material for tensile and hardness testing was done in circulating air furnaces.

Mechanical Testing

Tensile strength, yield strength, and percent elongation were obtained using a 0.250" x 1.00" gauge section for longitudinal and transverse samples with underaged, peak aged, and overaged samples.

Standard Kahn tear test blanks (2 1/4" x 1 7/16") were used to determine crack initiation and crack propagation energies. Kahn tear tests were performed on those alloys and aging conditions which exhibited the most tensile ductility.

Metallography

Metallographic sections of as-solutioned samples were examined as-polished. Overaged samples etched with Keller's reagent were used to determine subgrain size. An electrolytic etch was used to determine grain size.

Scanning electron microscopy (SEM) electron microprobe was used for examination of polished sections and fracture samples in the underaged, peak aged, and overaged tempers.

Transmission electron microscopy (TEM) was used to examine rolling plane sections of those samples of particular interest. TEM was carried out on an RCA EMU-3G electron microscope at 100 KV.

Results

Chemical Analysis

Chemical analysis results are given in Table 4-1.

Lithium levels were fairly well controlled, ranging from 3.0%-3.3% for the 3% aim. Magnesium, also prone to oxidation, showed a dramatic loss (approximately 50%) during melting and casting of the Al-Li-Mg-Si ingots. The resulting excess

silicon may lead to the precipitation of $\text{Li}_3\text{Al}_2\text{Si}_2$, a hardening precipitate found in Soviet investigation of an Al-Li-Si alloy. [33]

Alloys #23 and #24 in the Al-Li-Mn-Fe system had only a 25%-30% recovery of iron. In addition, bismuth was difficult to put in solution, with no detectable recovery (<0.005%), even with an addition of 0.01%.

The use of a new lithium hardner in casts 22-26 resulted in calcium levels dropping from 0.02% typical to 0.001%. Sodium levels were excellent (0.0001%) for all castings and well below the 0.004% level found to cause sub-boundary embrittlement. [18]

Hydrogen levels given in Table 4-2 are fairly low compared with other aluminum-lithium studies. [4,10] However, these levels are unacceptable in commercial aircraft alloys in that porosity is generally associated with hydrogen levels above 0.12 ml/100 g.

Microstructure

An electrolytic (Barker's) etch was used to determine degree of recrystallization of the sheet. Figures 4-1 through 4-10 show typical grain structures for the various samples. Recrystallization is evident in all samples without zirconium. Zirconium appears to be a more effective inhibitor of recrystallization, as evidenced by the lack of recrystallization seen in those samples.

Processing and heat treating variables have a strong influence on microstructure. The intermediate anneal before cold rolling caused #22 (Al-Li-Zr) to recrystallize totally with an elongated grain structure (Figure 4-2). #22--AR, cold rolled directly from hot line gauge, resulted in very little recrystallization. The high temperature (1050°F [565°C]/1 hour) solution heat treatment had little effect on the Mn+Fe alloys, but caused excessive grain growth in the manganese-only (#25) sheet (Figure 4-10).

As-polished metallographic sections were examined for all samples. A typical example from each system is shown in Figures 4-11 through 4-15. All samples show some evidence of porosity; however, the manganese-bearing alloys showed a minimal amount. Despite HIP treatment, #10 showed evidence of porosity, particularly in the as-HIPed ingot. Large insoluble phases were evident in the magnesium-silicon and manganese-containing alloys. The 1050°F (565°C)/1 hour solution heat treatment appears to result in somewhat fewer "fines" in the matrix than the 975°F (524°C)/30 minute solution heat treatment in the manganese-bearing alloys. The movement of manganese in aluminum is very sluggish, and significant change in the larger manganese-bearing particles should not be expected.

Subgrain structure as revealed using Keller's reagent is shown in Figures 4-16 through 4-19 for samples from each alloy system. Well overaged samples (e.g. 375°F (191°C)/480 hours) were used so as to decorate the subgrain boundaries.

Microstructural details for each alloy for each solution heat treatment and rolling condition are tabulated in Table 4-3.

Aging Study

Aging curves are presented in Figures 4-20 through 4-34. Of alloys #19-#26, the manganese-containing alloys show the slowest response to aging. The copper-bearing and magnesium-silicon-bearing alloys show the quickest response.

Aging curves for #22 (Al-Li-Zr), #24 (Al-Li-Mn-Fe), and #25 (Al-Li-Mn) were obtained for sheet cold rolled with and without an intermediate anneal. Aging response appears to be slightly quicker with no intermediate anneal, in some cases reaching a higher hardness in the no-anneal condition. This higher hardness is probably due to reduced recrystallization of the no-anneal material as reported under the section on metallography.

The high temperature (1050°F [565°C]) solution heat treatment given to the manganese-containing alloys had a minimal effect on the aging curves, though the Al-Li-Mn-Fe alloys (#23, #24) showed a somewhat higher peak hardness with the high temperature solution heat treatments.

Tensile Test Results

Tensile strength, yield strength, and elongation results are presented in Tables 4-4 through 4-13. Material was tested in the underaged, peak hardness, and overaged conditions for each alloy.

In general, elongation was very low for all but the Al-Li-Cu (#19) and Al-Li-Zr (#26) alloys. In addition, all but the Al-Li-Cu alloy were prone to fracture outside the gauge length. This may be due to large stress-concentrating insolubles found in the other alloys. However, as can be seen in the tensile, yield, and elongation tables, those fracturing outside the gauge length typically had the same elongation as those fracturing within the gauge marks. This indicates that the elongation is primarily uniform, with little contribution due to necking.

Fracture Characteristics

Binocular microscopic examination of the broken tensiles showed different fracture modes, such as 45° shear and intergranular failure, in the different alloys and tempers. In addition, various defects, such as porosity and inclusions, became apparent, which should be considered in interpreting the tensile data. In particular, a large number of samples showed centerline porosity, which resulted in a "delamination" through all or part of the width of the gauge section during testing. A summary of fracture characteristics and material defects in each sample is given in Table 4-14.

Of the aluminum-lithium binary alloys, #10 (2.87Li), #22 (3.26Li-0.06Zr), and #26 (3.23Li-0.08Zr), #10 showed the

lowest strength. Ductility was also poor, generally $\leq 6\%$ elongation. Despite HIP treatment for #10, porosity and inclusions apparently contributed to low strength and ductility, and this alloy/process combination was not included in further testing. SEM (Figures 4-35 through 4-37) showed the failure of #10 to be characteristically intergranular for all tempers. Al-Li-Zr (#22AR) also showed apparent intergranular failure (Figure 4-38). However, the "grains" correspond fairly closely to the observed subgrain size (using Keller's reagent), rather than to the grain size. This may indicate subgrain boundary rather than grain boundary failure.

Al-Li-Zr (#26A) showed fairly good ductility in the LT direction. Elongations were generally 6%-8% for all tempers. In contrast, the longitudinal elongation was very low. (#26B, with a low temperature homogenization, did not perform as well as #26A; therefore, emphasis was placed on #26A.)

The Al-Li-Cu alloy showed good elongations, especially in the underaged samples. Figure 4-39 shows the relationship between temper and elongation. Again, elongation is somewhat better in the LT direction, decreasing with increasing aging time.

The fracture of the Al-Li-Cu samples was predominantly transgranular 45° shear for both test directions. In general the fracture surface was bright for the underaged temper, progressing to a dull, or rougher (more typical of brittle fracture), surface for the overaged samples. These samples showed some necking at the fracture.

On a micro-scale the fractures showed dimples, which are normally associated with ductile fracture. The dimples became more prominent and well-defined with increased aging, as shown in Figures 4-40 through 4-42. Dimple size corresponds approximately to subgrain boundary size, indicating that fracture may be due to subgrain boundary failure. Subgrain boundaries generally show increased precipitation and wider precipitate-

free zones (PFZ) with increased aging. This may cause lower strength at the subgrain boundary, explaining the greater dimple definition with increased aging.

The Al-Li-Mg-Si alloys (#20, #21) showed strengths similar to the binary alloys. It appears that additions of magnesium and/or silicon decrease ductility somewhat. These alloys exhibit largely 45° shear in the underaged condition, progressing to flat, brittle failures in the overaged condition. In general little or no necking was seen. SEM of an overaged sample (Figure 4-43) showed some dimpling of the fracture surface.

The Al-Li-Mn (#25) and Al-Li-Mn-Fe (#23, #24) alloys showed poor ductility and no necking. SEM (Figure 4-44) examination showed largely intergranular failure. In addition, silicon-rich and manganese-rich insolubles were identified.

Kahn Tear Tests

Kahn tear test results are presented in Tables 4-15 through 4-20. The results in general were very poor, particularly in the T-L direction.

The Al-Li-Mg-Si and Al-Li-Mn-(Fe) alloys showed near zero crack propagation energy for the tempers tested. This was not unexpected considering the very low ductility seen in the tensile tests. The Al-Li-Zr alloys showed somewhat better crack propagation, but did not perform as well as the tensile test ductility might have indicated.

The Al-Li-Cu alloy, which showed good longitudinal and transverse elongation in tensile tests, also had poor tear test properties. Crack propagation energy was comparable only to that of the most brittle commercial alloys (see Discussion).

In all alloys the crack front tended to follow the grain direction. The crack front in the T-L samples propagated straight in the rolling direction, while in the L-T direction there was

a tendency in some samples to turn from perpendicular to parallel to the rolling direction.

Transmission Electron Microscopy (TEM)

Micrographs of Al-Li-Zr alloy #26A in the underaged condition are given in Figures 4-45 and 4-46. The spherical δ' precipitate is very small, but is resolvable at 46,000X. Note the grain boundary is pinning by small particles, presumably Al_3Zr .

A narrow grain boundary precipitate-free zone (PFZ) is visible in the underaged sample. The overaged samples show pronounced PFZ's (Figure 4-47), typically 7500Å for samples aged 400°F (204°C)/64 hours. It appears that the PFZ width is strongly orientation dependent in that some grain boundaries do not exhibit a perceptible PFZ. Figure 4-47B shows a triple point with two grain boundaries exhibiting a wide PFZ, while along the third grain boundary the PFZ diminishes to an imperceptible width.

Discontinuous precipitation (Figure 4-48) was observed in the Al-Li-Zr alloy, but was uncommon. Williams and Edington^[34] report that this phenomenon occurs at all grain boundaries with extended aging; however, it was observed infrequently in any of our material examined.

The Al-Li-Mn alloy aged 400°F (204°C)/64 hours (overaged) shows δ' of size similar to that of the Al-Li-Zr alloy in the same condition (Figure 4-49). In addition, there is a scattering of submicron size dense particles, presumably MnAl_6 . Grain boundaries (Figure 4-50) show a 7500Å PFZ similar to that seen in the Al-Li-Zr alloy. The high temperature solution heat treatment (1050°F [565°C]/1 hour) with the same aging practice (Figure 4-51) shows a PFZ around most of the dispersoid phases in what appears to be a greater degree than in the normal solution heat treated material.

No discontinuous precipitation was seen in the Al-Li-Mn alloy. It was thought that the high solution heat treatment temperature and water quench might provide a more uniform distribution of lithium near grain boundaries. Such a distribution of lithium (smaller PFZ) would be more likely to encourage discontinuous precipitation. [34]

Peak hardening of the Al-Cu-Li alloy appears to be related most closely to the aluminum-copper aging sequence. Figure 4-52 shows the alloy at peak hardening and is characterized by abundant coherency strains associated with θ'' growth. Precipitation of θ'' is responsible for the peak hardening of aluminum-copper binary alloys. [35] Diffraction patterns show string $L1_2$ superlattice reflections in this temper as well (Figure 4-53), indicating that δ' is present. Other diffracting conditions (Figures 4-54 and 4-55) show that there has also been some precipitation of the strain-free θ' plates in the peak aged material.

Further aging, to the overaged condition, promotes the formation of θ' -like plates, seen in Figures 4-56 through 4-60. There is extensive grain boundary or sub-boundary precipitation evident. As discussed earlier, extended aging (though as little as 100 minutes at 398°F--200°C) [31] in the Al-Li-Cu system can result in the diffusion of lithium into θ' and subsequent formation of T_B ($Al_{15}Cu_8Li_2$) with the same morphology as θ' . In addition, the plate-like ternary phase T_1 is expected with this composition. [30] Thus the precipitates referred to as θ' , or identified as θ' in these micrographs, are likely modified by diffusion of lithium or, in some cases, are actually a ternary phase as described below.

The displacement fringe contrast in the overaged Al-Li-Cu alloy in Figures 4-58 and 4-59 is identical to stacking fault contrast. However, the stacking fault energy of aluminum is high, and such faults are uncommon. The contrast is possibly due to an orientation of θ' nearly in the plane of the foil. [36] More likely, though, is that the T_1 phase is present, causing

such contrast due to the "stacking fault" arrangement of atoms at the matrix-precipitate interface. X-ray work has shown the interface to be a near perfect match of the precipitate hexagonal basal plane and the (111) FCC matrix plane.^[12] The atomic positions are then essentially in a stacking fault sequence at the precipitate-matrix interface, giving rise to the contrast seen in the overaged alloys. In this way the plate-like precipitates can be identified as T_1 .

Specimens overaged further (350°F [163°C]/480 hours), Figures 4-61 through 4-64, show similar features with larger and more pronounced θ' and/or T_1 . Some θ'' is retained as evidenced by coherency strains.

TEM of the gauge section of a tensile sample in an overaged condition (Figures 4-65 through 4-67) reveals heavy dislocations in some grains and intense planar slip. This is typical of the aluminum-lithium system and similar to the behavior reported by Sanders for 2020.^[4] Severe strain at grain boundaries occurs when the planar slip progresses to the degree seen in Figure 4-67.

Discussion and Conclusions of Phase III

Casting and Fabrication of Sheet

Bookmold ingots were cast and 0.063" sheet successfully fabricated. Significant problems occurred with hydrogen, the related problem of porosity, and inclusions.

Some samples were successfully cold rolled off the hot-line gauge, but in general the alloys needed an anneal before cold rolling to prevent edge cracking. The Al-Li-Mn and Al-Li-Mn-Fe alloys suffered particularly from edge cracking. Though an intermediate anneal (932°F [500°C]/1 hour) is sufficient to eliminate the problem, this treatment encourages recrystallization in the final gauge. Alternatives are a lower temperature anneal or a shorter anneal time at high temperature. Either may suffice and not cause recrystallization in the sheet.

The hydrogen and porosity problems are difficult to deal with. A delayed addition of the lithium until just prior to the casting may help decrease the hydrogen level. However, other research^[10,13,14] indicates that hydrogen content increases immediately upon addition of lithium.

Centerline porosity may be reduced by using a mold with insulated sides so as to produce directional solidification. This may act to drive porosity to the top rather than the center of the ingot.

Grain Structure

The present work indicates that as little as 0.06% zirconium is effective in inhibiting recrystallization, while up to 1.4% manganese proves ineffective. Fridlyander^[17] had similar results comparing 0.1% zirconium and 0.6% manganese in alloy 01420, as did Sanders^[4] in comparing 0.13% zirconium and 0.32% manganese in an Al-2.85Li binary alloy.

An intermediate anneal following hot rolling strongly encourages recrystallization. This effect may be reduced with shorter time at the annealing temperature.

Though there are few direct comparisons, the particular grain structure (recrystallized or not) does not appear to significantly affect the elongation or strength.

Precipitation and Aging Response

Aging curves show that the alloys containing copper or magnesium and silicon have the quickest response to aging, with the binary and magnesium-containing alloys showing a slower response.

There are indications that peak hardening in the Al-Cu-Li alloy is associated primarily with θ'' formation and less with θ' . TEM of sheet in the peak aged condition shows θ'' , while

δ' (typically 500Å in peak aged binary alloys) is not resolved. If this is the case, it would at least partially explain the greater tensile ductility seen in this alloy. If peak hardening can be reached with a minimal ripening of δ' , then the optimum strength/ductility combination might be realized.

Discontinuous precipitation of δ' , reported by Williams and Edington^[34], was observed in the Al-Li-Zr alloy. The reaction was uncommon and was not seen in the Al-Li-Mn and Al-Li-Cu alloys examined. The occurrence of the phenomenon is rare enough that it should present no problem in the system, such as associated grain boundary weakening found in some alloy systems.

Tensile and Yield Strengths and Elongation

Though showing moderate strength, the Al-Li-Mg-Si, Al-Li-Mn, and Al-Li-Mn-Fe systems showed no promise as far as acceptable ductility.

The Al-Li-Cu system exhibited strengths comparable to the Al-Li-Zr alloys in comparable tempers, but showed much improved ductility. The properties given in Table 4-6 can be compared with other alloys in the Al-Li-Cu system below.

Description	UTS (ksi)	YS (ksi)	Elong. (%)
VAD Nominal (Nom. Al-5.2Cu-1.2Li-0.6Mn) [37, 38]	68	58	6-8
2020-T6 Typical ^[5] --L	82	77.5	7.4
2020-T4 Typical ^[5] --L	50	34.2	16.5
Al-2.2Li-2.0Cu (#19)	L	63	50
(Present study--typical)	LT	56	43
			5-8
			6-12

Thus the properties of the sheet in the current study, of higher lithium content, show values somewhat lower than other

Al-Li-Cu alloys in terms of the tensile strength/ductility combination.

Tensile Fracture Characteristics

The more brittle alloys, in the Al-Li-Mg-Si and Al-Li-Mn-(Fe) systems, showed predominantly a flat, brittle fracture. The more ductile alloys, in the Al-Li-Cu and Al-Li systems, generally showed a 45° shear in the underaged samples, with an increasing degree of flat-face fracture with continued aging.

In general the alloys showed a dimpled fracture surface. The dimples were more pronounced with increased aging time. The dimple size may be related to subgrain size. TEM has shown formation of a PFZ on grain and subgrain boundaries. The formation of the PFZ and consequent weakening and failure at the subgrain boundaries may be the mechanism for failure. If this is the case, then an aging practice or thermomechanical treatment (TMT) to produce significant hardening without PFZ formation could lead to a better strength/ductility combination.

Fracture Toughness--Kahn Tear Tests

The Kahn tear tests showed poor toughness values in general for the alloys and tempers tested. The Al-Li-Mg-Si and Al-Li-Mn-(Fe) alloys showed near zero unit propagation energy. The Al-Li-Cu and Al-Li-Zr alloys showed somewhat better crack propagation energy values, but even the better tempers are comparable only to those commercial alloys with the poorest tear behavior.

For comparison Table 4-21 gives tensile and tear values for some commercial alloys including AA2020. Of those listed, all performed significantly better than the Al-Li-Cu alloy, except 2020-T6 and 2024-T86, which have significantly higher tensile and yield strengths.

The Al-Cu-Li alloy was the only alloy under study which indicated any significant resistance to crack propagation.

Possible methods to improve the toughness of this alloy include those methods discussed previously to increase ductility. These include an aging sequence, TMT, or alloying addition to encourage more rapid θ'' precipitation than δ' precipitation and treatments to discourage the formation of a PFZ at grain boundaries or subgrain boundaries.

TABLE 4-1
CHEMICAL ANALYSES OF ALLOYS PRODUCED IN PHASE III

Sample I.D.	Composition (%)											
	Li	Si	Fe	Cu	Mn	Mg	Zn	Zn	Na	Ca	Ba	Be
<u>Al-Li-(Zr)</u>												
10*	2.87	0.03	0.06	<0.01	<0.01	<0.01	<0.01	<0.01	<0.0001	--	--	--
22	3.26	--	--	--	--	--	0.06	0.06	<0.0001	0.001	<0.005	0.004
26*	3.23	0.02	0.02	<0.01	0.01	<0.01	0.02	0.08	<0.0001	--	<0.01	--
<u>Al-Li-Cu</u>												
19*	2.22	0.03	0.05	2.01	<0.01	<0.01	0.02	0.10	<0.0001	0.02	<0.01	0.001
<u>Al-Li-Mg-Si</u>												
20*	3.12	0.73	0.06	0.20	<0.01	0.62	0.02	0.08	<0.0001	0.02	<0.01	0.005
21	3.16	0.37	--	--	--	0.20	--	0.09	<0.0001	0.021	<0.005	0.002
<u>Al-Li-Mn-Fe</u>												
23	3.07	0.06	0.40	0.14	1.41	--	--	0.01	<0.0001	0.001	<0.005	<0.0005
24	3.27	0.05	0.32	0.15	1.28	--	--	<0.01	<0.0001	0.001	<0.005	<0.0005
<u>Al-Li-Mn</u>												
25	3.23	0.09	--	0.16	1.36	--	--	<0.01	<0.0001	0.001	<0.005	0.004

*Cr, Ni, and Ti = <0.01% each.

TABLE 4-2
HYDROGEN LEVELS IN PHASE III INGOTS

<i>Sample Number</i>	<i>Hydrogen Content (ml/100 gm)</i>	
	<i>Surface</i>	<i>Volume</i>
47850-19	0	0.236
-20	0	0.574
-21	0.006	0.748
-22	0	0.418
-23	0	0.386
-24	0	0.912
-25	0	0.652

TABLE 4-3

MICROSTRUCTURAL DETAILS OF PHASE III SHEET

<i>Alloy Description</i>	<i>Grain Structure Recrystallized?</i>	<i>Subgrain Dimensions (μm) Longitudinal Cross-Section</i>	<i>Insolubles</i>	<i>Porosity</i>
<u>Al-Li</u> #10 (HIP)	Yes, coarse equiaxed		No	Yes
<u>Al-Li-Zr</u> #22 #22--AR #26A--AR #26B	Yes, elongated Slight Slight 50% recrystallized	6 x 10 4 x 6 5 x 10 in unrecrystallized area	No No Yes Yes	Yes Yes Yes Yes
<u>Al-Li-Cu</u> #19--AR	Slight	2 x 5	Little	Yes
<u>Al-Li-Mg-Si</u> #20--AR #21	No No	2 x 4	Yes Yes	Yes Yes
<u>Al-Li-Mn-Fe</u> #23--AR #23-h #24--AR #24-h	Yes, fine equiaxed		{ (Mn,Fe)Al ₆	Little No No No
<u>Al-Li-Mn</u> #25 #25--AR #25-h	Yes, elongated Yes, elongated Yes, coarse elongated		{ MnAl ₆	{ Little

TABLE 4-4

LONGITUDINAL AND TRANSVERSE TENSILE PROPERTIES OF
Al-Li (#10-HIP) SHEET SHT 975°F/30 MINUTES

Age Temp. (°F)	Age Time (Hrs.)	Longitudinal			Transverse		
		UTS (ksi)	YS (ksi)	Elong. (%)	UTS (ksi)	YS (ksi)	Elong. (%)
325	168	47.7	37.5	2.0*			
		46.7	36.1	2.0*			
	480	51.1	39.7	3.0			
		50.7	39.6	*			
350	960	51.0	40.0	2.0*			
		52.1	39.9	4.0			
	32	46.0	33.7	2.0*	¹ 43.0	33.4	2.0*
		48.2	33.9	3.0*	45.8	34.6	3.0*
375	168	49.8	37.4	3.0*			
		50.0	37.6	5.0			
	817	49.6	37.6	6.0			
		48.8	37.8	5.0			
400	32	45.9	34.4	2.0*	¹ 43.9	35.0	3.0
		46.3	36.4	2.0*	46.7	35.7	3.0*
	64	49.2	36.1	2.0*			
		47.1	36.4	3.0			
400	240	42.2	35.4	1.0	¹ 46.9	35.6	5.0
		48.7	35.7	6.0	45.1	35.2	5.0
	2	45.3	30.1	8.0	¹ 41.2	30.3	5.0
		44.3	30.2	6.0*	42.2	28.9	7.0
400	32	47.3	35.1	7.0*	¹ 46.2	34.0	4.0*
		48.9	35.4	4.0*	47.1	35.9	4.0
	64	44.3	37.3	3.0*	¹ 47.5	35.2	6.0
		44.1	36.6	1.0*	47.3	34.9	5.0

*Fracture outside of gauge length.

¹AR--Those cold rolled directly from hot line gauge; no intermediate anneal.

TABLE 4-5

LONGITUDINAL AND TRANSVERSE TENSILE PROPERTIES OF
Al-Li-Zr (#22) SHEET SHT 975°F/30 MINUTES

Age Temp. (°F)	Age Time (Hrs.)	Longitudinal			Transverse		
		UTS (ksi)	YS (ksi)	Elong. (%)	UTS (ksi)	YS (ksi)	Elong. (%)
325	168	¹ 58.5	46.4	3.0*			
		57.1	45.4	2.0*			
	240	50.9	43.0	*			
		53.9	43.2	5.0			
	480	59.3	46.4	4.0*			
		59.7	45.4	5.0*			
350	16	44.2	38.6	1.0*	45.3	34.8	5.0
					44.3	34.2	2.0*
	64	¹ 56.8	44.8	2.0*	47.1	39.2	1.0*
		57.6	44.4	3.0*	47.9	38.5	3.0
		56.7	48.7	1.0*			
		51.0	43.8	2.0*			
	240	¹ 58.8	44.0	7.0*			
		55.2	44.0	3.0*			
	270	50.4	41.7	3.0			
		47.7	40.9	2.0			
375	2	41.9	32.4	6.0	41.1	30.1	4.0*
					43.7	30.7	5.0*
	16	¹ 57.3	44.1	3.0*			
		58.0	46.1	4.0			
	64	53.8	40.3	6.0	46.9	39.5	2.0*
		55.4	42.1	3.0	47.9	39.8	2.0*
	120	¹ 55.5	42.5	6.0			
		54.7	41.5	6.0			
168	53.6	40.2	3.0*				
	49.2	38.3	2.0*				
400	1	¹ 46.3	35.4	5.0			
		49.2	38.2	5.0			
		40.9	33.7	2.0*			
		41.1	34.1	2.0*			
	8	¹ 54.9	42.7	2.0*	46.1	36.5	3.0
		58.2	44.5	4.0*	46.6	35.9	3.0
		47.6	39.0	4.0			
		45.6	39.9	2.0*			

*Fracture outside of gauge length.

¹AR--Those cold rolled directly from hot line gauge; no intermediate anneal.

TABLE 4-6

LONGITUDINAL AND TRANSVERSE TENSILE PROPERTIES OF
Al-Li-Zr (#26A--AR¹) SHEET SHT 975°F/30 MINUTES

Age Temp. (°F)	Age Time (Hrs.)	Longitudinal			Transverse		
		UTS (ksi)	YS (ksi)	Elong. (%)	UTS (ksi)	YS (ksi)	Elong. (%)
325	24				53.4	45.3	4.0*
					55.4	45.1	6.0
	120	61.6 57.6	49.6 50.4	4.0 2.0*	59.4 59.6	48.3 48.2	6.0 4.0*
350	4	51.1 52.0	42.6 41.8	2.0* 3.0*	54.5 54.6	49.1 42.9	7.0 6.0*
		58.4 60.4	49.1 48.1	1.0* 3.0*	60.8 58.8	48.2 47.2	6.0* 4.0*
	270	58.0 57.0	45.4 44.1	4.0* 4.0*	55.4 55.4	-- 43.8	8.0 5.0
375	3				55.6 57.2	42.9 42.9	6.0* 6.0*
	24	56.7 60.1	48.1 47.2	2.0* 3.0*	58.9 59.4	45.7 46.7	7.0 8.0
400	50 min.				56.2 52.7	42.4 42.1	6.0* 4.0*
	2	55.9 54.3	44.9 45.4	2.0* 2.0*	58.6 58.5	45.0 44.8	12.0 8.0

*Fracture outside of gauge length.

¹AR--Those cold rolled directly from hot line gauge; no intermediate anneal.

TABLE 4-7

LONGITUDINAL AND TRANSVERSE TENSILE PROPERTIES OF
Al-Li-Zr (#26B) SHEET SHT 975°F/30 MINUTES

Age Temp. (°F)	Age Time (Hrs.)	Longitudinal			Transverse		
		UTS (ksi)	YS (ksi)	Elong. (%)	UTS (ksi)	YS (ksi)	Elong. (%)
325	24				55.1	44.5	5.0*
					55.2	43.8	7.0
	120	55.2	48.5	1.0*	59.4	46.2	6.0
		58.4	49.2	1.0*	53.6	45.7	2.0*
480	61.0	48.7	5.0*				
600	59.6	49.9	2.0*				
		61.8	49.0	3.0*			
350	8	50.4	45.2	1.0*	54.3	42.1	6.0*
		50.7	43.7	1.0*	53.5	42.6	5.0*
	45	52.9	48.8	1.0*	58.9	46.8	6.0
56.1		49.6	1.0*	58.9	46.0	5.0*	
300	60.7	46.8	4.0*	52.1	--	4.0*	
	58.7	45.6	6.0	53.5	42.2	5.0*	
375	2	45.4	41.7	1.0	52.8	42.2	4.0*
		49.5	40.7	2.0*	54.3	41.9	6.0*
32	61.2	46.7	4.0	57.9	46.3	5.0*	
	56.5	48.1	1.0*	56.8	45.6	6.0	
400	1	45.7	42.3	1.0*			
		50.3	41.5	2.0*			
8	53.5	44.6	4.0	57.2	44.9	5.0*	
	60.9	46.1	5.0	57.2	45.2	5.0*	

*Fracture outside of gauge length.

TABLE 4-8

LONGITUDINAL AND TRANSVERSE TENSILE PROPERTIES OF
Al-Li-Cu (#19--AR¹) SHEET SHT 975°F/30 MINUTES

Age Temp. (°F)	Age Time (Hrs.)	Longitudinal			Transverse		
		UTS (ksi)	VS (ksi)	Elong. (%)	UTS (ksi)	VS (ksi)	Elong. (%)
325	16	59.6	50.0	12.0*	58.0	43.6	11.0
		62.3	50.7	5.0	57.2	44.2	6.0
	64	66.5	55.7	5.0			
66.9		55.7	5.0				
168	63.1	47.8	8.0				
	64.4	52.9	8.0				
350	3	59.0	45.7	9.0	55.4	41.8	12.0
		57.2	44.1	5.0*	55.0	40.7	12.0
	32	63.1	50.6	6.0	57.7	43.8	6.0*
63.4		52.7	4.0*	58.2	45.9	11.0	
90	60.1	48.8	5.0	55.0	44.2	8.0	
	60.1	48.0	6.0	55.2	43.8	8.0	
375	2	58.8	44.7	6.0*	55.7	42.5	12.0
		56.0	43.7	8.0	54.5	41.6	11.0
	16	59.9	49.7	8.0	54.1	42.8	10.0
60.3		49.7	8.0	53.5	41.7	8.0	
45	54.5	43.3	8.0	49.4	38.6	8.0	
	53.6	39.0	8.0	50.3	39.4	8.0	
Natural age	6 months				40.3	23.8	21.0
					39.5	23.7	21.0

*Fracture outside of gauge length.

¹AR--Those cold rolled directly from hot line gauge; no intermediate anneal.

TABLE 4-9

LONGITUDINAL AND TRANSVERSE TENSILE PROPERTIES OF
Al-Li-Mg-Si (#20) SHEET SHT 975°F/30 MINUTES

Age Temp. (°F)	Age Time (Hrs.)	Longitudinal			Transverse		
		UTS (ksi)	YS (ksi)	Elong. (%)	UTS (ksi)	YS (ksi)	Elong. (%)
325	120	62.6	53.5	2.0*	¹ 60.7	51.9	2.0
		58.2	51.5	1.0*			
325	480	54.9	49.2	*			
		57.6	50.7	2.0*			
350	3	52.6	45.1	2.0*			
		59.4	45.6	3.0			
350	16	60.4	50.6	2.0*	¹ 54.0	49.0	2.0
		57.3	50.9	2.0			
375	2	60.4	47.4	3.0*			
		55.3	48.8	1.0*			
	8	63.2	51.9	2.0*			
375	45				¹ 52.8	45.7	2.0*
400	40 min.				¹ 54.6	45.2	4.0
	2	62.8	49.2	4.0	¹ 54.7	48.1	2.0
54.0		--	--	54.9			
400	16	54.9	42.4	4.0			
		55.1	40.0	1.0*			

*Fracture outside of gauge length.

¹AR--Those cold rolled directly from hot line gauge; no intermediate anneal.

TABLE 4-10

LONGITUDINAL AND TRANSVERSE TENSILE PROPERTIES OF
Al-Li-Mg-Si (#21--AR¹) SHEET SHT 975°F/30 MINUTES

Age Temp. (°F)	Age Time (Hrs.)	Longitudinal			Transverse		
		UTS (ksi)	YS (ksi)	Elong. (%)	UTS (ksi)	YS (ksi)	Elong. (%)
325	8	46.6	45.9	2.0	57.2	45.5	6.0
		51.7	46.4	1.0*	57.4	45.7	6.0
	64	56.9	52.3	3.0			
		57.0	52.1	1.0*			
	300	60.8	49.2	5.0	58.1	48.8	4.0
		58.9	49.8	4.0	58.0	48.5	3.0*
350	1.5	50.3	44.7	1.0*	51.0	41.8	6.0
		51.8	44.3	2.0*	54.1	43.1	6.0
	16	58.5	50.5	2.0*	56.8	47.7	4.0
		47.2	--	1.0*	57.0	48.4	2.0*
	200				55.4	44.7	2.0*
					52.1	45.5	2.0
375	1.5	46.8	--	1.0*	49.4	44.1	3.0
		56.0	--	2.0	56.7	44.8	6.0
	8	54.1	49.8	2.0	57.8	48.3	4.0*
		56.3	49.7	2.0	57.7	47.6	4.0
400	30 min.	53.6	46.3	2.0*	54.9	43.6	6.0
		51.4	46.1	2.0	54.0	44.3	5.0
	1	55.2	47.3	2.0	48.7	45.1	3.0
		57.2	47.5	4.0	54.3	45.4	4.0
	16	53.8	45.0	2.0*			
		53.5	45.6	2.0			

*Fracture outside of gauge length.

¹AR--Those cold rolled directly from hot line gauge; no intermediate anneal.

TABLE 4-11

LONGITUDINAL AND TRANSVERSE TENSILE PROPERTIES OF
Al-Li-Mn-Fe (#23) SHEET SHT 975°F/30 MINUTES

Age Temp. (°F)	Age Time (Hrs.)	Longitudinal			Transverse		
		UTS (ksi)	YS (ksi)	Elong. (%)	UTS (ksi)	YS (ksi)	Elong. (%)
325	240	56.8	43.4	3.0*			
		56.8	44.1	2.0*			
350	16	50.3	41.3	2.0*			
		53.8	38.8	2.0*			
	90	59.2	41.8	4.0*	¹ 45.7	42.2	1.0*
		56.6	42.5	3.0*	47.9	42.9	1.0
375	4	51.5	37.5	2.0*			
		52.9	38.7	3.0*			
	375	55.5	41.8	2.0*	¹ 48.5	42.9	1.0
		51.4	38.7	2.0*	51.0	42.4	1.0*
400	8	57.1	40.4	4.0*			
		49.2	35.6	4.0*			
	45				¹ 49.8	40.0	2.0*
					48.8	39.6	2.0*

*Fracture outside of gauge length.

¹AR--Those cold rolled directly from hot line gauge; no intermediate anneal.

TABLE 4-12

LONGITUDINAL AND TRANSVERSE TENSILE PROPERTIES OF
Al-Li-Mn-Fe (#24) SHEET SHT 975°F/30 MINUTES

Age Temp. (°F)	Age Time (Hrs.)	Longitudinal			Transverse		
		UTS (ksi)	YS (ksi)	Elong. (%)	UTS (ksi)	YS (ksi)	Elong. (%)
325	480	61.4	47.2	3.0*			
		62.1	46.5	3.0*			
350	90	¹ 47.2	--	1.0*			
		57.0	44.3	2.0*			
375	4	¹ 55.3	36.7	4.0*			
		54.9	38.9	4.0*			
	64	¹ 56.8	43.3	2.0*			
		55.9	43.6	2.0*			

*Fracture outside of gauge length.

¹AR--Those cold rolled directly from hot line gauge; no intermediate anneal.

TABLE 4-13

LONGITUDINAL AND TRANSVERSE TENSILE PROPERTIES OF
Al-Li-Mn (#25) SHEET SHT 975°F/30 MINUTES

Age Temp. (°F)	Age Time (Hrs.)	Longitudinal			Transverse		
		UTS (ksi)	YS (ksi)	Elong. (%)	UTS (ksi)	YS (ksi)	Elong. (%)
325	480	¹ 61.0	45.6	*			
		60.5	45.9	3.0			
		53.7	46.3	*			
		57.0	45.8	3.0			
350	32				46.8	38.1	2.0
					46.9	38.6	2.0*
350	120				52.4	41.1	2.0*
					52.8	41.4	2.0*
375	4	¹ 58.1	38.1	5.0*			
		56.7	38.8	4.0*			
	8				44.6	38.2	1.0
					49.1	37.2	2.0*
	64	57.6	42.3	2.0*			
		58.9	43.2	4.0			
375	90				51.2	42.3	2.0*
					50.7	41.6	1.0*
375	480	54.5	51.2	*			
		55.0	41.6	3.0			
400	1.5				47.3	33.6	4.0
					50.8	34.6	6.0
	8	¹ 61.1	42.7	4.0*			
		59.8	41.4	3.0*			
	16	¹ 35.3	--	1.0	52.7	38.4	4.0
53.1		40.7	2.0*	54.6	39.1	4.0	
49.9		40.4	4.0				
	52.4	40.7	4.0				

*Fracture outside of gauge length.

¹AR--Those cold rolled directly from hot line gauge; no intermediate anneal.

TABLE 4-14

TENSILE TEST FRACTURE SURFACE CHARACTERISTICS OF PHASE III SHEET

I.D.	Inter- fracture	Flat/ 45° Shear	Necking	Porosity	Dimples	General Observations
#10	Yes	Flat	None	Centerline	Yes	About half showed inclusions on fracture surface.
#22	Yes	Mixed	Very little	None	Yes	Regardless of anneal, samples showed some mostly shear, some flat, and most mixed type of fracture.
#20A Long.	No	Shear	Very little	Very little	Yes	Up to 75% shear in underaged condition, increasingly flat-faced with aging.
Underaged	No	Flat	None	Much centerline	Yes	Underaged--bright surface; Overaged--dull surface.
Trans.	Partly	Flat	None		Yes	
#19	No	Shear	Yes	Much centerline	Yes	Increased (up to 30%) flat-faced fracture with overaging. Dimples more pronounced with increased aging. Porosity in several cases caused a "delamination" of layer in sample.
#20--Underaged	No	Shear	Very little	Very little	Yes	Dramatic change from shear to flat fracture with increased aging.
Overaged	Partly	Flat/ shear lips	Very little			
#21--Underaged	No	Shear	Little	Some centerline	Yes	Similar to #20.
Overaged	Yes	Flat	None	Some centerline	Yes	
#23	Yes	Flat	None	None	Yes	Brighter facets in underaged.
#24	Yes	Flat	None	None	Yes	
#25	Yes	Flat	None	Little	Yes	

TABLE 4-15

KAHN TEAR TEST RESULTS*

#10--A1-2.8Li

Aging Condition	L-T				T-L			
	Tear/Yield Strength	Unit Init. Energy (in-lb/in ²)	Unit Prop. Energy ₂ (in-lb/in ²)	Unit Total Energy	Tear/Yield Strength	Unit Init. Energy (in-lb/in ²)	Unit Prop. Energy (in-lb/in ²)	Unit Total Energy
400°F/2 hours	1.55	225	103	328	1.52	186	72	258
400°F/32 hours	1.20	136	14	150	1.10	112	8	119

*Triplicate specimens.

TABLE 4-16

KAHN TEAR TEST RESULTS*
#22--Al-3.3Li-0.08Zr

Aging Condition	L-T				T-L			
	Tear/Yield Strength	Unit Init. Energy ² (in-lb/in ²)	Unit Prop. Energy ² (in-lb/in ²)	Unit Total Energy	Tear/Yield Strength	Unit Init. Energy ² (in-lb/in ²)	Unit Prop. Energy ² (in-lb/in ²)	Unit Total Energy
350°F/240 hours (AR)					0.65	74	0	74 ¹
375°F/120 hours (AR)	0.97	124	58	182	0.76	74	0	74
350°F/240 hours	1.00	141	15	156	0.86	106	6	113 ²
375°F/2 hours	1.55	238	140	140 ²	1.53	206	111	317
0.125" sheet (no cold roll)								
350°F/240 hours	0.98	184	0	184 ²	0.74	95	0	95
375°F/2 hours	1.84	433	241	674	1.73	275	19	294

*Duplicate specimens.

¹Single specimen--duplicate specimen fracture angle > 30°.

²All specimens fracture angle > 30°.

TABLE 4-17

KAHN TEAR TEST RESULTS*
 #26A--Al-3.2Li-0.08Zr

Aging Condition	L-T				T-L			
	Tear/Yield Strength	Unit Init. Energy (in-lb/in ²)	Unit Prop. Energy (in-lb/in ²)	Unit Total Energy	Tear/Yield Strength	Unit Init. Energy (in-lb/in ²)	Unit Prop. Energy (in-lb/in ²)	Unit Total Energy
350°F/4 hours	1.28	265	295	560 ¹	1.08	189	78	266
350°F/32 hours	0.99	171	34	206	0.93	130	0	130
350°F/270 hours	0.89	105	11	116	0.73	74	0	74
400°F/2 hours	1.20	232	194	426 ¹	1.10	225	9	233

*Triplicate specimens.

¹All specimens fracture angle > 30°.

TABLE 4-18

KAHN TEAR TEST RESULTS*
 #19--Al-2.2Li-2.0Cu-0.10Zr

Aging Condition	L-T				T-L			
	Tear/Yield Strength	Unit Init. Energy ² (in-lb/in ²)	Unit Prop. Energy (in-lb/in ²)	Unit Total Energy	Tear/Yield Strength	Unit Init. Energy ² (in-lb/in ²)	Unit Prop. Energy (in-lb/in ²)	Unit Total Energy
325°F/16 hours	1.16	265	86	351	1.34	272	80	351
350°F/3 hours	1.39	309	236	544	1.48	349	138	487
375°F/2 hours	1.40	347	194	541 ¹	1.47	361	80	442
375°F/16 hours	1.12	244	41	286	1.33	273	43	316

*Duplicate specimens.

¹Single test result, duplicate specimen fracture angle >30°.

TABLE 4-19

KAHN TEAR TEST RESULTS*
 #21--Al-3.2Li-0.37Si-0.20Mg

Aging Condition	L-T				T-L			
	Tear/Yield Strength	Unit Init. Energy ₀ (in-lb/in ²)	Unit Prop. Energy ₀ (in-lb/in ²)	Unit Total Energy	Tear/Yield Strength	Unit Init. Energy (in-lb/in ²)	Unit Prop. Energy ₀ (in-lb/in ²)	Unit Total Energy
325°F/8 hours AR ¹	1.04	164	25	189 ²	1.04	161	19	180
325°F/300 hours AR	0.87	131	7	138	0.73	85	1	86
325°F/8 hours	0.99	139	33	172	1.07	174	16	190
325°F/300 hours	0.79	101	9	111	0.70	83	0	83

*Triplicate specimens.

¹AR--Those cold rolled directly from hot line gauge; no intermediate anneal.

²Single specimen--duplicate specimen fracture angle >30°.

TABLE 4-20

KAHN TEAR TEST RESULTS*

#25--A1-3.2Li-1.26Mn

Aging Condition	L-T				T-L			
	Tear/Yield Strength	Unit Init. Energy (in-lb/in ²)	Unit Prop. Energy (in-lb/in)	Unit Total Energy	Tear/Yield Strength	Unit Init. Energy (in-lb/in ²)	Unit Prop. Energy (in-lb/in)	Unit Total Energy
375°F/4 hours	1.26	194	70	264	1.18	142	42	184
375°F/64 hours	0.91	106	6	112	0.78	74	6	79

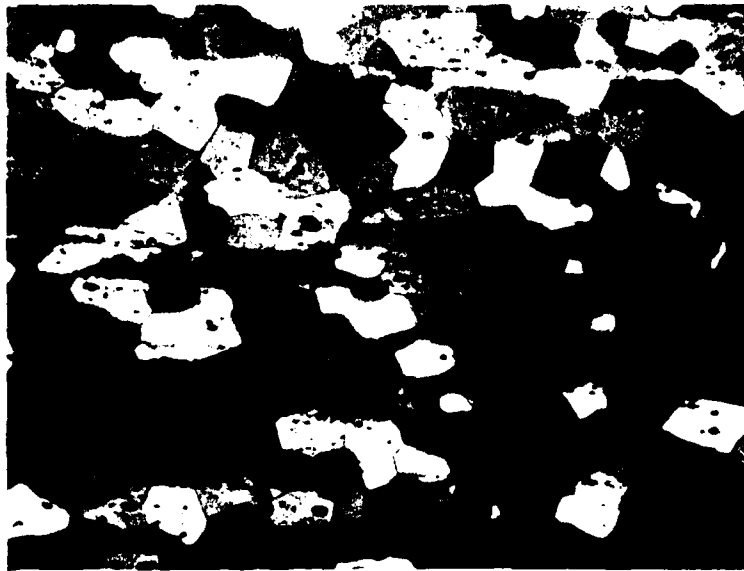
*Triplicate specimens.

TABLE 4-21

TYPICAL TENSILE AND TEAR PROPERTIES
OF SOME COMMERCIAL ALLOYS

Alloy I.D.	Longitudinal				Transverse			
	TS (psi)	YS (psi)	Elong. (%)	UPE (in-lb/in ²)	TS (psi)	YS (psi)	Elong. (%)	UPE (in-lb/in ²)
2020-T4	50,000	34,200	16.5	1110	49,400	31,600	16.5	1060
-T6	82,000	77,500	7.4	30	81,800	75,400	7.0	15
2024-T3	69,600	52,400	19.5	710	67,400	46,400	19.7	600
-T6	67,200	53,200	9.5	275	66,300	51,800	8.8	245
-T86	77,100	72,400	6.4	130	76,100	71,200	6.1	115
7075-T6	82,300	74,900	11.2	290	82,300	72,500	10.8	220
-T73	71,600	60,300	10.6	510	72,900	61,000	10.3	400

From Reference 5



100μ

FIGURE 4-1. LONGITUDINAL CROSS-SECTION OF Al-Li (#10)
Intermediate anneal before cold rolling.
As-solution heat treated.
Electrolytic etch, 100X.



A. Intermediate anneal before cold rolling.
As solution heat treated.



B. No anneal.
As solution heat treated.

100μ

FIGURE 4-2. LONGITUDINAL CROSS-SECTIONS OF Al-Li-Zr (#22)
Electrolytic etch, 100X.

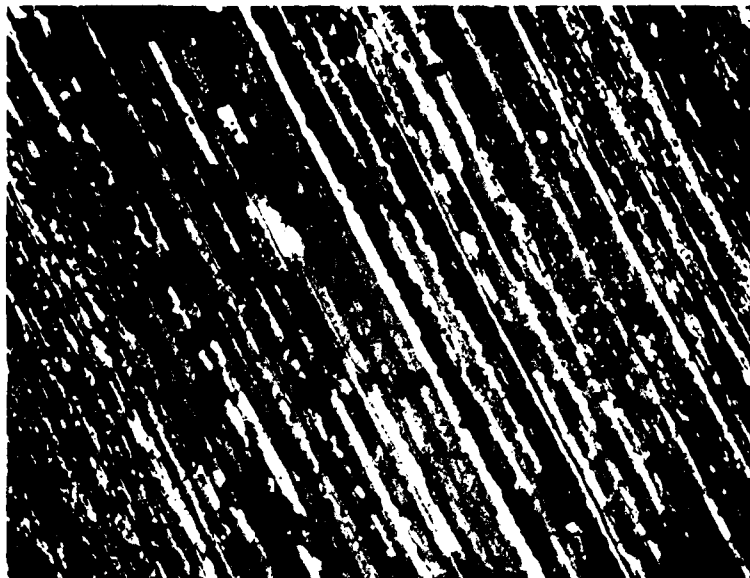


FIGURE 4-3. LONGITUDINAL CROSS-SECTION OF Al-Li-Zr
(#26A--AR)

No anneal, as solution heat treated.
Electrolytic etch, 100X.

100 μ

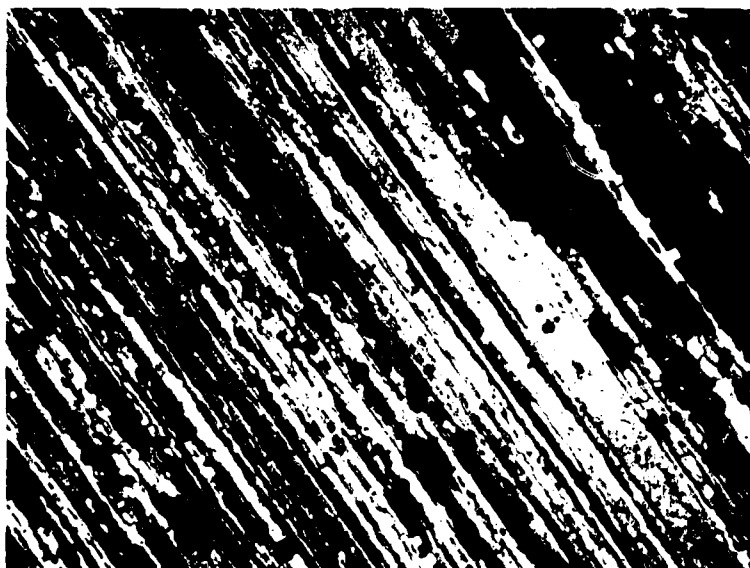


FIGURE 4-4. LONGITUDINAL CROSS-SECTION OF Al-Li-Zr
(#26B)

Intermediate anneal before cold rolling.
As solution heat treated.
Electrolytic etch, 100X.

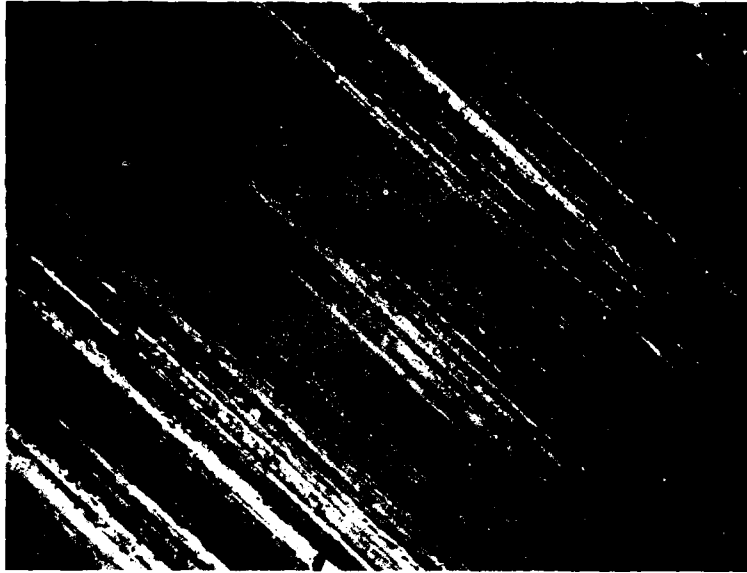


FIGURE 4-5. LONGITUDINAL CROSS-SECTION OF Al-Li-Cu
(#19--AR)

No anneal, as solution heat treated.

Electrolytic etch, 100X.

100 μ

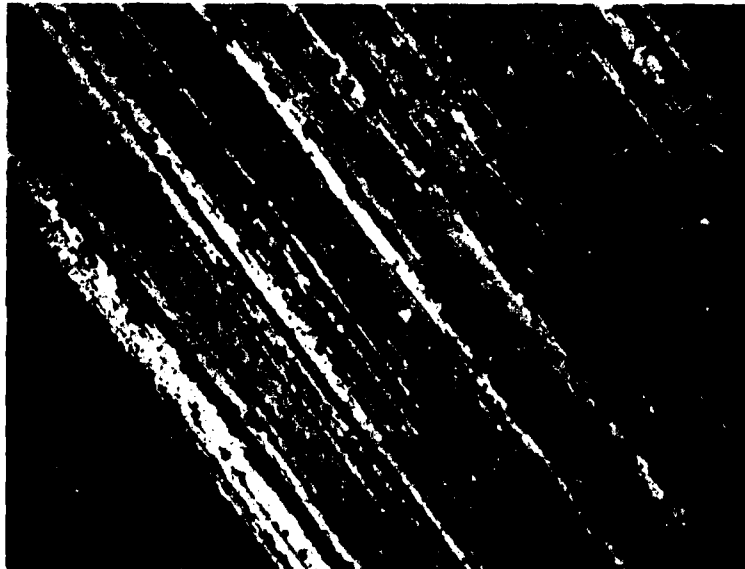


FIGURE 4-6. LONGITUDINAL CROSS-SECTION OF Al-Li-Mg-Si
(#20--AR)

No anneal, as solution heat treated.

Electrolytic etch, 100X.

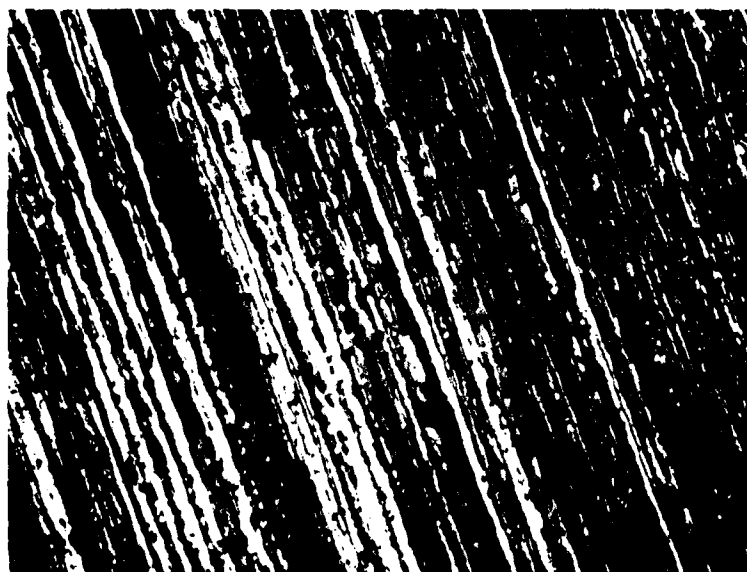
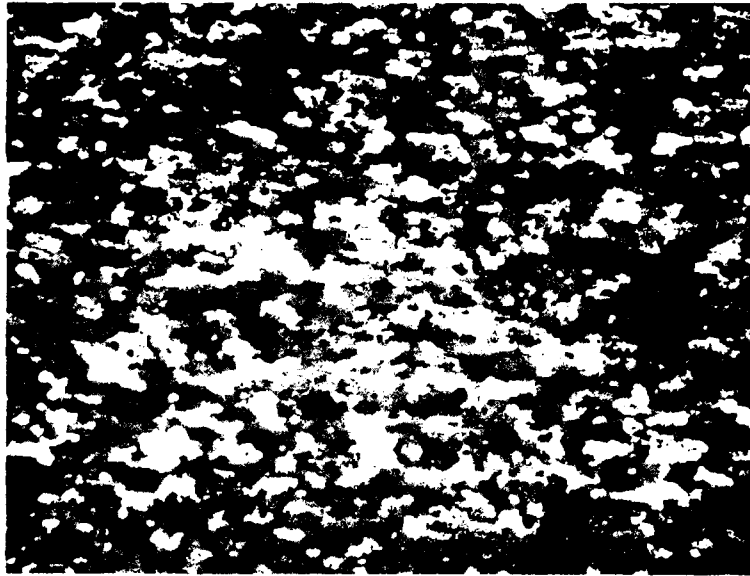
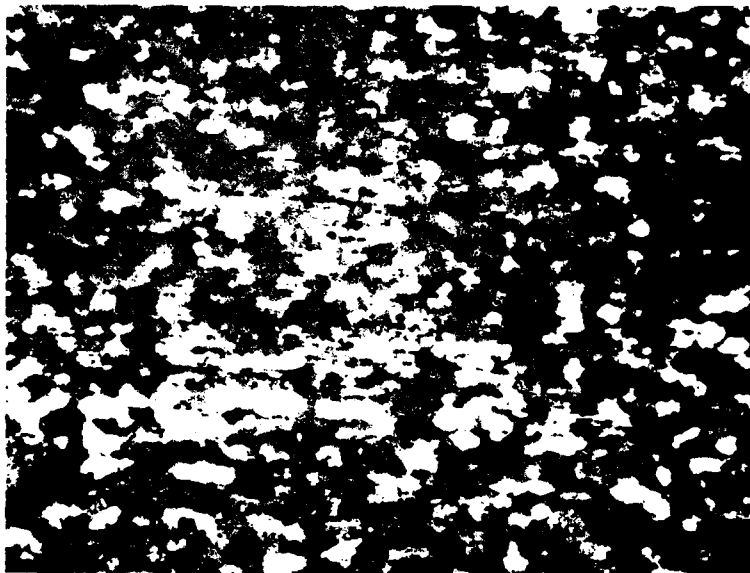


FIGURE 4-7. LONGITUDINAL CROSS-SECTION OF Al-Li-Mg-Si
(#21--AR)
No anneal, as solution heat treated.
Electrolytic etch, 100X.



A. No anneal.
Solution heat treatment 975°F (524°C)/30 minutes.

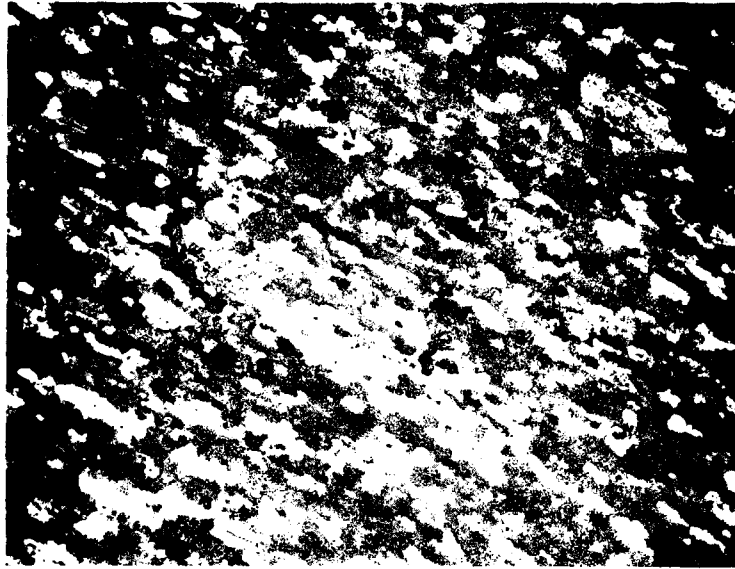


100 μ

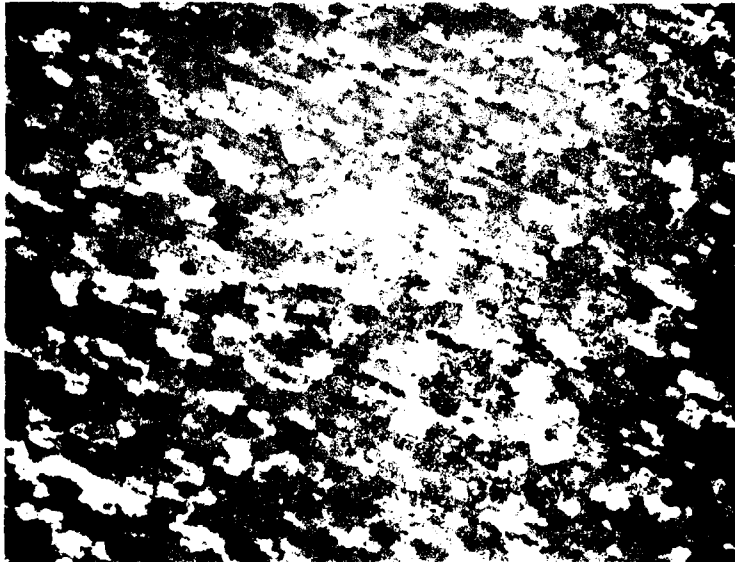
B. #23-h.
Solution heat treatment 1050°F (565°C)/1 hour.

FIGURE 4-3. LONGITUDINAL CROSS-SECTIONS OF Al-Li-Mn-Fe
(#23)

Electrolytic etch, 100X.



A. #24--AR, no anneal.
Solution heat treatment 975°F (524°C)/30 minutes.



B. #24-h.
Solution heat treatment 1050°F (566°C)/1 hour.

100μ

FIGURE 4-9. LONGITUDINAL CROSS-SECTIONS OF Al-Li-Mn-Fe
(#24)
Electrolytic etch, 100X.



C. #25-h.
Solution heat treatment 1050°F (565°C) /
1 hour.

100μ

FIGURE 4-10

LONGITUDINAL CROSS-SECTIONS OF Al-Li-Mn (#25)
Electrolytic etch, 100X.



A. Intermediate anneal before cold rolling.
Solution heat treatment 975°F (524°C) /
30 minutes.



B. #25--AR.
Solution heat treatment 975°F (524°C) /
30 minutes.



FIGURE 4-11. LONGITUDINAL CROSS-SECTION OF Al-Li-Zr (#22--AR)
As solution heat treated.
As-polished, 500X.

20 μ



FIGURE 4-12. LONGITUDINAL CROSS-SECTION OF Al-Li-Cu (#19--AR)
As solution heat treated.
As-polished, 500X.

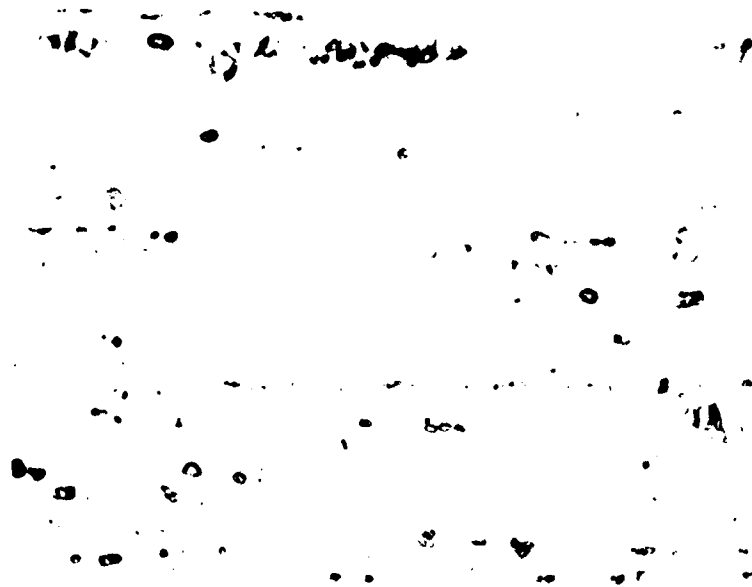


FIGURE 4-13. LONGITUDINAL CROSS-SECTION OF Al-Li-Mg-Si (#20)
As solution heat treated.
As-polished, 500X.

20 μ



FIGURE 4-14. LONGITUDINAL CROSS-SECTION OF Al-Li-Mn-Fe (#24--AR)
As solution heat treated.
As-polished, 500X.



FIGURE 4-15. LONGITUDINAL CROSS-SECTION OF Al-Li-Mn (#25--AR)
As solution heat treated.
As-polished, 500X.

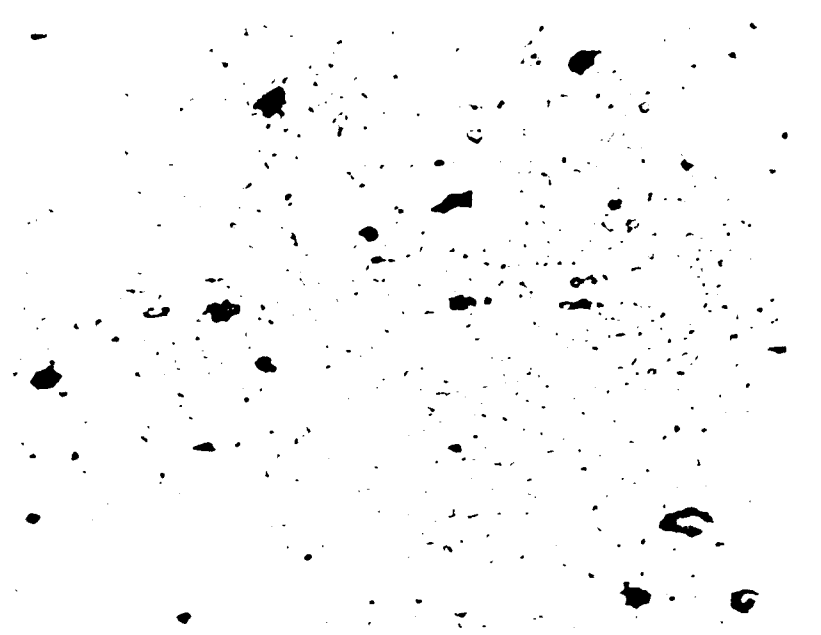
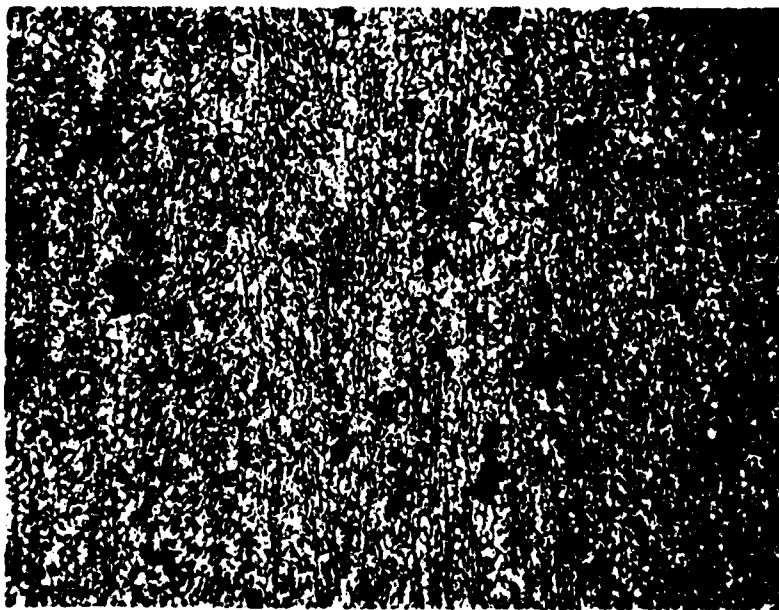


FIGURE 4-16. TRANSVERSE CROSS-SECTION OF Al-Li-Zr (#26A--AR)
975°F (524°C)/30 minutes + 375°F (177°C)/480 hours.
Keller's reagent used to reveal subgrain structure.
500X.



20 μ

FIGURE 4-17. LONGITUDINAL CROSS-SECTION OF Al-Li-Cu (#19--AR)
975°F (524°C)/30 minutes + 375°F (177°C)/480 hours.
Keller's reagent used to reveal subgrain structure.
500X.

FIGURE 4-18. LONGITUDINAL CROSS-SECTION OF Al-Li-Mg-Si (#20)
975°F (524°C)/30 minutes + 375°F (177°C)/480 hours.
Keller's reagent used to reveal subgrain structure.
500X.

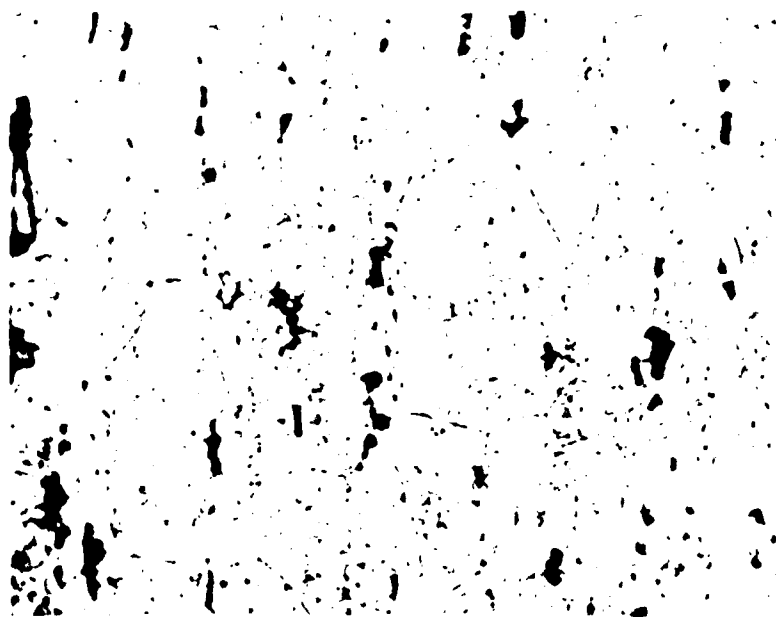


FIGURE 4-19. LONGITUDINAL CROSS-SECTION OF Al-Li-Mn-Fe (#24-h)
1050°F (565°C)/1 hour + 375°F (177°C)/480 hours.
Keller's reagent used to reveal subgrain structure.
500X.

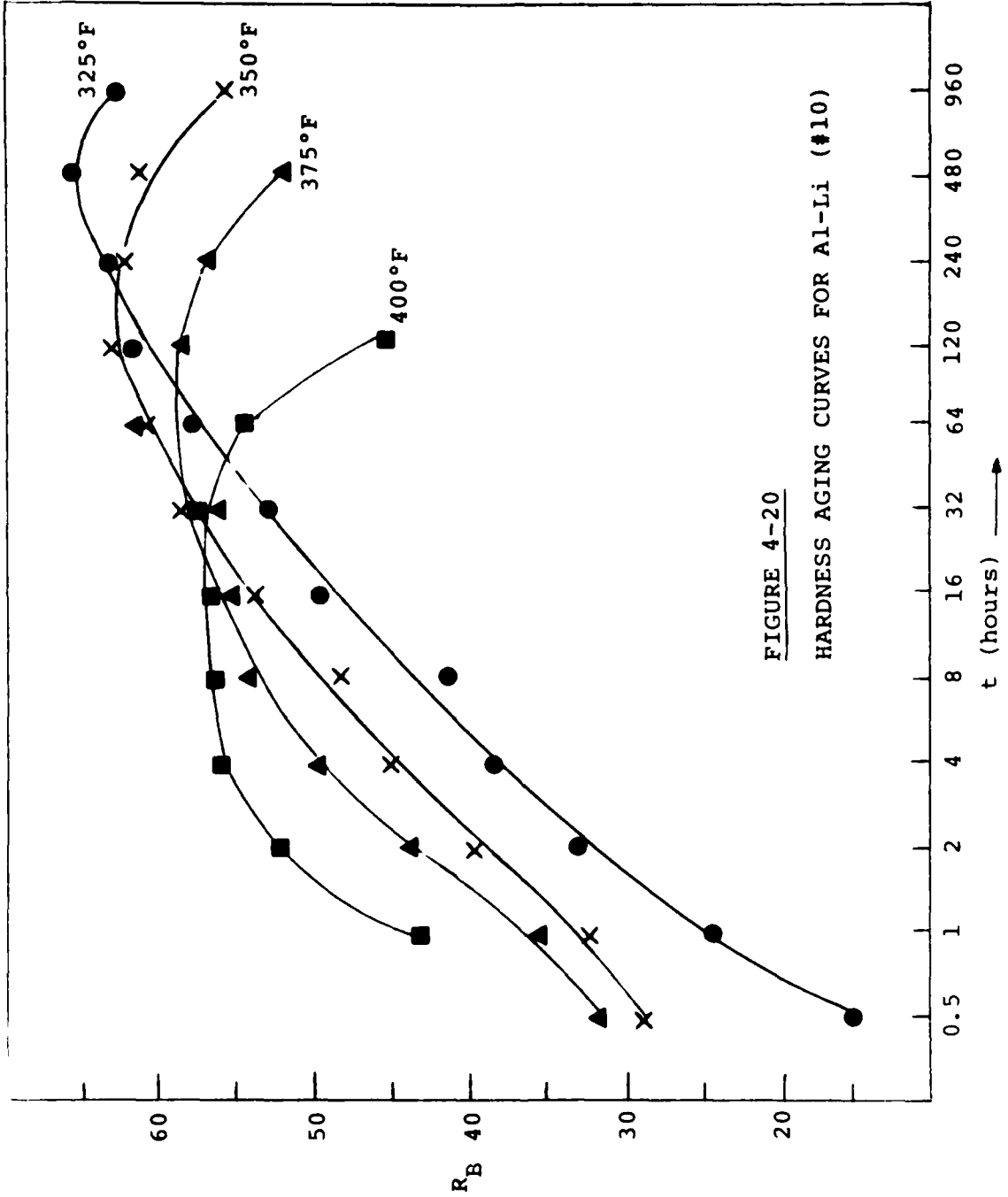


FIGURE 4-20
HARDNESS AGING CURVES FOR Al-Li (#10)

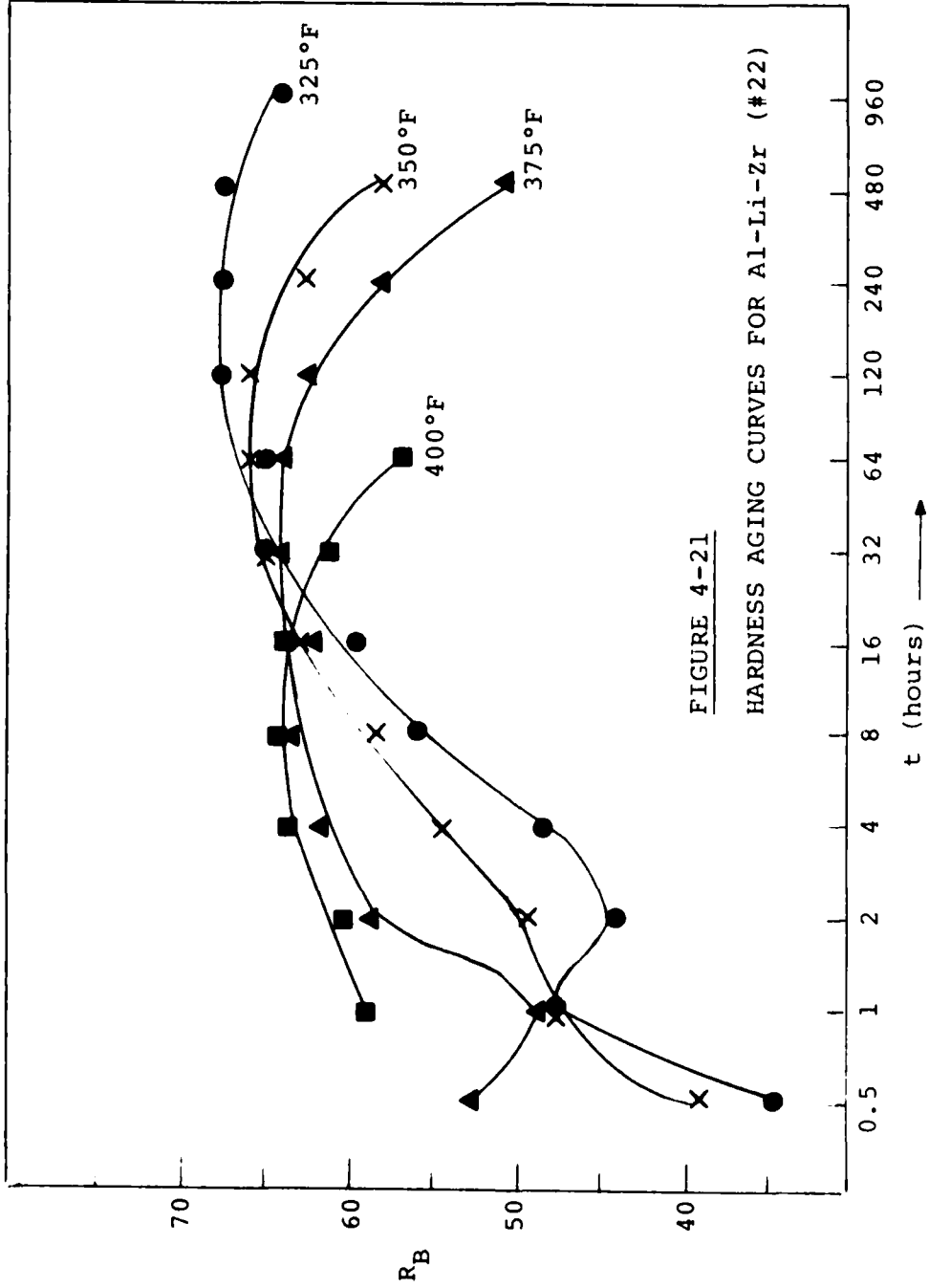
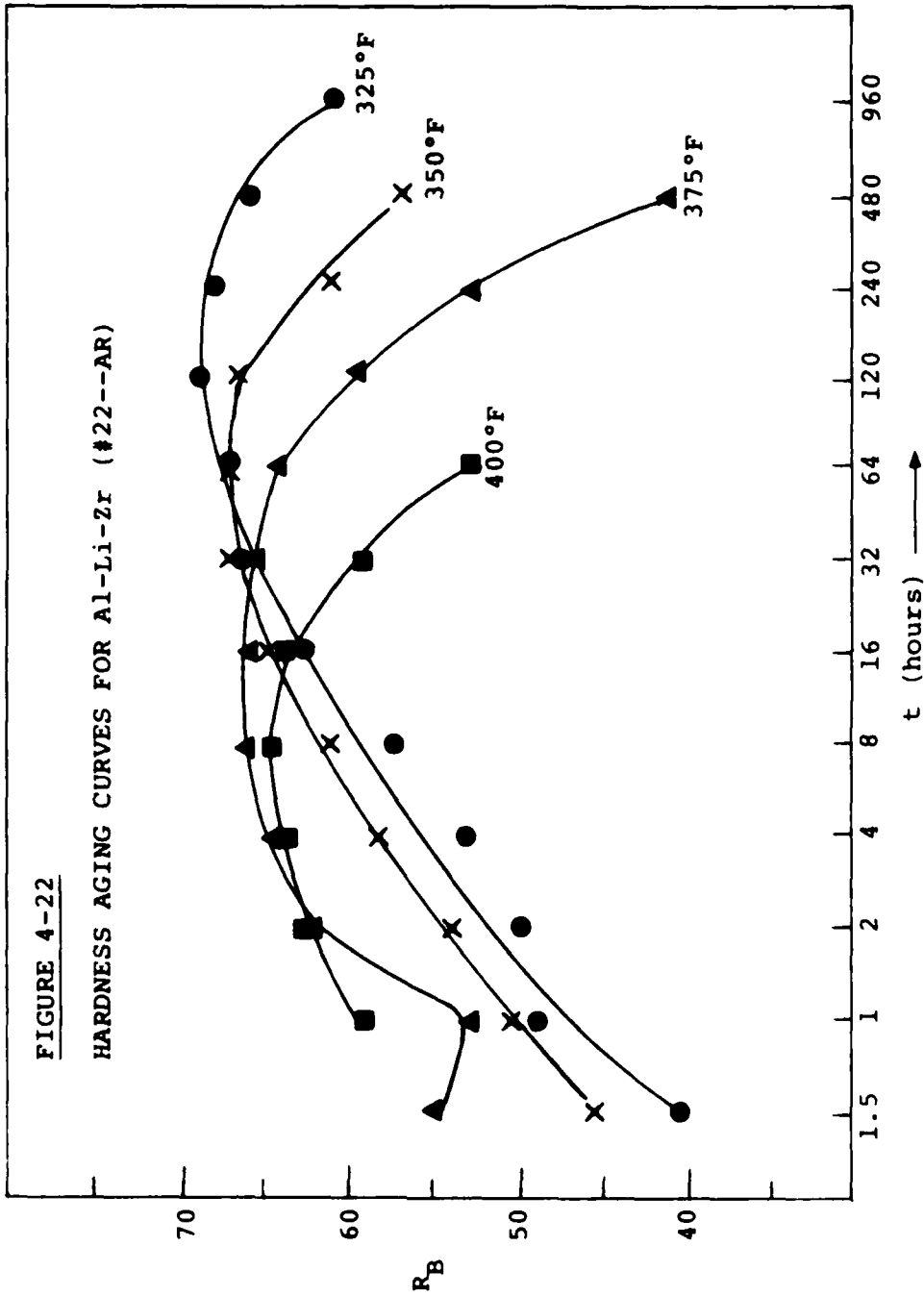


FIGURE 4-21
HARDNESS AGING CURVES FOR Al-Li-Zr (#22)



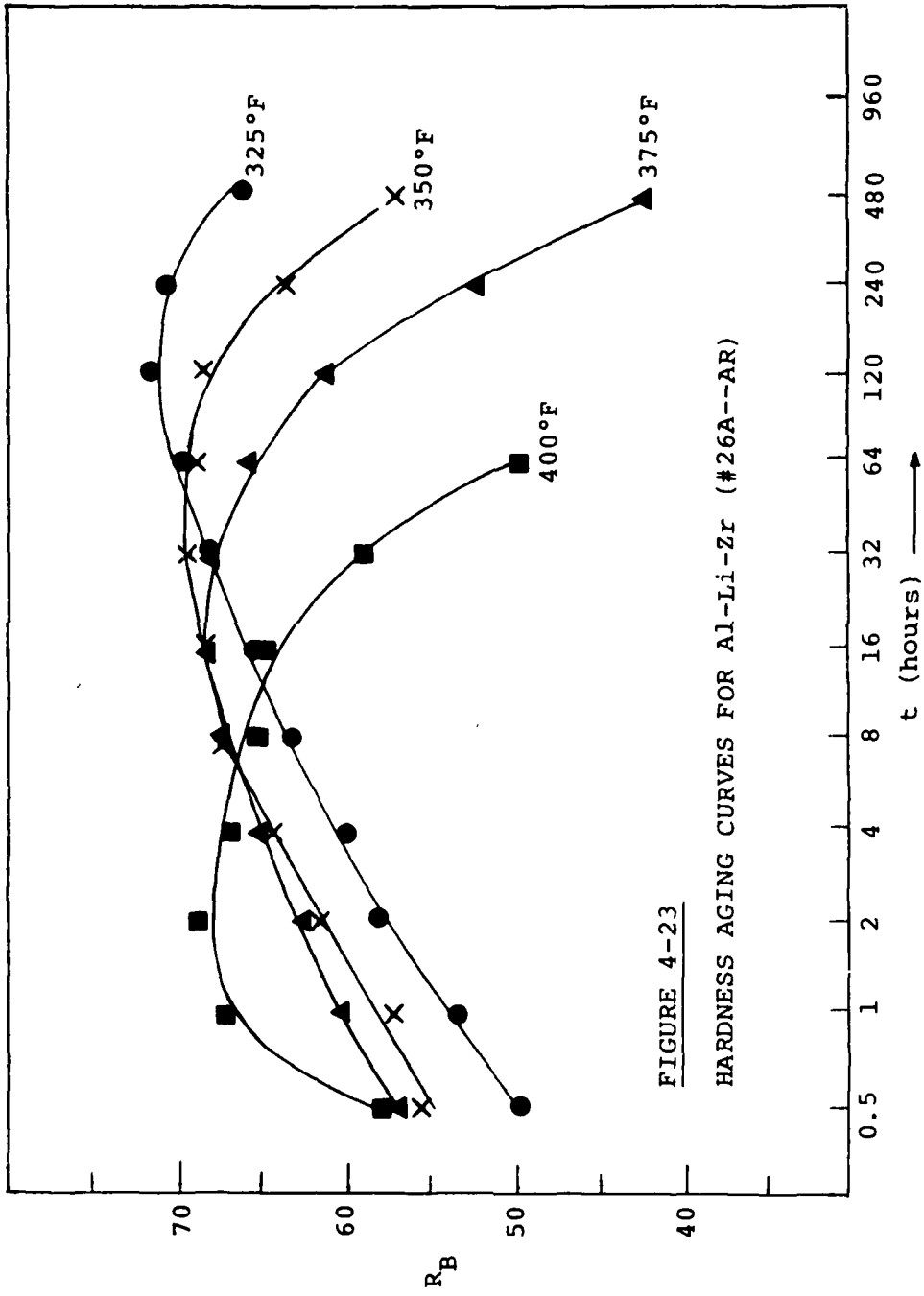


FIGURE 4-23

HARDNESS AGING CURVES FOR Al-Li-Zr (#26A--AR)

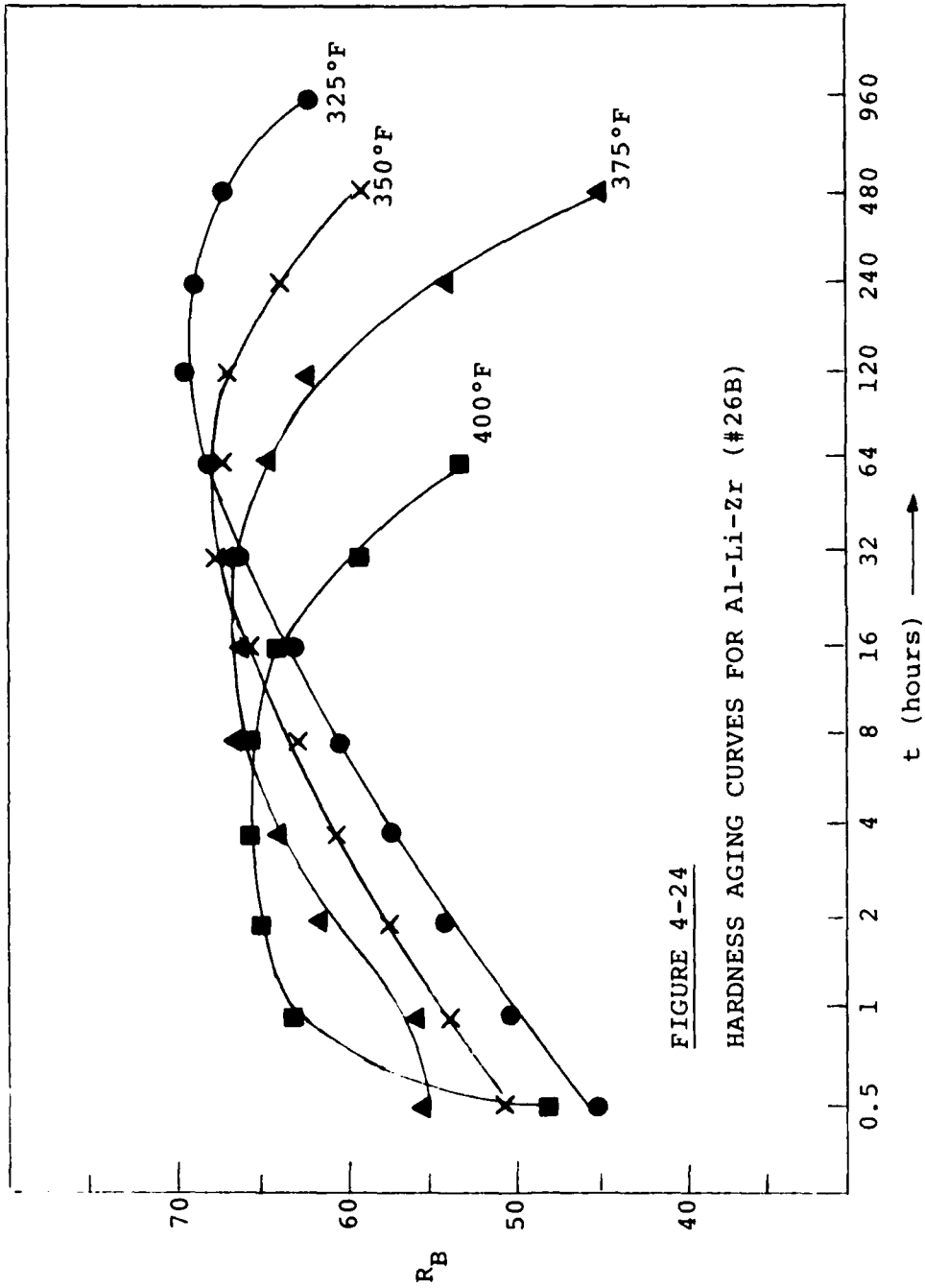


FIGURE 4-24
HARDNESS AGING CURVES FOR Al-Li-Zr (#26B)

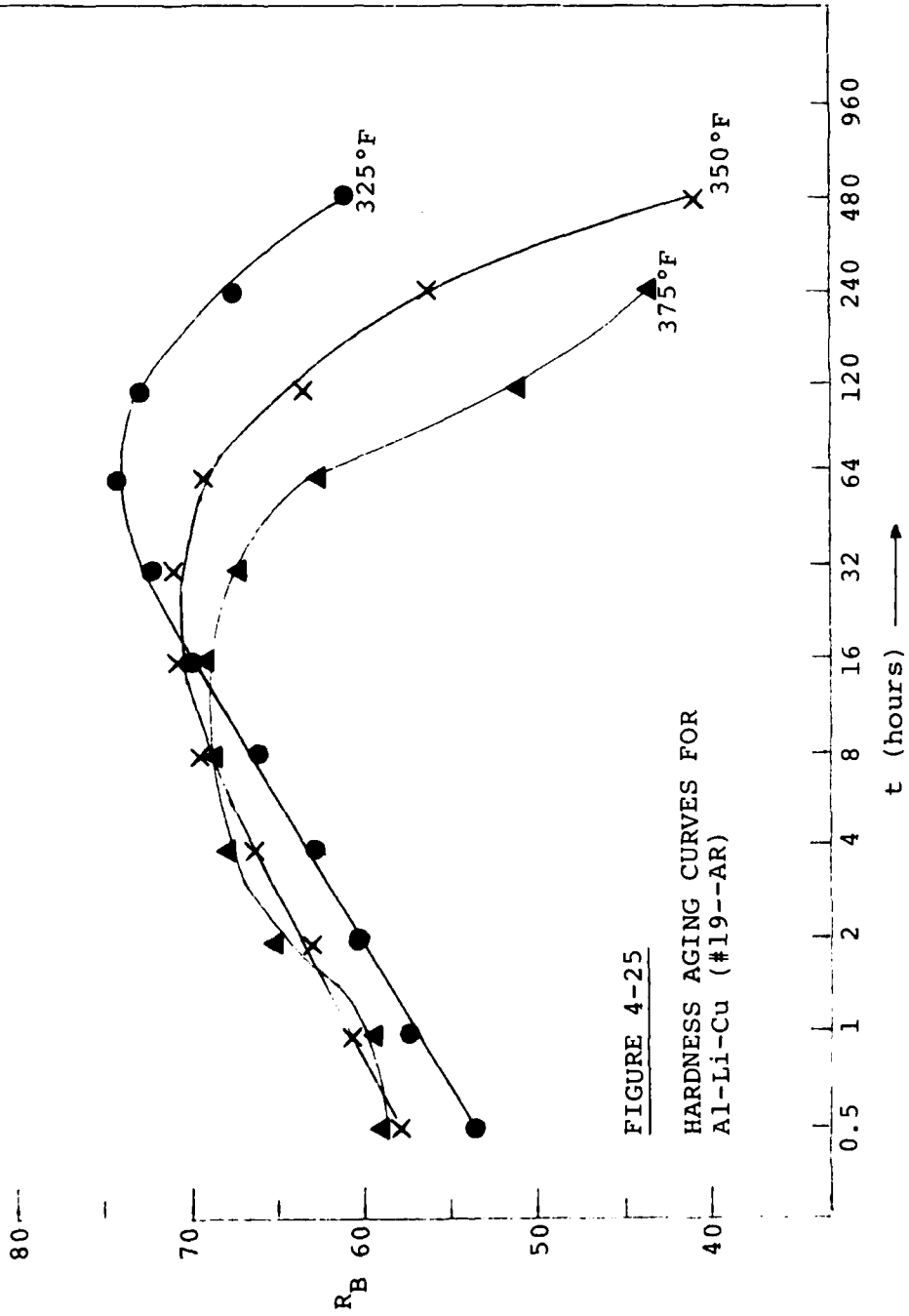


FIGURE 4-25
HARDNESS AGING CURVES FOR
Al-Li-Cu (#19--AR)

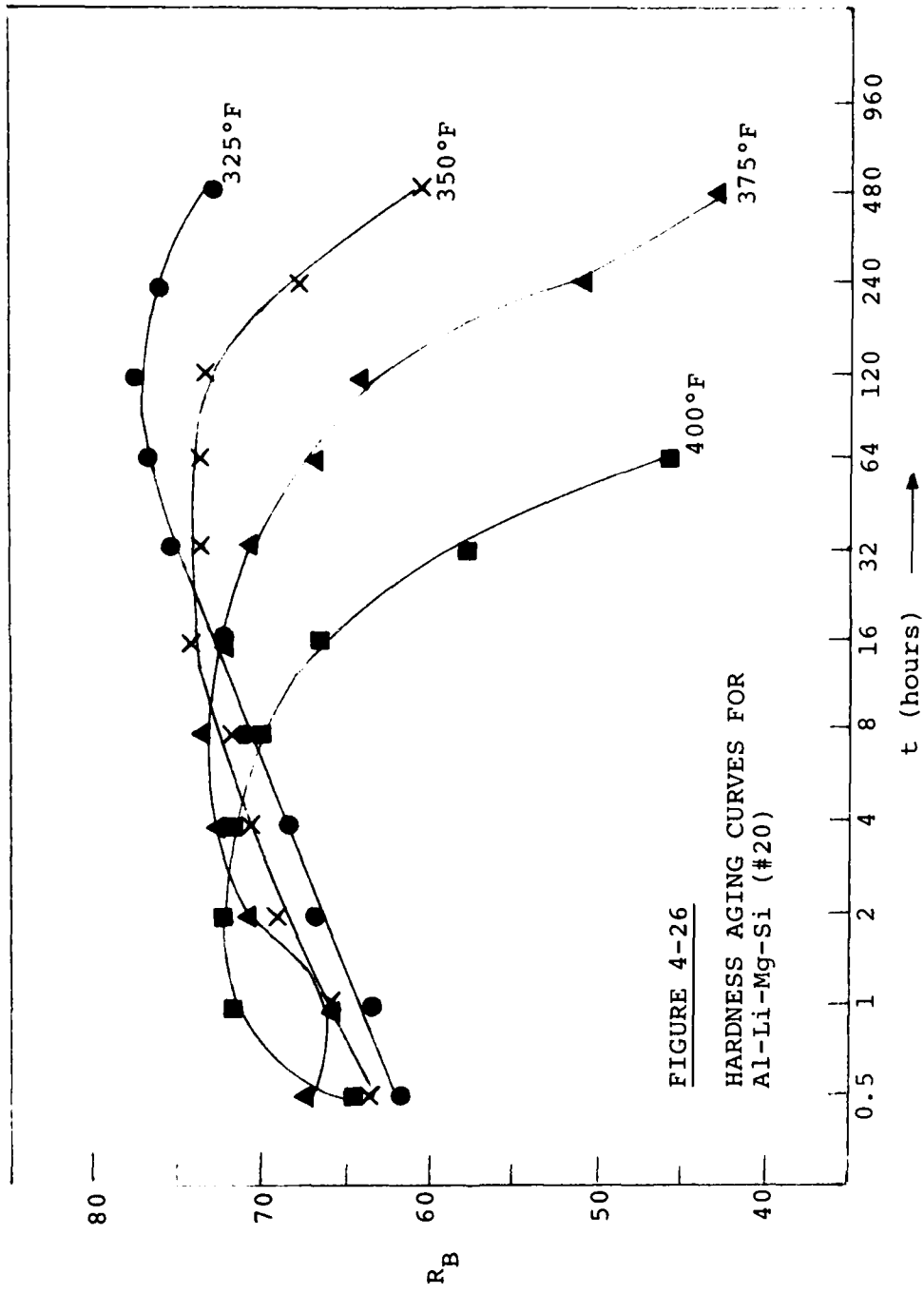


FIGURE 4-26
HARDNESS AGING CURVES FOR
Al-Li-Mg-Si (#20)

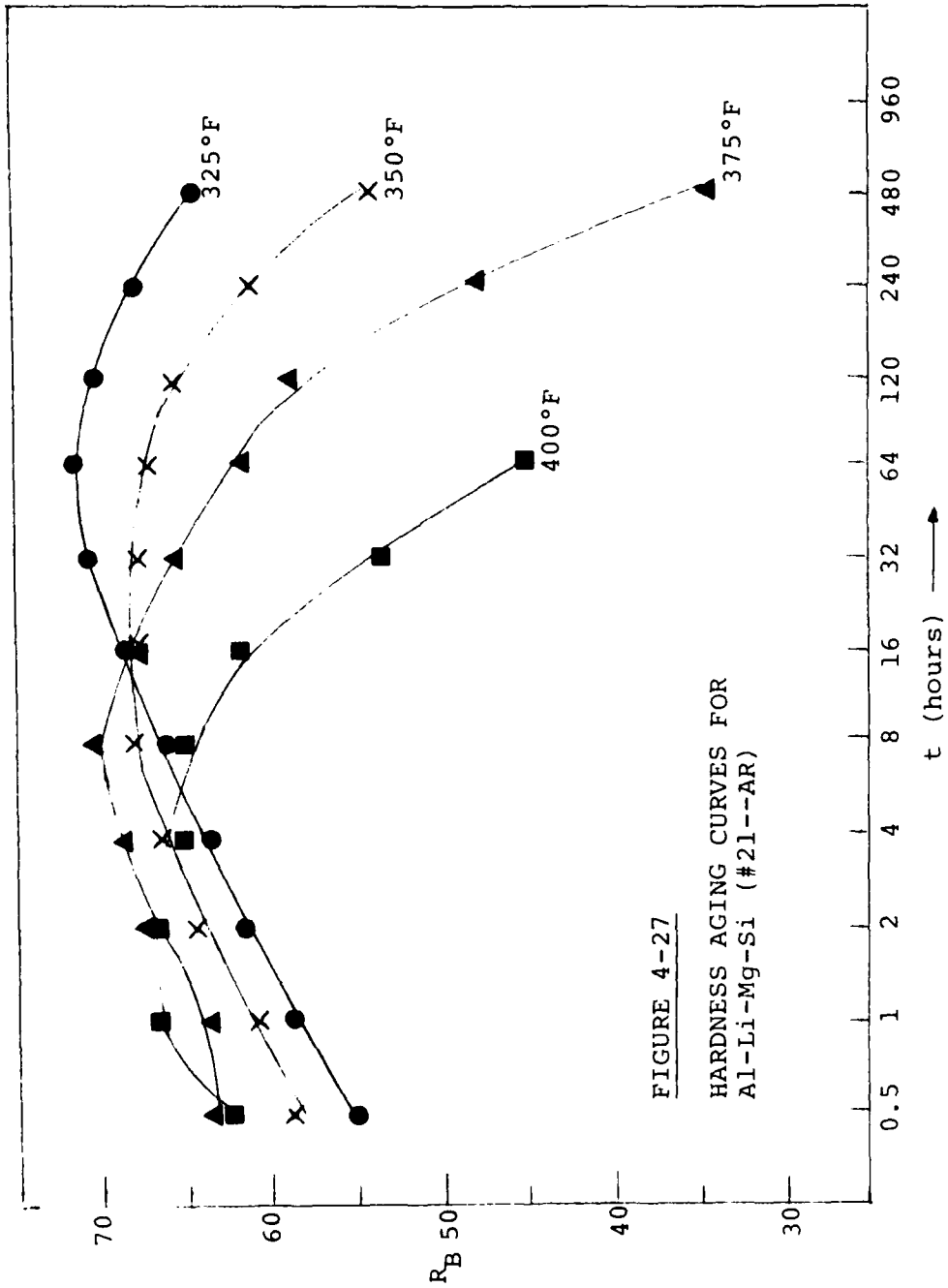


FIGURE 4-27

HARDNESS AGING CURVES FOR
Al-Li-Mg-Si (#21--AR)

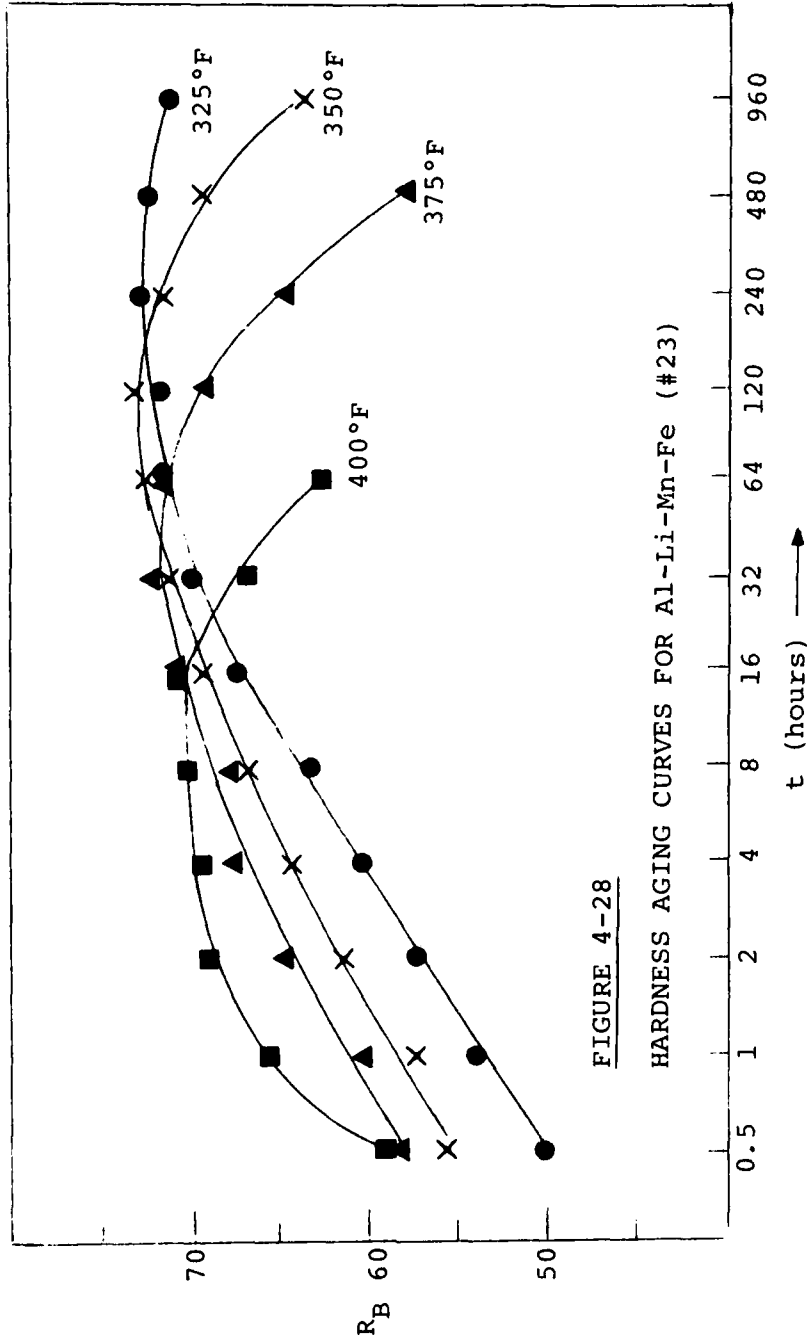


FIGURE 4-28

HARDNESS AGING CURVES FOR Al-Li-Mn-Fe (#23)

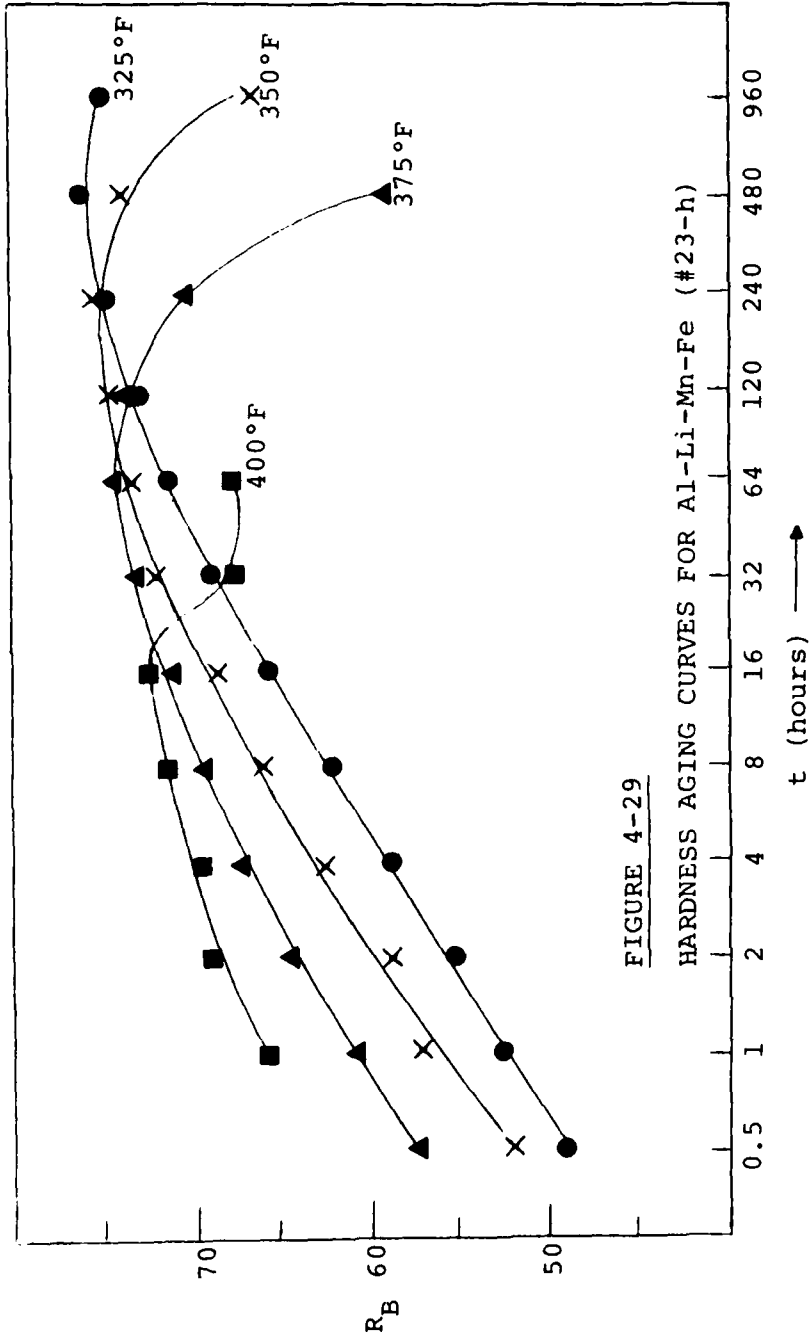
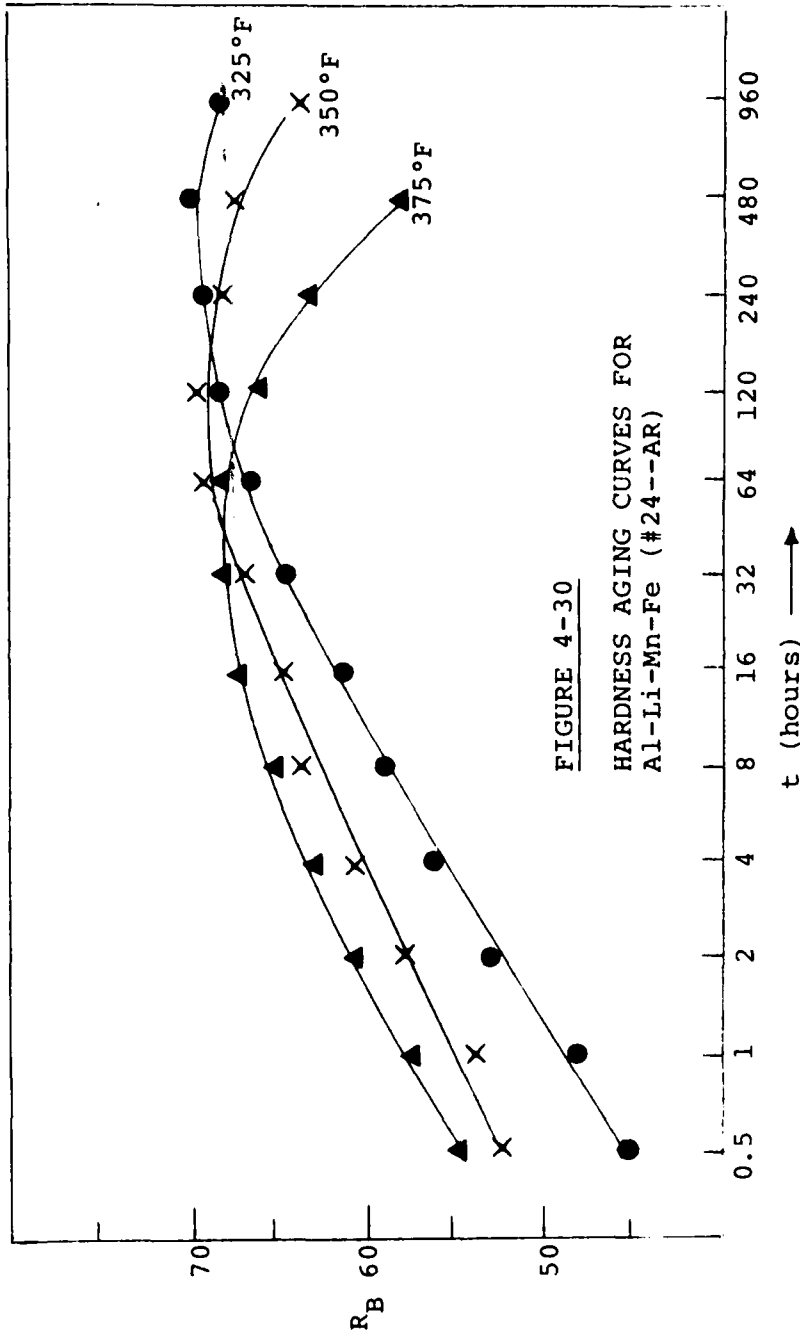


FIGURE 4-29

HARDNESS AGING CURVES FOR Al-Li-Mn-Fe (#23-h)



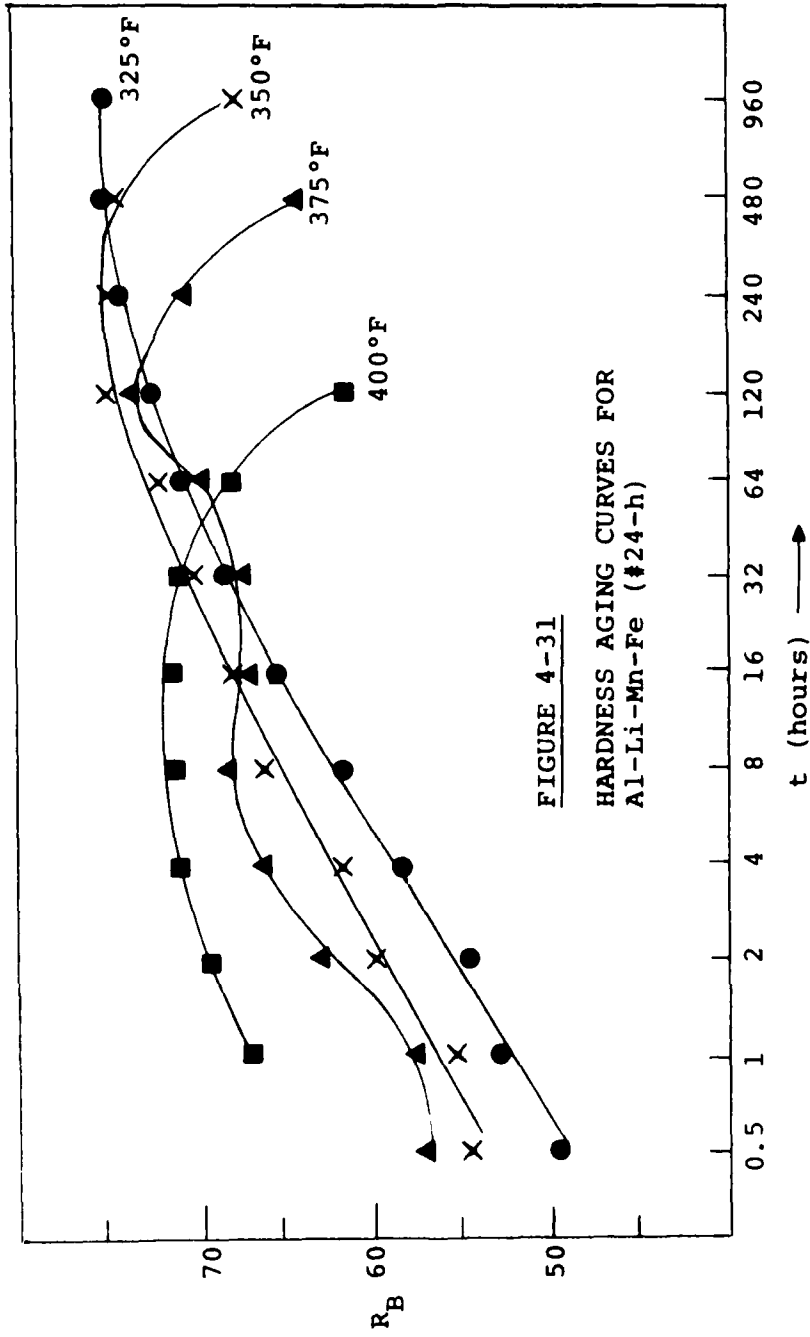


FIGURE 4-31
HARDNESS AGING CURVES FOR
Al-Li-Mn-Fe (#24-h)

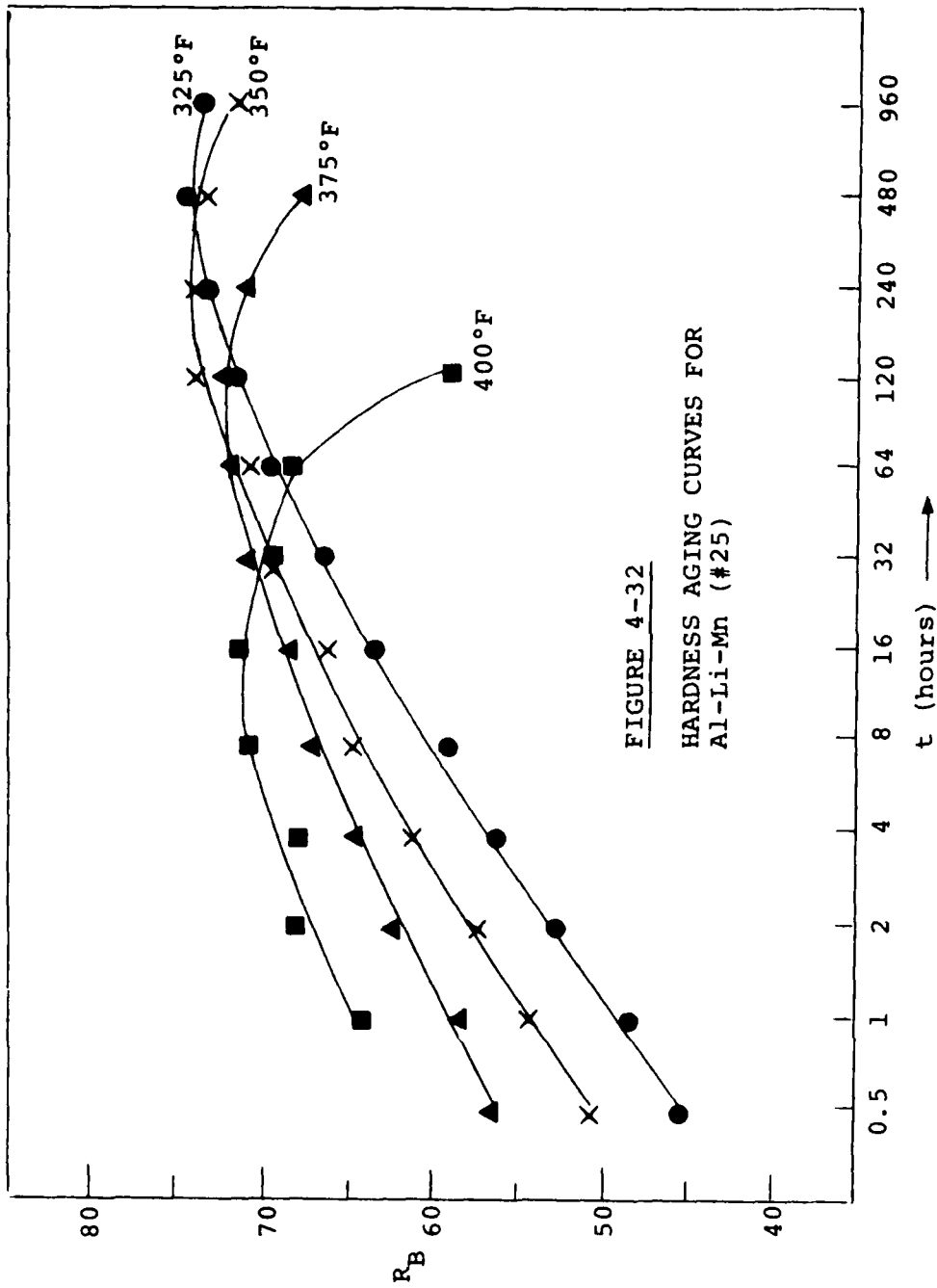


FIGURE 4-32
HARDNESS AGING CURVES FOR
Al-Li-Mn (#25)

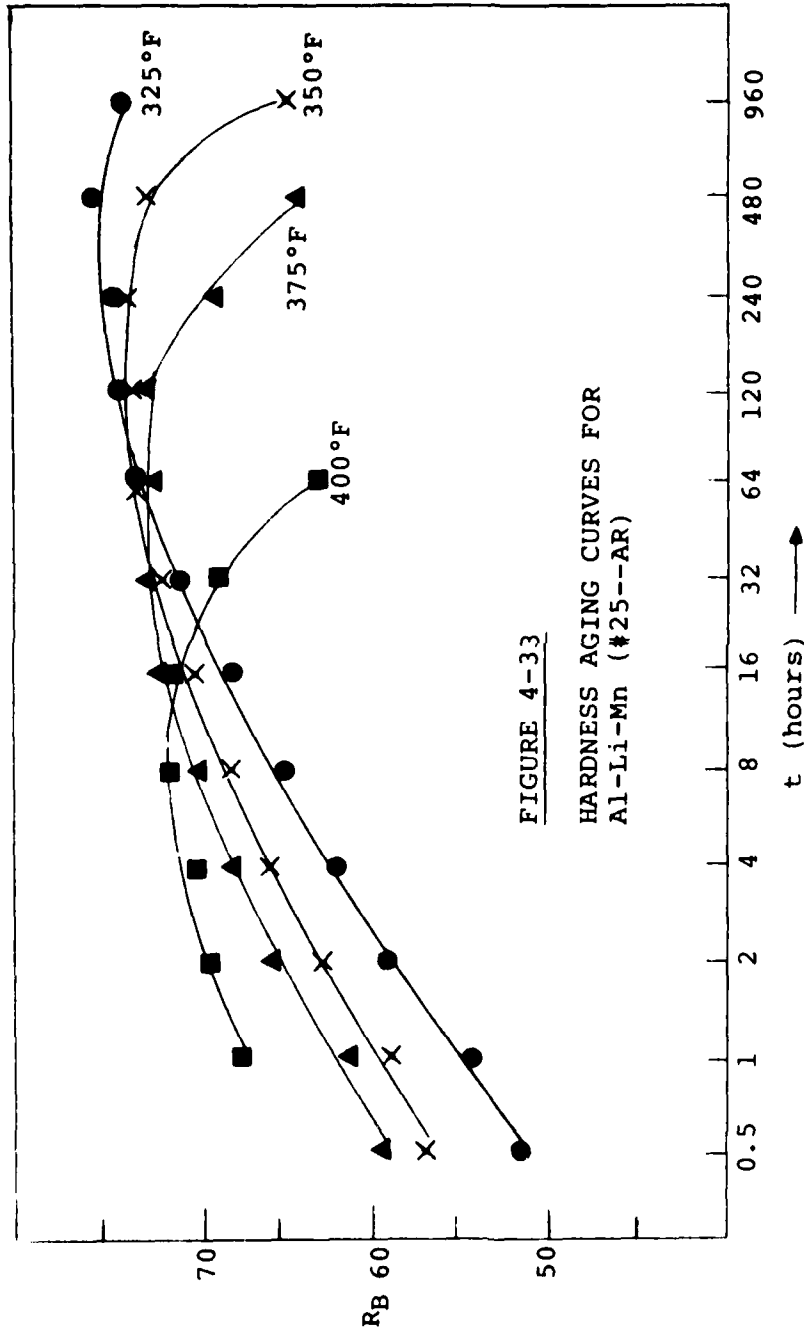


FIGURE 4-33
HARDNESS AGING CURVES FOR
Al-Li-Mn (#25--AR)

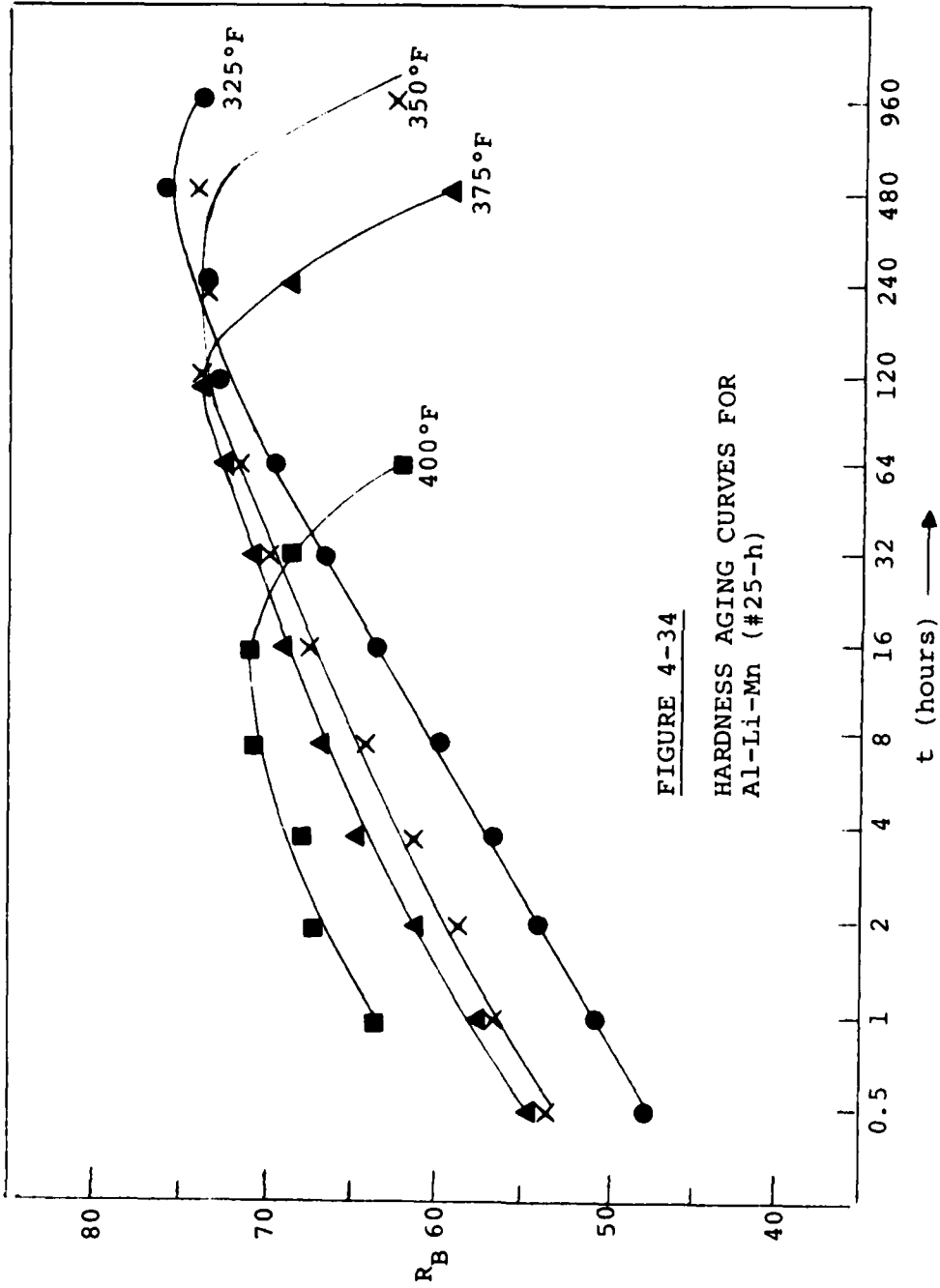
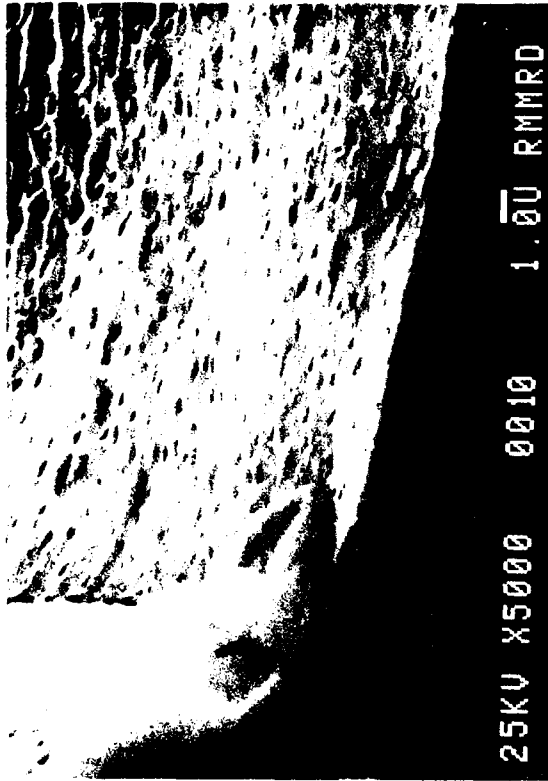


FIGURE 4-34
HARDNESS AGING CURVES FOR
Al-Li-Mn (#25-h)

C.



A.



B.



FIGURE 4-35

SEM OF Al-Li (#10--AR)
Aged 400°F/2 hours (underaged).
Transverse tensile fracture surface.
Typical intergranular fracture.

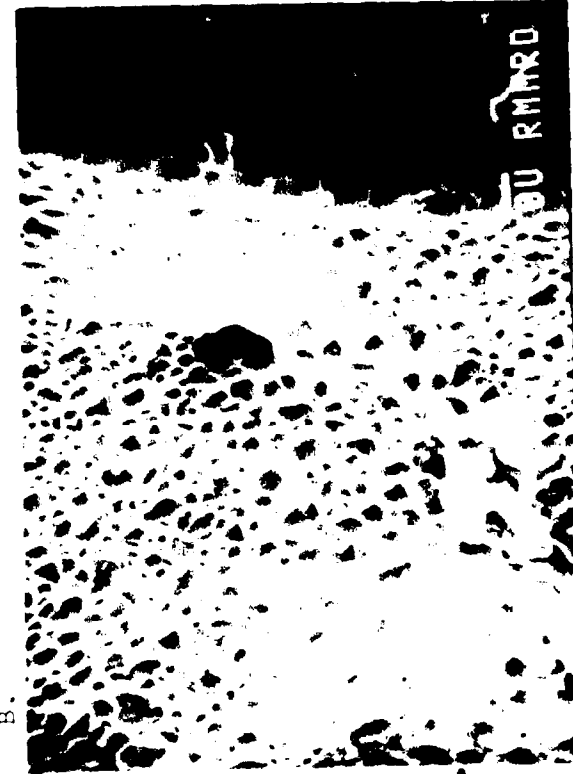
FIGURE 4-36

SEM OF Al-Li (#10)

Aged 375°F/64 hours (peak hardness).
Transverse tensile fracture surface.

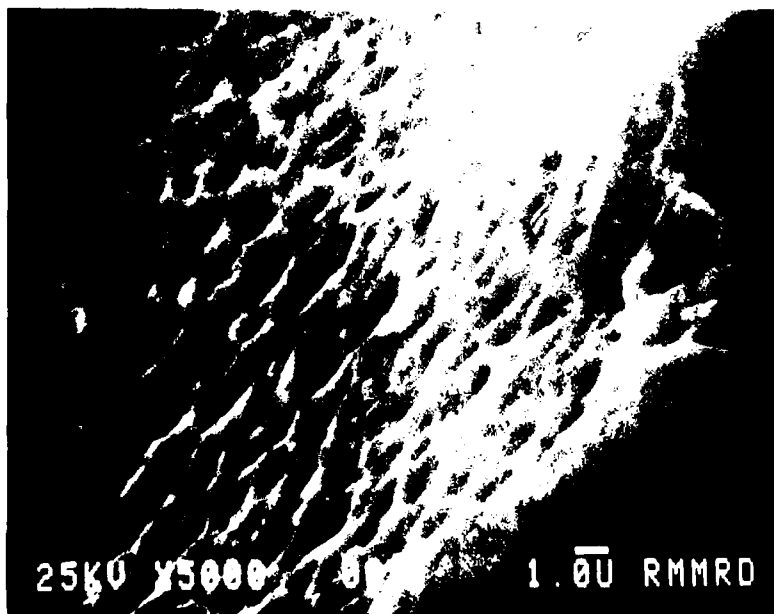
A. Typical intergranular fracture.

B. & C. Left and right faces of center
grain in A. showing different
dimple morphology. Arrows mark
typical iron-rich inclusion
approximately 1 μ m across.





A.



B.

FIGURE 4-37. SEM of the surface of the
A) at 300°C/764 h. The surface is highly porous.
B) after the thermal treatment at 300°C/764 h.
The final interfacial structure is shown.

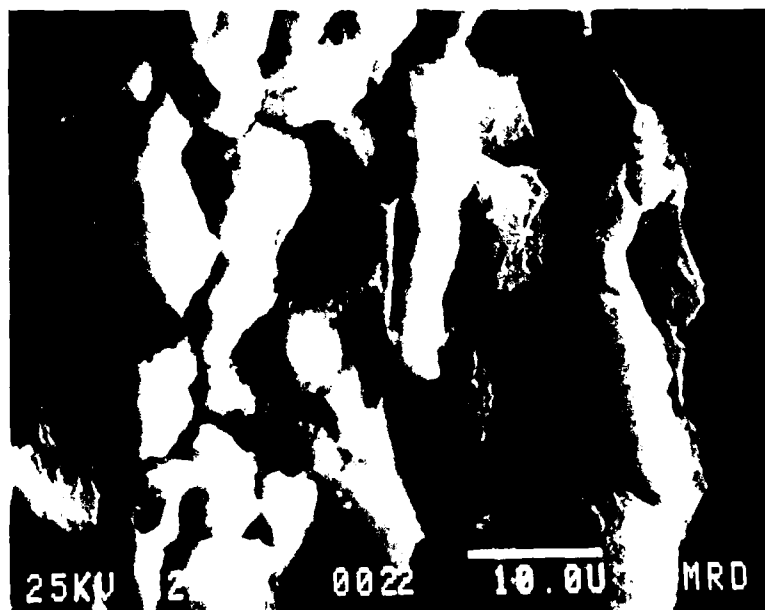
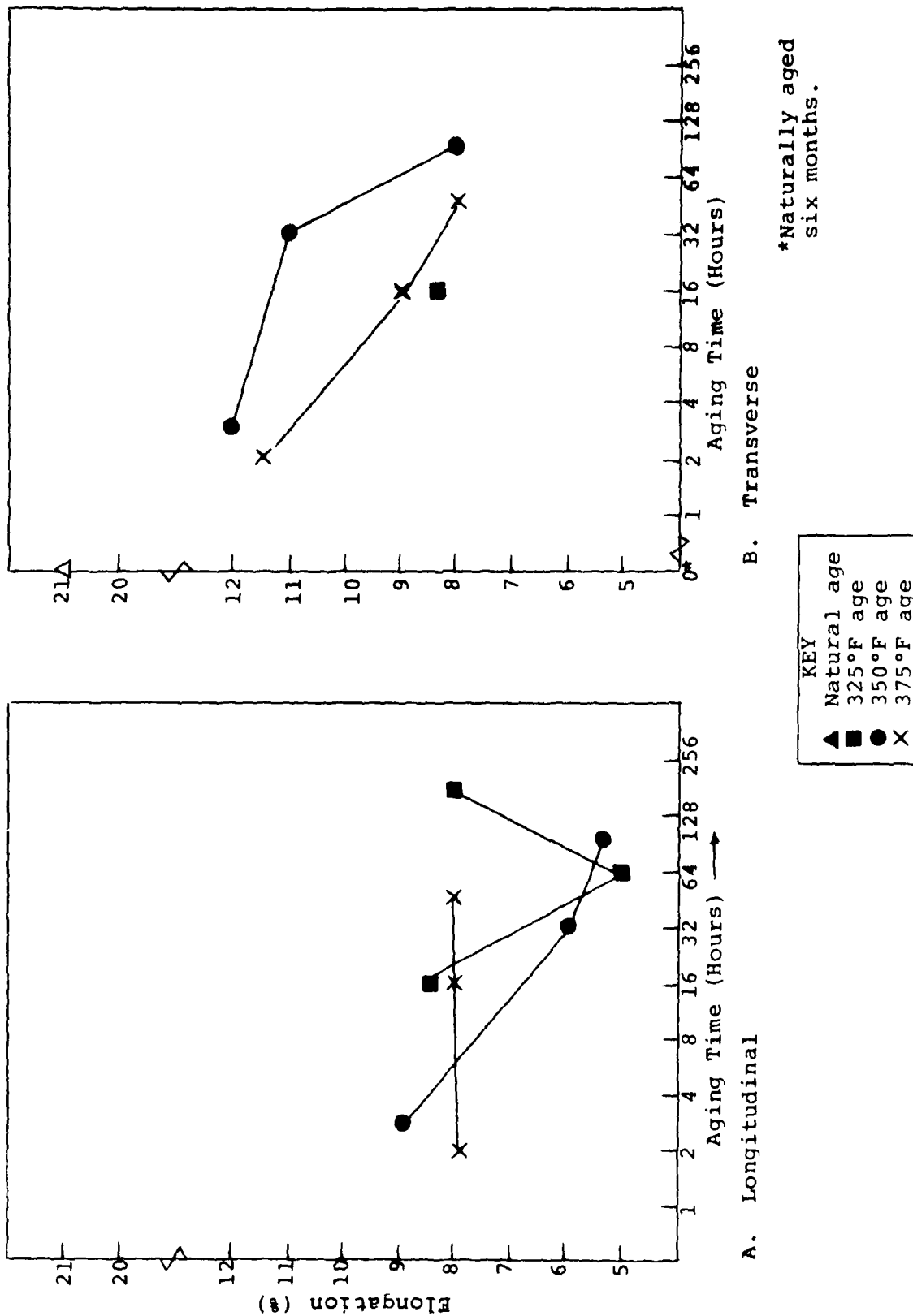


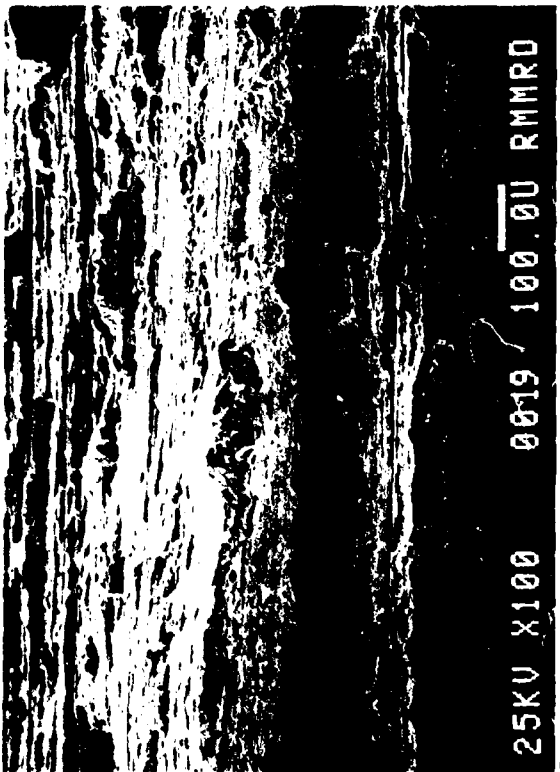
FIGURE 4-38. SEM OF Al-Li-Zr (#22--AR)
Aged 350°F/64 hours.
Longitudinal tensile fracture surface.

FIGURE 4-39. Al-Li-Cu (#19--AR) TENSILE TEST ELONGATION VERSUS AGING TIME

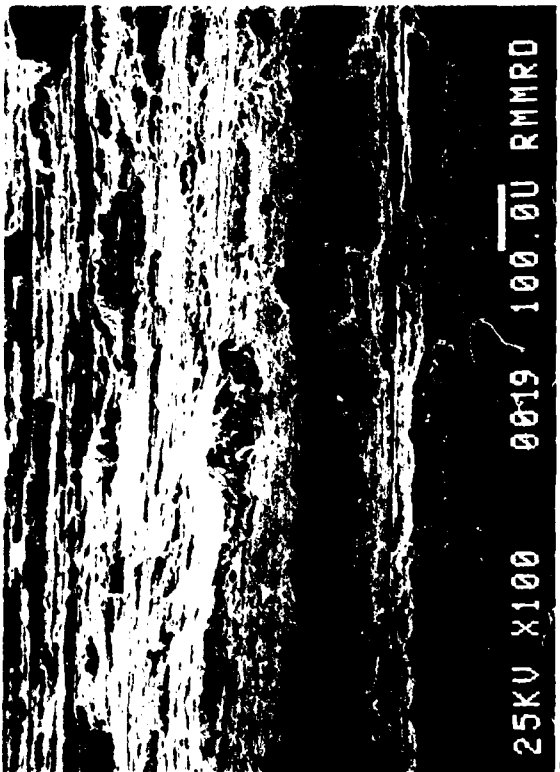




A.



B.



C.

FIGURE 4-40. SEM OF Al-Li-Cu (#19--AR)
Aged 350°F/3 hours (underaged).
Transverse tensile fracture surface.

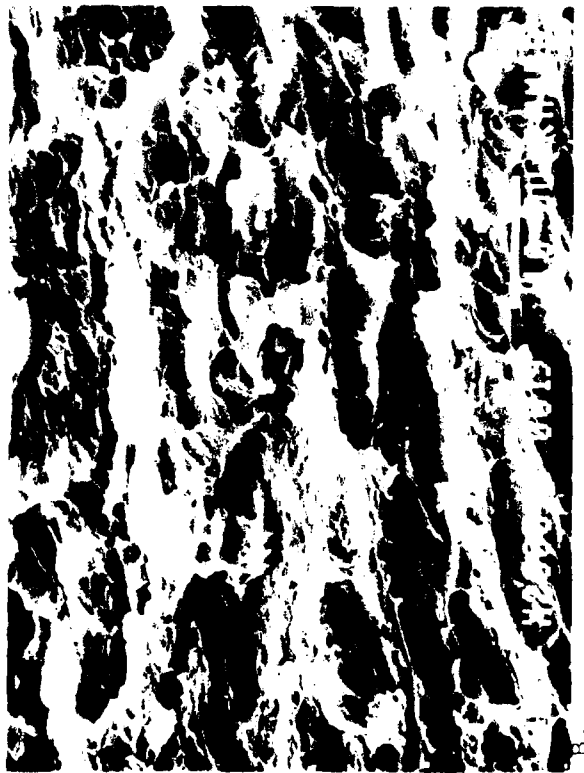
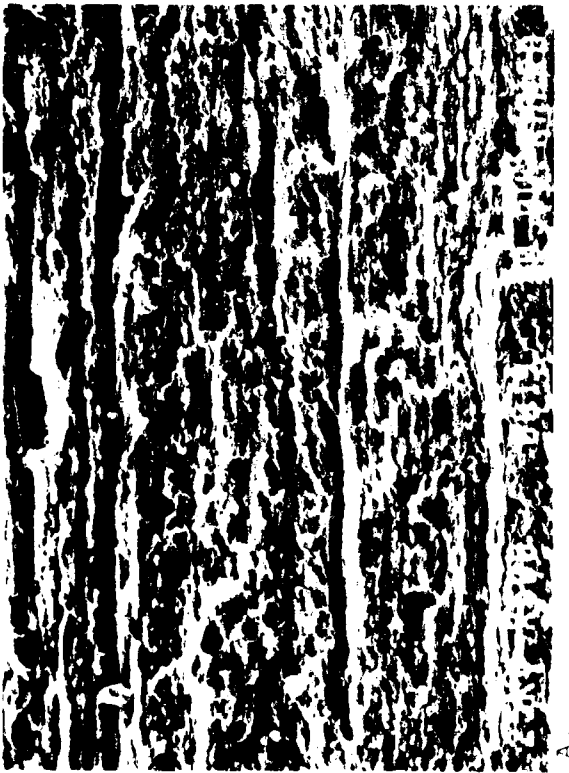
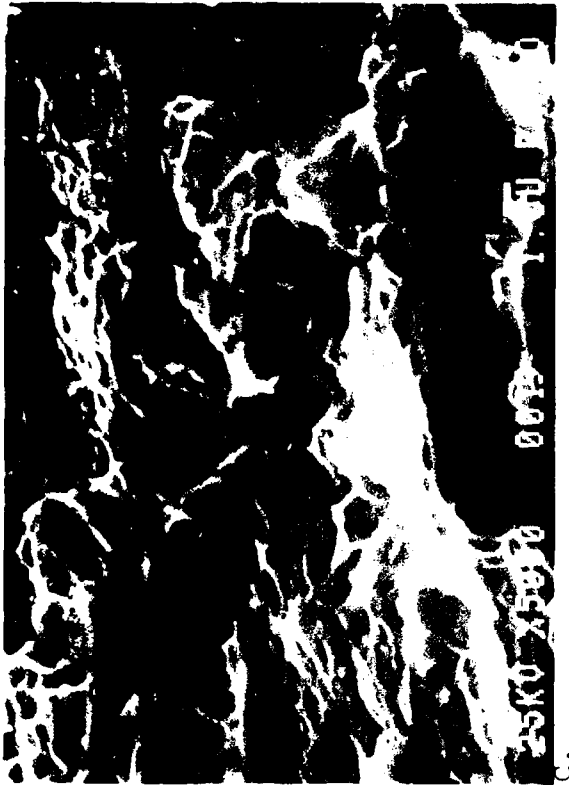
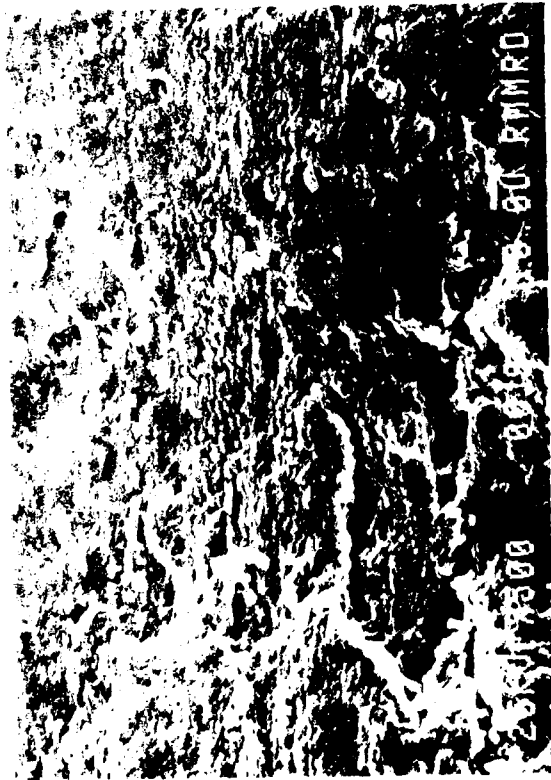
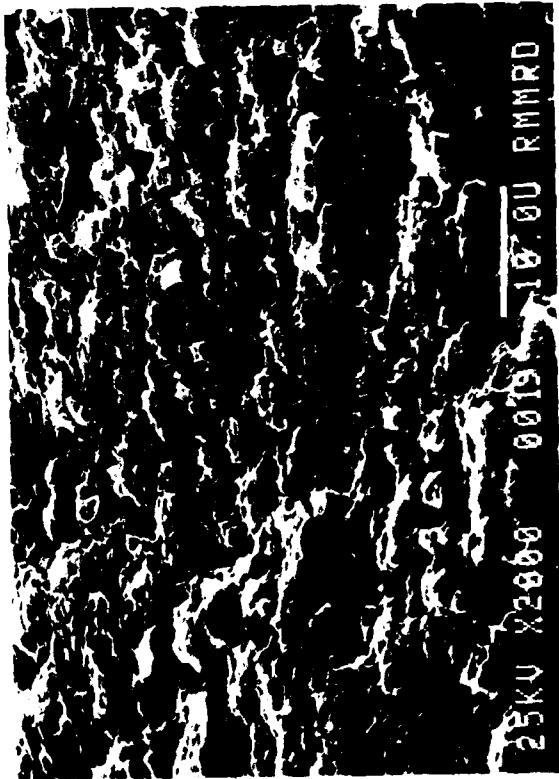


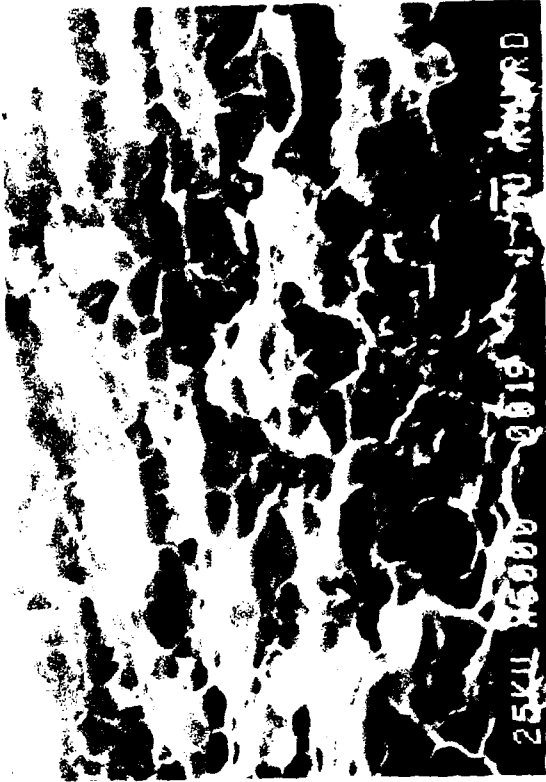
FIGURE 4-41. SEM OF Al-Li-Cu (#19--AR)
Aged 375°F/16 hours (peak aged).
Transverse tensile fracture surface.



A.



B.



C.

FIGURE 4-42. SEM OF Al-Li-Cu (#19--AR)
Aged 375°F/45 hours (overaged).
Transverse tensile fracture surface.



A.



B.



C.

FIGURE 4-43. SEM OF Al-Li-Mg-Si (#20--AR)
Aged 375°F/45 hours (overaged).
Transverse tensile fracture surface.

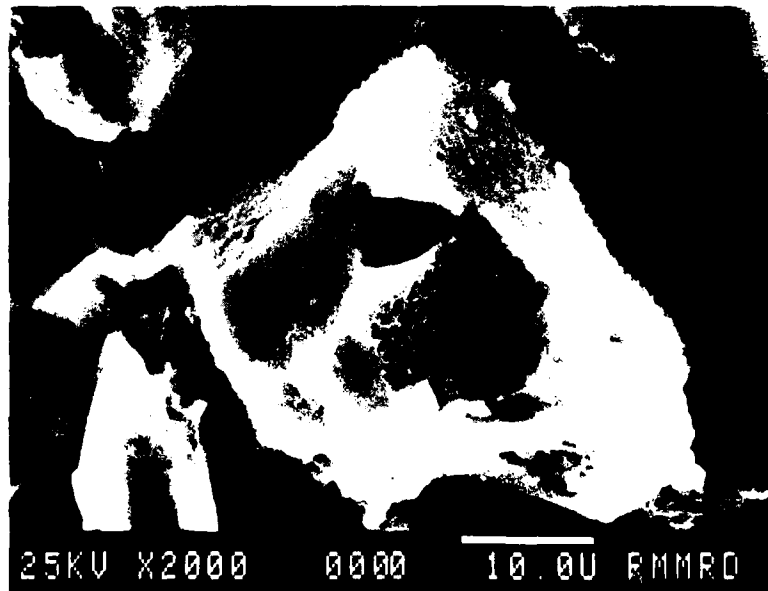
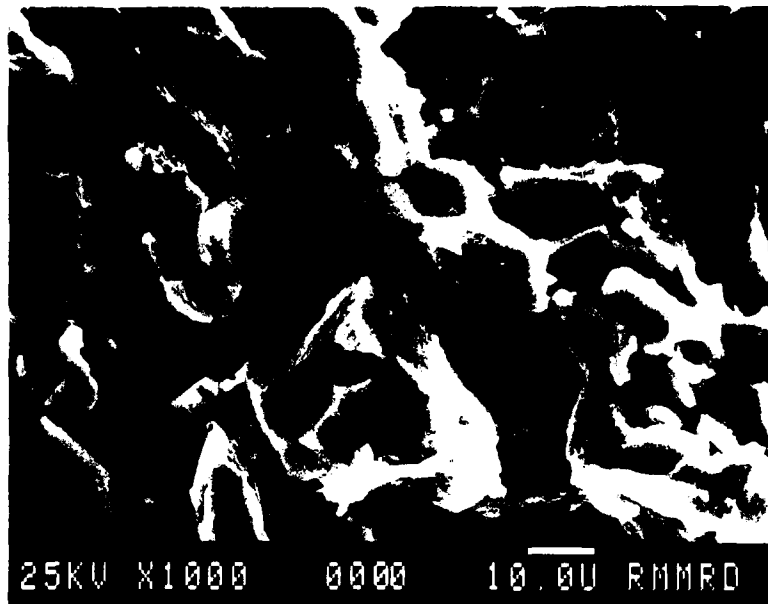


FIGURE 4-44. SEM OF AL-LI-MG-Fe (643-AR)
As of 400°F/45 hours.
Transverse tensile fracture surface showing
typical intergranular fracture.



FIGURE 4-45. TEM OF Al-Li-Zr (#26A) SHEET
Aged 400°F/50 minutes (underaged). 11,500X.



FIGURE 4-46. TEM OF Al-Li-Fe (#265) SHEET
Aged 400°F/50 minutes (under load).
Note grain boundary pinning by FeAl. $\times 46,000X$.

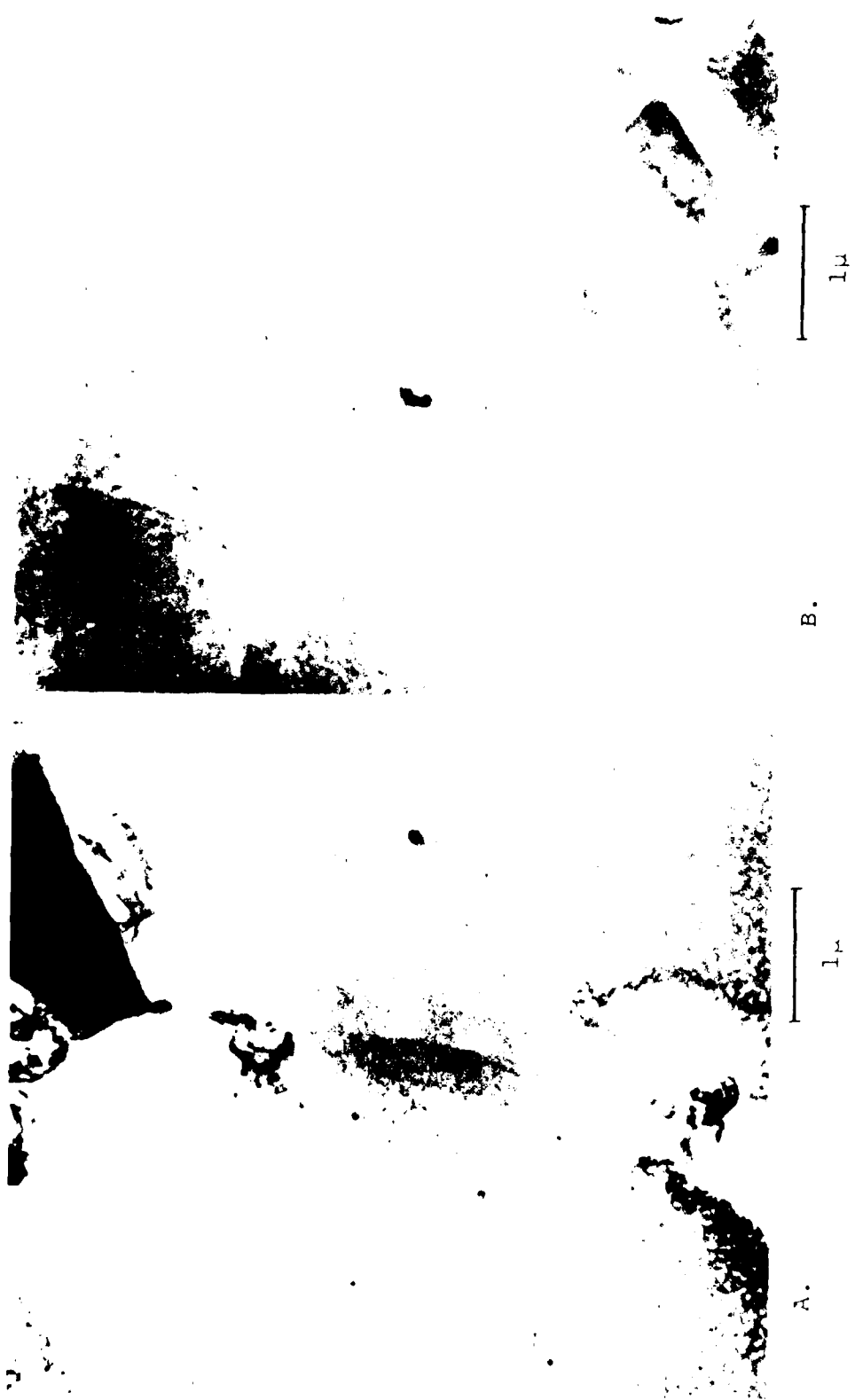


FIGURE 4-47. TEM OF Al-Li-Zr (#26A) SHEET

Aged 400°F/64 hours (overaged).
Coarsened δ' and wide PFZ on some grain
boundaries are apparent. 22,000X.



1 μ

FIGURE 3-47. TEM OF Al-Li-7 (#26A) SHEET
X-ray 400°C for 60 minutes (under load).
Note direction of lamellar precipitation. $\times 22,000X$.

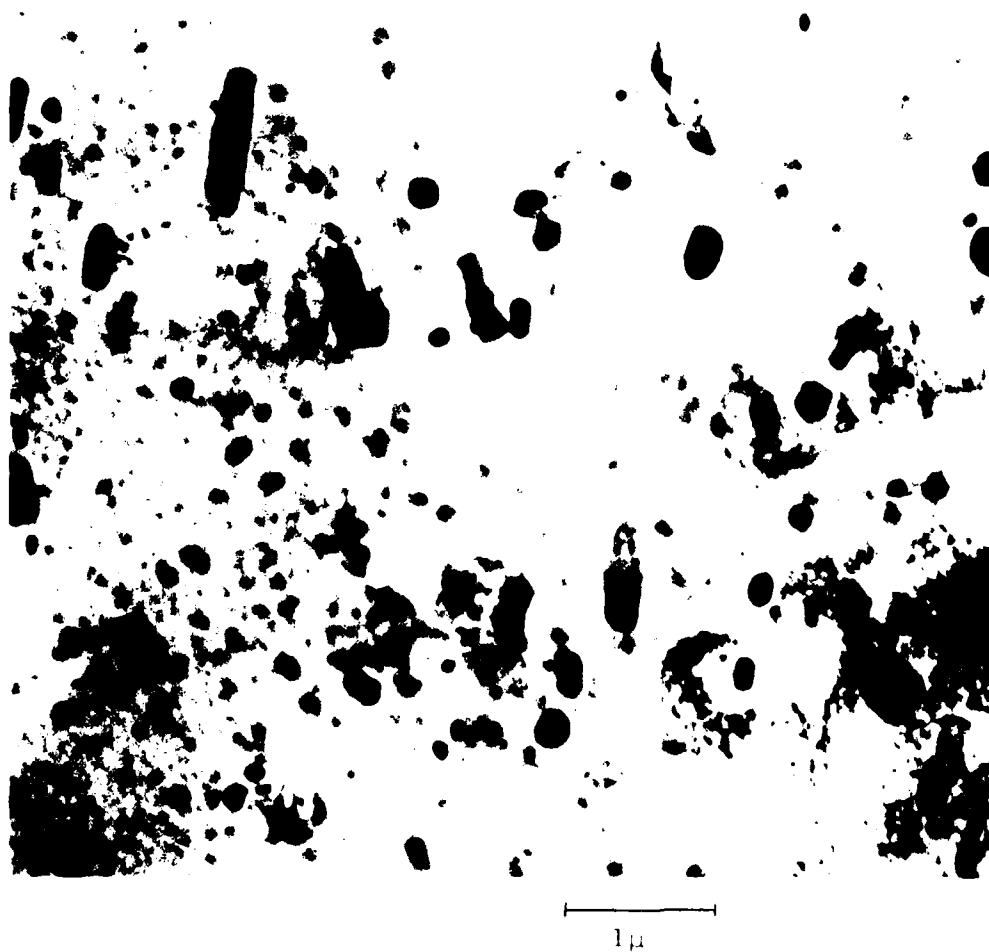
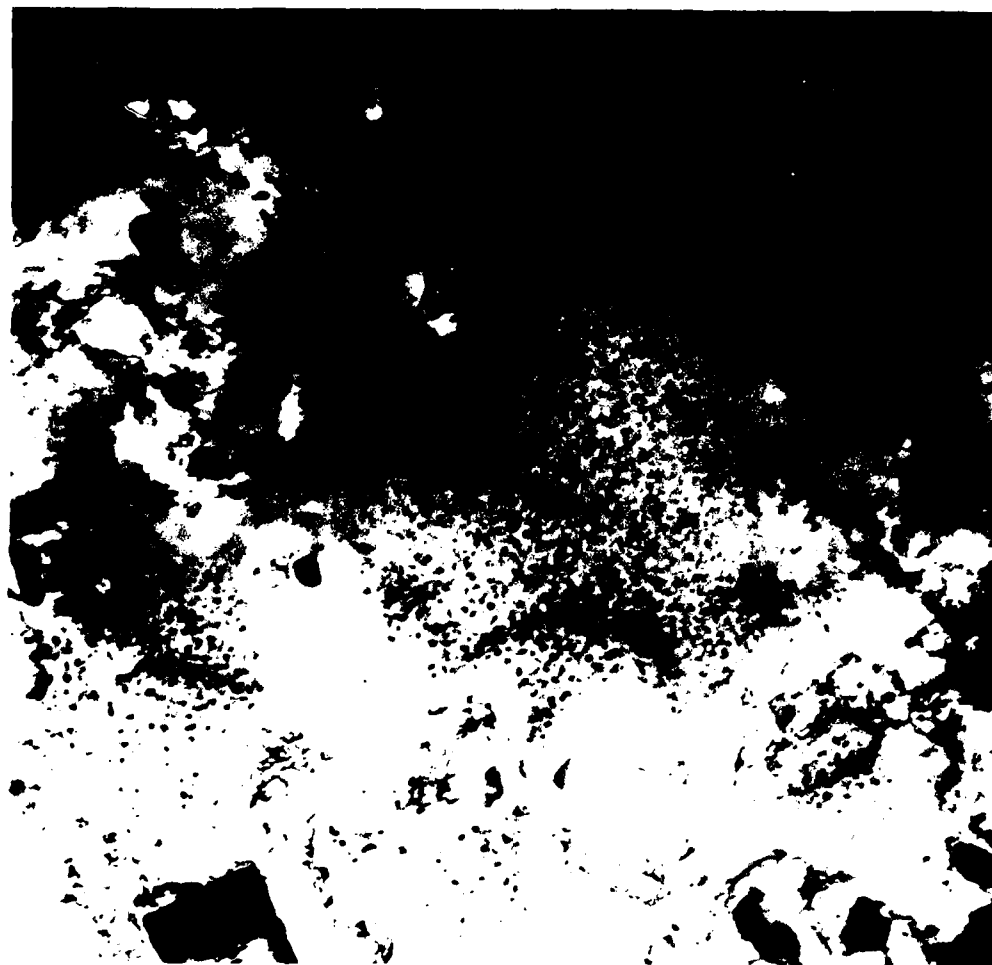


FIGURE 4-49. TEM OF Al-Li-Mn (#25--AR) SHEET
Aged 400°F/64 hours.
Typical of matrix showing $MnAl_6$ insolubles.
22,000X.



1 μ

FIGURE 4-51. TEM OF Al-Li-Mn (#25-h) SHEET
Solution heat treated 1050°F/1 hour + aged
400°F/64 hours.
PFZ around MnAl₆ insolubles. 22,000X.

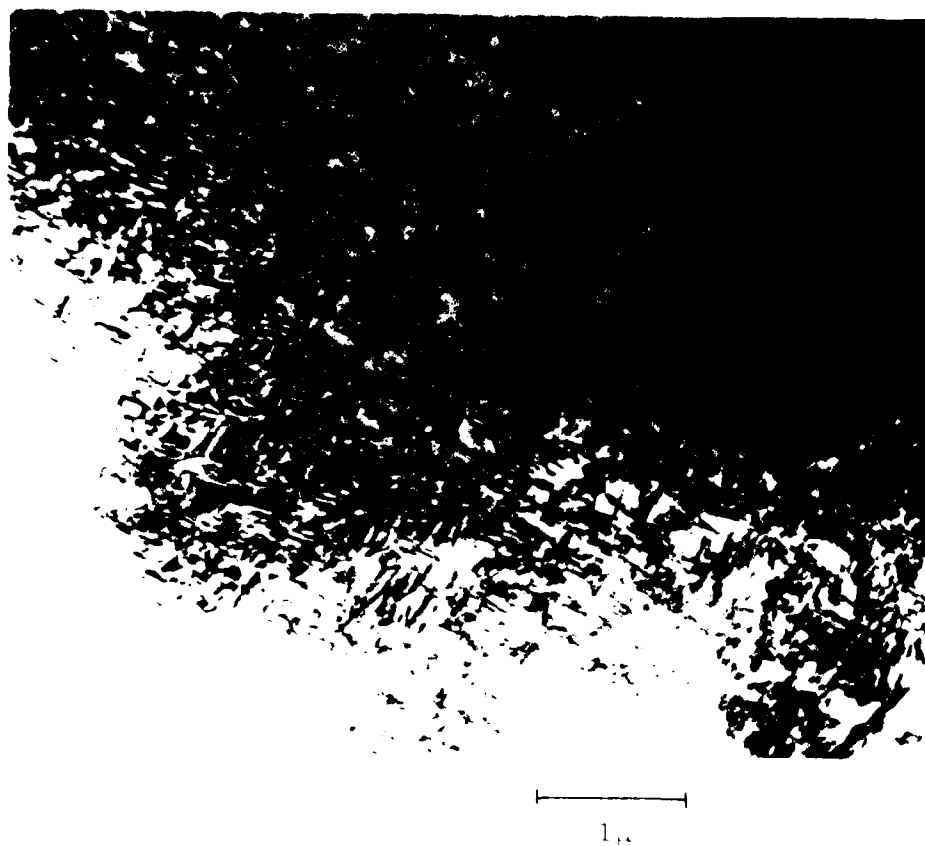


FIGURE 4-52. TEM OF Al-Li-Cu (#19--AB) SHEET
Aged 375°C/16 hours.
Coherency strain contrast started with "0". 22,000X.

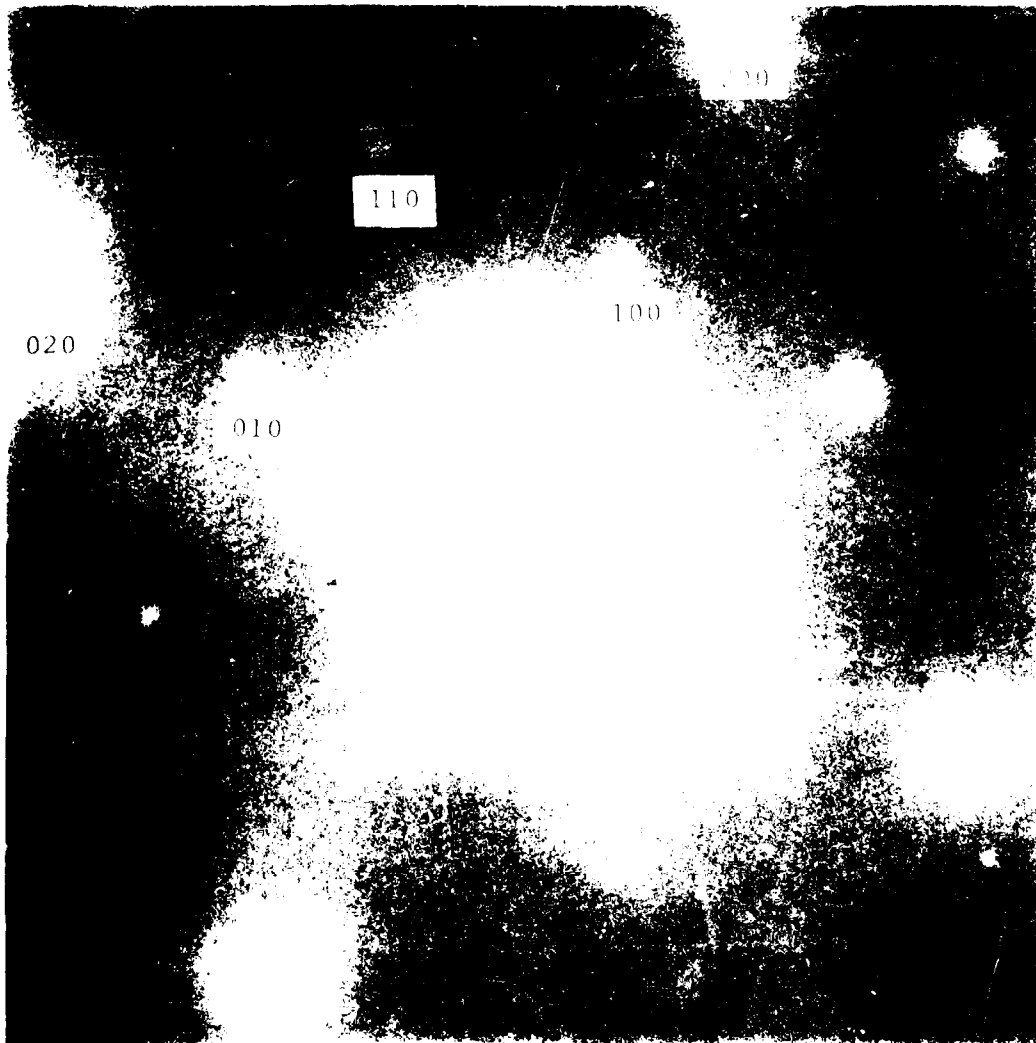
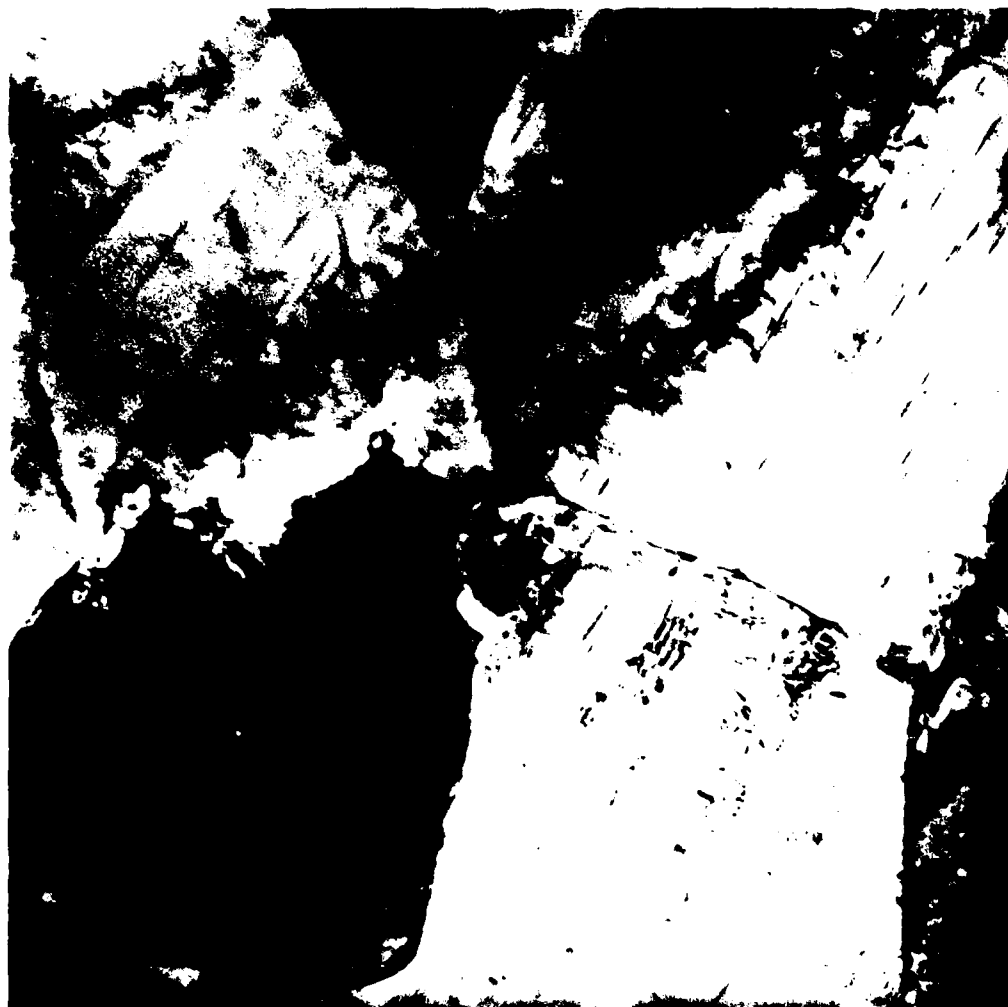


FIGURE 4-53. TEM OF Al-Li-Cu (#19--AP) SHEET
Aged 375°F/16 hours.
Selected area diffraction pattern on $\{111\}$ pole
of matrix showing superlattice reflections.



1μ

FIGURE 4-34. TEM OF Al-Li-Cu (#19--AR) SHEET
Aged 175°C (16 hours (peak hardness),
Photo-etch reagent (C', T_J, or T_R). 22,000X.



FIGURE 4-55. TEM OF Al-Li-Cu (#19--AR) SHEET
Aged 375°F/16 hours (peak hardness). 22,000X.



1 μ

FIGURE 4-56. TEM OF Al-Li-Cu (#19--AR) SHEET
Aged 375°F/45 hours (overaged).
Note precipitate nucleation at subgrain
boundaries. 22,000X.



FIGURE 4-57. TEM OF Al-Li-Cu (#19--AR) SHEET
Aged 375°F/45 hours (overaged) typical. 22,000X.



FIGURE 4-58. TEM OF Al-Li-Cu (#19--AR) SHEET
Aged 375°F/45 hours (overaged).
Platelike T₁ precipitates and heavy subgrain
boundary precipitation. 46,000X.

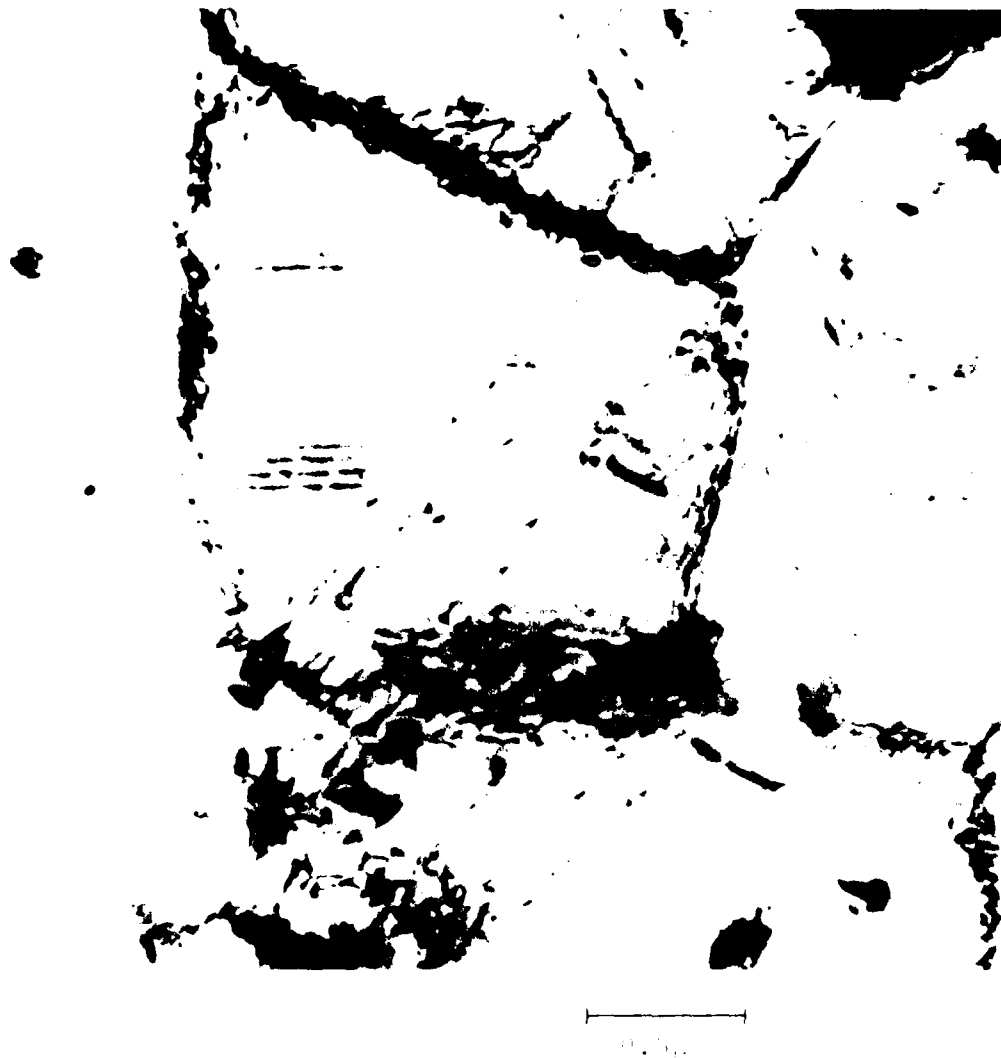


FIGURE 4-59. TEM OF Al-11-cu-0.5#19. 200,000X
Aged 275°F/45 hours. (courtesy Dr. J. C. Williams)

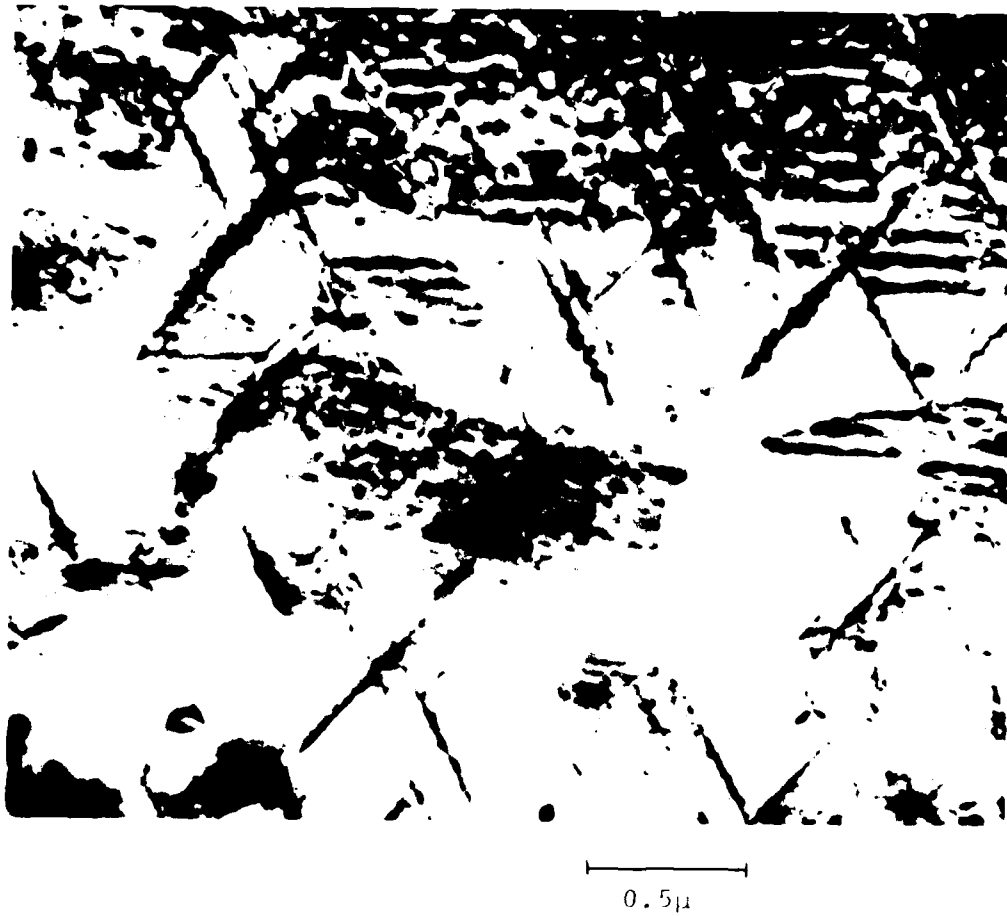


FIGURE 4-60. TEM OF Al-Li-Cu (#19--AR) SHEET
Aged 375°F/45 hours (overaged). 46,000X.

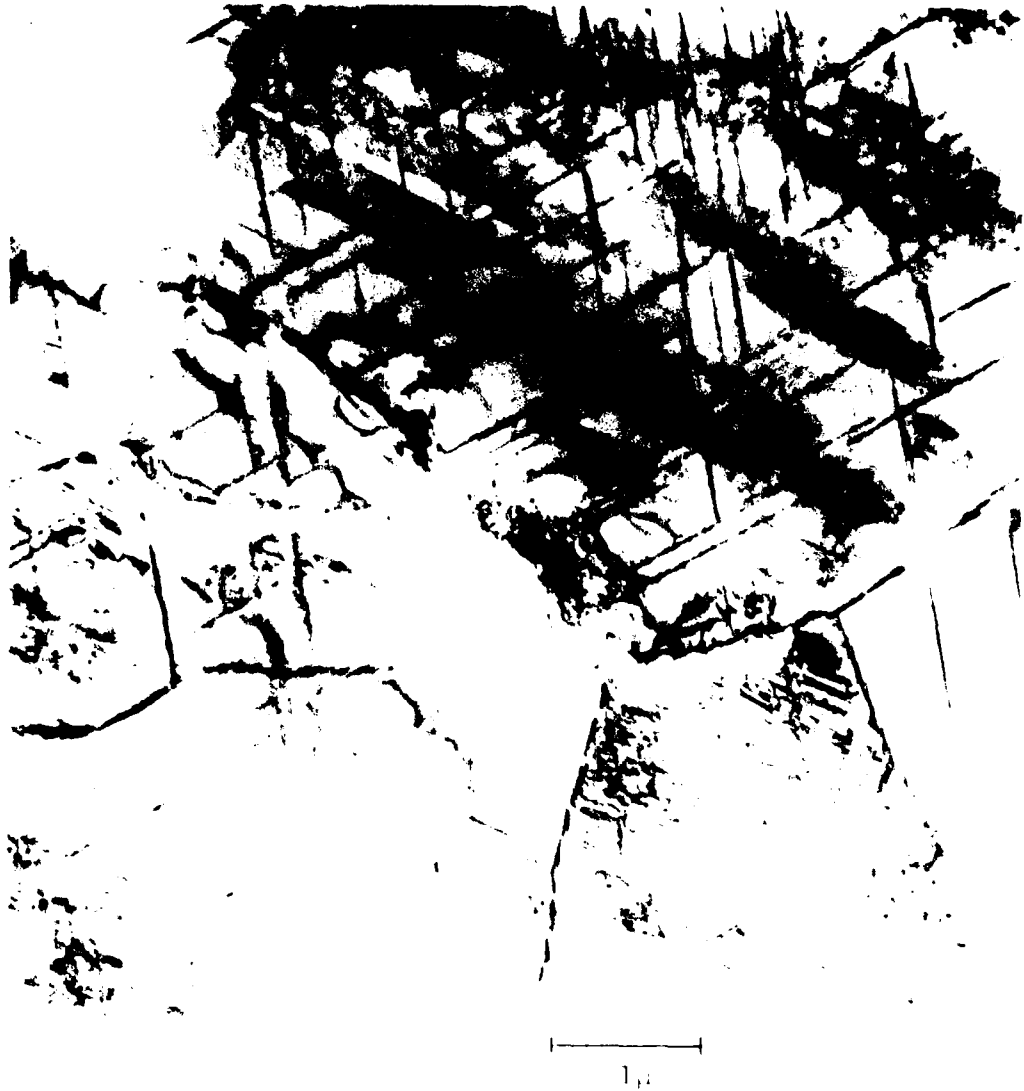


FIGURE 4-61. TEM OF Al-Li-Cu (#19--AB) SHEET
Aged 350°F/480 hours (overaged). 22,000X.

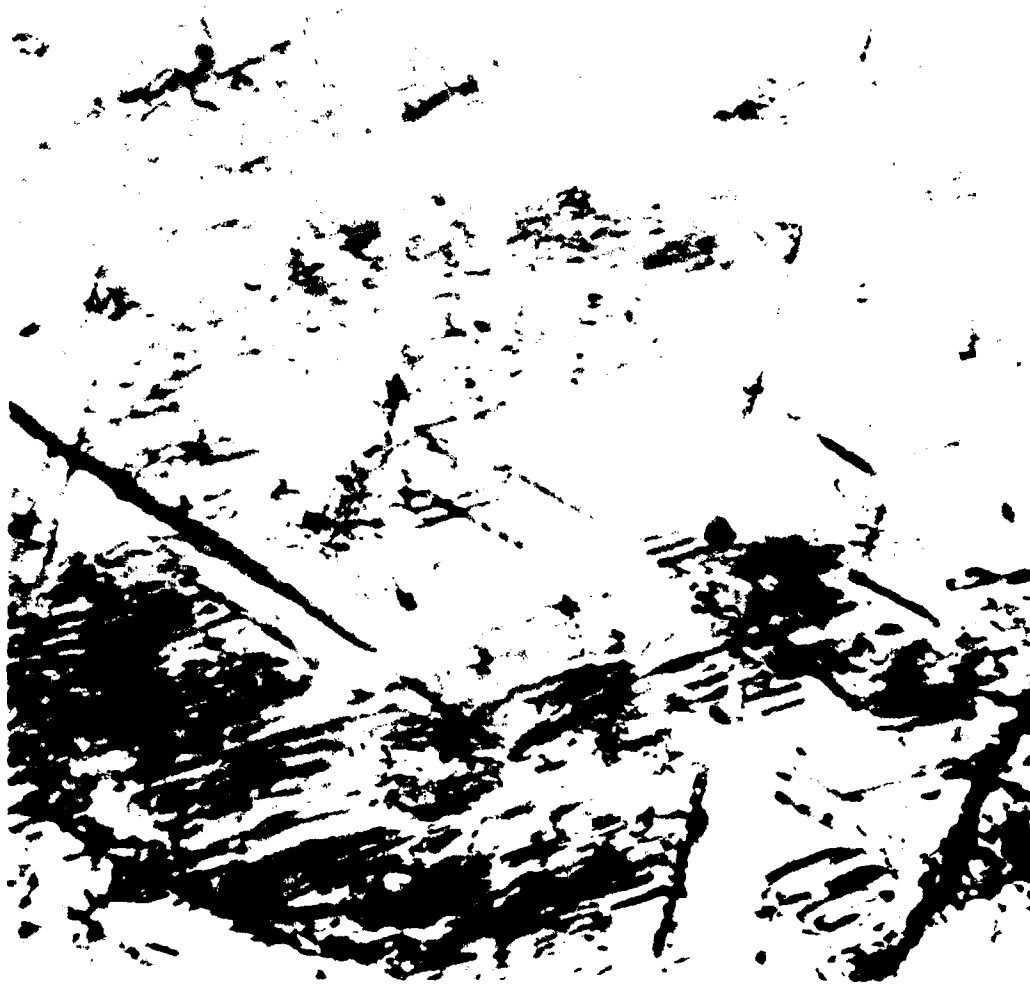


FIGURE 4-62. TEM OF Al-Li-Cu (#19--AR) SHEET
Same sample as in Figure 4-61, under different
diffracting conditions. Aged 350°F/480 hours
(overaged). Much T_1 precipitation is apparent.
22,000X.



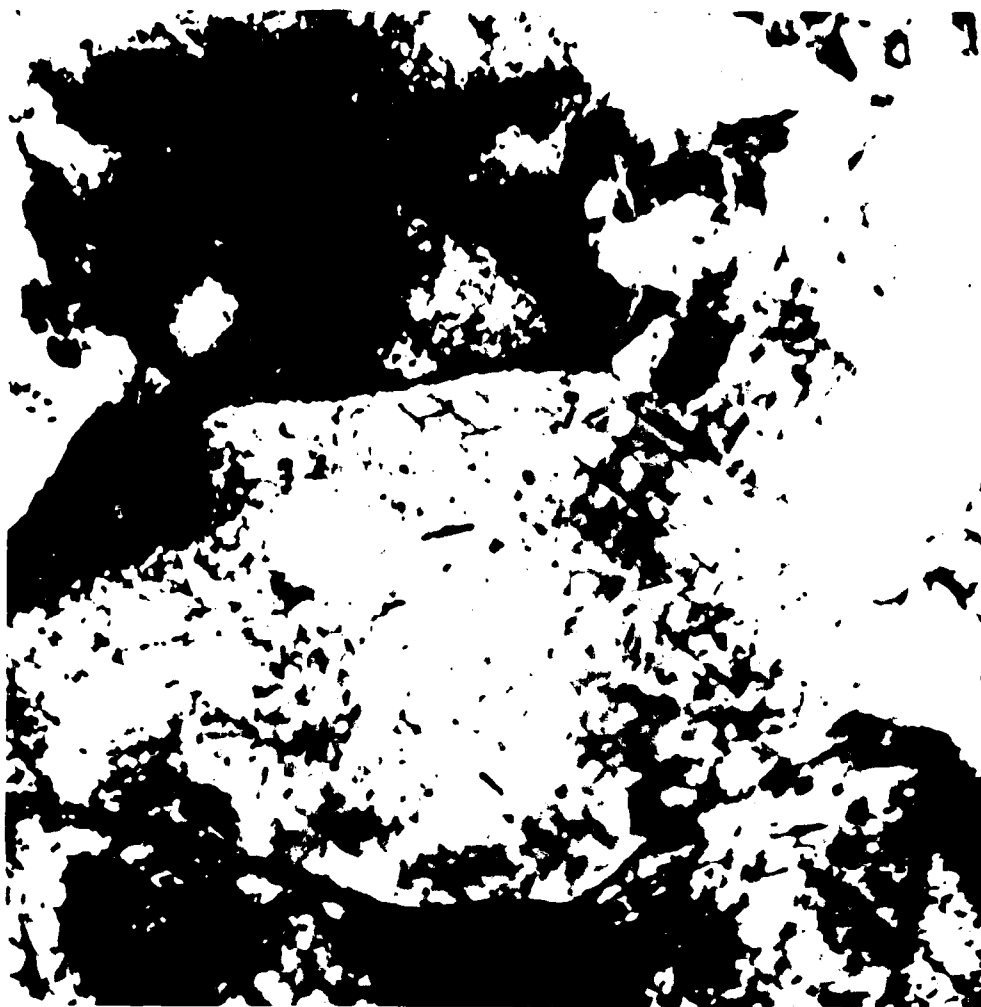
100μ

FIGURE 4-61. TEM OF Al-14.0% Cu-1.0% Ag-0.05% Zn
Same sample as in Figures 4-54 and 4-55, under
different diffraction conditions. Scale: 50 Å,
430 hours (overexposed). Magnification: 100,000X.



0.5 μ

FIGURE 4-64. TEM OF Al-Li-Cu (#19--AR) SHEET
Aged 350°F/480 hours (overaged). Extensive
T₁ precipitation. 46,000X.



1 μ

FIGURE 4-66. TEM OF Al-Li-Cu (#19--AR) SHEET
Same sample as in Figure 4-65, under different
diffracting conditions. Aged 375°F/45 hours
(overaged) from transverse tensile test gauge
section. 22,000X.

SECTION 5

CONCLUSIONS AND RECOMMENDATIONS

Process Development

Aluminum-lithium sheet of lithium content up to 3.3% can be fabricated using the casting and rolling procedures outlined. There are problems with hydrogen, porosity, and inclusions. No immediate solution to the hydrogen and porosity problems has been found in the high lithium alloys.

Alloy Development

The Al-Li-Zr, Al-Li-Mg-Si, and Al-Li-Mn-(Fe) alloys studied do not offer any improved fracture properties over high lithium alloys in other studies.

The Al-Li-Cu alloys offer better fracture properties in that elongation is 8%-12% and Kahn tear test results are somewhat improved. However, crack propagation energy is quite low. There is evidence that fracture is associated with failure at subgrain boundaries. It has been shown that such boundaries exhibit significant grain boundary precipitation and the growth of a precipitate-free zone with extended aging.

On a microscale the fracture surfaces of each alloy showed dimples, which are normally associated with ductile fracture. The reason for such pronounced dimples in relatively brittle material has not been completely defined. The dimples become more prominent and well-defined with increased aging. In the Al-Li-Cu alloy the dimple size corresponds approximately to subgrain size, indicating that fracture may be associated with subgrain boundary failure. Dimples in such a case may be present due to a relatively ductile precipitate-free zone (PFZ), which forms on grain and subgrain boundaries. Such PFZ's grow with aging, possibly explaining the increased prominence of dimples in the overaged samples. A major consideration, though, should be given to the role of hydrogen in these alloys. The high hydrogen levels found in lithium-containing alloys may be a controlling factor in microvoid coalescence and early grain

boundary failure. The dimples may result from some combination of the above factors. Further study is needed to answer these questions.

The precipitation mechanism in the Al-Li-Cu alloy appears to follow the sequence observed by workers with alloys of lower lithium content, i.e. the independent precipitation sequences of the Al-Cu and Al-Li systems.

Solid solution \rightarrow GP \rightarrow θ'' \rightarrow θ' , and
solid solution \rightarrow δ' .

However, TEM of the current alloy indicates that there is copious precipitation of the ternary hexagonal phase, T_1 , as described by Silcock^[30] in the overaged tempers. T_1 may form from the solid solution or from a transformation of θ' after diffusion of lithium into the θ' takes place.

Though fracture toughness properties are not good, there are methods which may be useful to improve the behavior in some of the alloy systems. In the Al-Li-Cu system manipulation of the aging program, thermomechanical treatment (TMT), or addition of an alloying element to form a nucleating phase may be useful in stimulating the precipitation of θ'' while inhibiting the ripening of δ' . In this way high strength, due to the θ'' , could be realized, while the planar slip and brittle fracture, due to δ' ripening, could be reduced.

In two systems, Al-Li-Mn-(Fe) and Al-Li-Sc, the use of rapid solidification methods such as powder metallurgy may prove useful. In the dispersoid system, Al-Li-Mn-(Fe), a rapid solidification may provide a dispersion of $(Mn,Fe)Al_6$ of a fine enough scale to require cross-slip for dislocation movement. This would alleviate the embrittling planar slip problem while providing an additional strengthening mechanism.

The application of rapid solidification to the Al-Li-Sc system may provide an interesting modification to the Al-Li

precipitation system. The Al_3Sc precipitate is isomorphous with δ' . A substitution of scandium for lithium in δ' may significantly affect the precipitate lattice parameter or matrix-precipitate interfacial energy. The equilibrium solubility of scandium in aluminum is so low, however, that at normal aging temperatures virtually no precipitation involving scandium takes place when using conventional ingot metallurgy.

A comparison of the alloys shows that zirconium affords very good recrystallization inhibition, even with relatively high SHT temperatures, while such an effect due to manganese/iron was not seen. It should be noted, though, that no improvement in mechanical properties in the unrecrystallized material over the recrystallized material was observed. However, if an unrecrystallized microstructure is sought, it is probably desirable to use zirconium, even in high manganese/iron alloys.

Recommendations for Future Work

Casting and Fabrication

1. Insulated sidewalls of bookmold or DC casting. A directional solidification may drive porosity to the top rather than the center of the ingot.
2. Investigation of the effect of time and temperature during intermediate anneal. A lower temperature or shorter anneal time before cold rolling may solve the edge cracking problem, yet allow an unrecrystallized microstructure to be retained in the final sheet product.

Alloy Development

1. Application of rapid solidification technology to the Al-Li-Mn-(Fe) system. The casting of these alloys in bookmold form resulted in large insoluble particles of $(Mn,Fe)Al_3$. A rapid solidification rate process, such as in powder metallurgy, may provide a high volume fraction of fine dispersoid. Such a dispersion might encourage cross-slip and decrease planar slip in the alloy.

2. Application of rapid solidification technology to the Al-Li-Sc and other systems. Scandium forms Al_3Sc , which is isomorphous with δ' (Al_3Li). In conventional ingot metallurgy scandium has virtually no solubility in aluminum. Using rapid solidification rate methods, the solubility of scandium in aluminum can be increased. It may be possible to precipitate, or form by diffusion, a δ' with at least some scandium, or $\text{Al}_3(\text{Li},\text{Sc})$. This would change the δ' lattice parameter and $\alpha\text{Al}-\delta'$ interfacial energy, possibly decreasing the planar slip encouraged by the small lattice misfit and interfacial energy in the Al-Li system.

This technique may be useful in other aluminum alloy systems. A high zirconium alloy is such a possibility since an ordered coherent face-centered cubic Al_3Zr precipitate is formed in the Al-Zr system with a lattice parameter close to that of the aluminum matrix.

3. Modification of precipitation sequence in the Al-Li-Cu system. The concept involved is to encourage strengthening by ν'' while slowing the ripening of δ' . In this way δ' , which controls fracture behavior in the system, may be retained fine enough so that ductility is not too severely reduced. In this way the benefits of lowered density and increased modulus may be obtained while the severe planar slip is minimized. Possible methods to accomplish this precipitation modification include thermomechanical treatment (TMT), an appropriate aging program, or modification with other alloying elements.

ACKNOWLEDGMENT

We wish to thank John Carson and especially John Yahley for their work in developing the casting procedures for this study.

REFERENCES

- [1] J. W. Evancho, "Development of an Al-Mg-Li Alloy," Naval Air Development Center Contract No. N62269-74-C-0438, Alcoa Quarterly Report, 1974 October 25.
- [2] V. G. Kovrizhnykh, V. A. Tikhomirov, N. I. Zaitseva, and M. V. Ermanok, "Mechanical Properties of Extruded Panels of Alloy 01420," translated from Metallovedenie i Termicheskaya Obrabotka Metalloy, No. 2, 1969 February, pp. 20-21.
- [3] Fulmer Research Institute (England), "Low Density, High Strength Al-Mg Alloys Containing Lithium," undated advertising flyer.
- [4] J. H. Sanders, "Factors Influencing Fracture Toughness and Other Properties of Aluminum-Lithium Alloys," Naval Air Development Center Contract No. N62269-76-C-0271, Final Report, 1979 June 14.
- [5] J. G. Kaufman and M. Holt, "Fracture Characteristics of Aluminum Alloys," Aluminum Company of America, Pittsburgh, Pennsylvania, 1965.
- [6] J. M. Silcock, "The Structural Aging Characteristics of Aluminum-Copper-Lithium Alloys," J. Inst. Metals, 88, 1959-60, p. 357.
- [7] T. Joski-yama, K. Hasabe, and M. Mannami, J. Phys. Soc. Japan, V. 25, 1968, p. 908, ref. in T. V. Shchegoleva and O. F. Rybalko, "On the Question of the Ageing Mechanism of the Alloy Al-Li," translated from Fiz. Metal Metalloved., V. 42, N. 3, 1976, pp. 546-556.
- [8] B. Noble and G. E. Thompson, "Precipitation Characteristics of Aluminum-Lithium Alloys," Metal Sci. J., V. 5, 1971, p. 114.
- [9] R. F. Decker, "Alloy Design Using Second Phases," Met. Trans., V. 4, 1973 November, p. 2495.

- [10] D. A. Bennett, "The Production and Assessment of an Al-Mg-Li-Zr Alloy," Progress Report, British Aluminium, 1977 November 24.
- [11] V. I. Elagin, V. V. Zakharov, and L. I. Levin, "Effect of Lithium on the Properties of Al-Zn-Mg Alloys," All-Union Institute of Light Alloys, translated from Metallovedenie i Termicheskaya Obrabotka Metallov, N. 12, 1977 December, pp. 34-38.
- [12] I. N. Fridlyander, A. I. Litvintseu, R. M. Gabidullin, S. I. Dudkina, L. W. Klimova, and N. V. Shiryaeva, Alyum Splyvy, translation, N. 5, 1968, pp. 335-341.
- [13] V. P. Ivanov, "Effect of Small Lithium Additions on the Gas Content and Mechanical Properties of Aluminum," translated from Izv. Vyssh. Uchebn. Zaved. Isvet. Metall., V. 14, N. 3, 1971, pp. 118-121.
- [14] Y. I. Morozov et al, Tr. VAMI, 1977, (99), pp. 16-18, as abstracted in World Aluminum Abstracts 1979 July, p. 11.
- [15] G. E. Kainova and T. I. Malinkina, translation, Metallovedenie i Termicheskaya Obrabotka Metallov, N. 2, 1969 February, pp. 22-23.
- [16] I. N. Fridlyander, Y. M. Dolzhanskii, V. S. Sandler, B. V. Tyurin, and T. I. Nikol'skaya, "Structure and Properties of Al-Mg-Li-Zr Alloys," translated from Metallovedenie i Termicheskaya Obrabotka Metallov, N. 12, 1977 December, pp. 29-33.
- [17] I. N. Fridlyander, T. I. Nikol'skaya, V. S. Sandler, and B. V. Tyurin, "The Structure of Alloy 01420 With Zirconium," translated from Metallovedenie i Termicheskaya Obrabotka Metallov, N. 8, 1972 August, pp. 7-9.
- [18] Y. N. Vaynblat, B. A. Kopelliovich, and Yu. G. Gol'der, "Subboundary Embrittlement of the Alloy Al-Mg-Li by Horophile Impurity Sodium," translated from Fiz. Metal Metalloved., 42, N. 5, 1976, pp. 1021-1028.

- [19] Z. A. Sviderskaya, E. S. Kadaner, N. I. Turkina, and V. I. Kuz'mina, "Boundary of the Solid Solution in the Aluminum Corner of the Aluminum-Manganese-Lithium System," translated from Metallovedenie i Termicheskaya Obrabotka Metallov, N. 12, 1963 December, pp. 2-6.
- [20] Z. A. Sviderskaya, E. S. Kadaner, and N. I. Turkina, "Phase Diagram of the Aluminum Rich Corner of the Al-Mn-Li System," Russian Metallurgy, N. 2, 1967, translated from Izv. Akad. Nauk, SSR, Metally.
- [21] G. E. Thompson and B. Noble, "Precipitation Characteristics of Aluminum-Lithium Alloys Containing Magnesium," J. Inst. Metals, V. 101, 1973, p. 111.
- [22] I. N. Fridlyander, S. M. Ambartsumyan, N. V. Shiryaeva, and R. M. Gavidullin, "New Light Alloys of Aluminum With Lithium and Magnesium," Metal Science and Heat Treatment, No. 3, 1968, pp. 211-212, translated by Consultants Bureau from Metallovedenie i Termicheskaya Obrabotka Metallov, N. 3, 1968, pp. 50-52.
- [23] T. H. Sanders, "Factors Influencing Fracture Toughness and Other Properties of Aluminum-Lithium Alloys," Naval Air Development Center Contract No. N62269-76-C-0271, Semi-Annual Report, 1977 March.
- [24] H. K. Hardy, "Trace-Element Effects in Some Precipitation-Hardening Alloys," J. Inst. Metals, V. 84, 1955-56, p. 429.
- [25] D. W. Levinson and D. J. McPherson, "Phase Relations in Magnesium-Lithium-Aluminum Alloys," Trans. ASM, V. 48, 1956, pp. 689-705.
- [26] T. H. Sanders, "Development of an Al-Mg-Si Alloy," Naval Air Development Center Contract No. N62269-74-C-0438, Final Report, 1976 June.
- [27] E. S. Kadaner and N. I. Turkina, "New Aluminum Alloy Based on the System Al-Mn-Li," Redkiye Metally v Tsvetnykh Splovakh, Moscow, 1975, p. 102.

- [28] H. W. L. Phillips, "The Constitution of Alloys of Aluminum With Manganese, Silicon, and Iron," J. Inst. Metals, V. 69, 1943, p. 275.
- [29] H. K. Hardy and J. M. Silcock, "The Phase Sections at 500° and 350°C of Aluminum-Rich Aluminum-Copper-Lithium Alloys," J. Inst. Metals, V. 84, 1955, p. 423.
- [30] J. M. Silcock, "The Structural Aging Characteristics of Aluminum-Copper-Lithium Alloys," J. Inst. Metals, V. 88, 1959-60, p. 357.
- [31] K. Schneider and M. von Heimendahl, Z. Metallkde, V. 64 (5), 1973, pp. 342-347, translated by Information Corporation of America.
- [32] Francis Degreve, "New Methods for Determining Hydrogen Content in Aluminum and Its Alloys," J. of Metals, V. 27, 1975 March, p. 21.
- [33] E. S. Kadaner et al, Izvestiya AN SSSR Metally, No. 5, 1976, p. 206.
- [34] D. B. Williams and J. W. Edington, "The Discontinuous Precipitation Reaction in Dilute Al-Li Alloys," Acta Met., V. 24, 1976, p. 323.
- [35] R. B. Nicholson and J. Nutting, "Direct Observation of the Strain Field Produced by Coherent Precipitated Particles in an Age-Hardened Alloy," Phil. Mag. (8th Series), V. 3, 1958, p. 531.
- [36] G. C. Weatherby and C. M. Sargent, "Electron Diffraction Contrast From Ledges at the Interfaces of Faceted θ' Precipitates," Phil. Mag., V. 22, 1970, p. 1049.
- [37] N. I. Kolobnev, M. B. Ovodenko, G. T. Shvirin, and E. V. Makagon, "Effect of Thermomechanical Processing Parameters on the Structure and Properties of Strip Made From VAD 23 Aluminum Alloy," Light Metal Age, 1979 October, p. 20.

- [38] I. N. Fridlyander et al, "High Strength, Heat Resistant, and Structural Alloys of Aluminum With Lithium," Alyuminiyevyye Splavy, Moscow, 1972, p. 204, Translation FSTC-HT-23-0911-74, dated 1974 September 18.

One copy unless otherwise noted

(1 copy + balance after distribution)
Mr. R. Steskal
AIR-5163C5
Naval Air Systems Command
Washington, DC 20361

Commander
Naval Air Development Center
Code 302
Warminster, PA 18974

Naval Sea Systems Command
Code 03423
Department of the Navy
Washington, DC 20360

Naval Ships Research and
Development Center
Code 2812
Annapolis, MD 21402

Commander
Naval Surface Weapons Center
Metallurgy Division
White Oak
Silver Spring, MD 20910

Director
Naval Research Laboratory
Washington, DC 20390
(Codes: 6380, 6490, 6601, 8430
1 copy each)

Office of Naval Research
The Metallurgy Program
Code 471
Arlington, VA 22217

Dr. T. R. McNelley
Department of Mechanical Engineering
Code 59
Naval Postgraduate School
Monterey, CA 93940

(14 copies--12 copies for DDC,
2 copies for AIR-954)
Commander
Naval Air Systems Command
AIR-954
Washington, DC 20361

Wright-Patterson Air Force Base
Ohio 45433
Attention W. Griffith, AFML/LLS

Wright-Patterson Air Force Base
Ohio 45422
Attention C. L. Harmsworth, AFML/MXE

Commanding Officer
Office of Ordnance Research
Box CM, Duke Station
Durham, NC 27706

U. S. Army Armament R&D Command
ARRADCOM
Dover, NJ 07801
Attention Dr. J. Waldman
DRDAR-SCM-P, Bldg. 3409

National Aeronautics & Space Admin.
Code RWM
600 Independence Avenue, S.W.
Washington, DC 20546

National Aeronautics & Space Admin.
Langley Research Center
Materials Division, Langley Station
Hampton, VA 23365
Attention Mr. H. F. Hardrath
Stop 188M

National Aeronautics & Space Admin.
George C. Marshall Space Flight Center
Huntsville, AL 35812
Attention Mr. J. G. Williamson
S&E-ASTN-MMC

National Academy of Sciences
Materials Advisory Board
Washington, DC 20418
Attention Dr. J. Lane

Director
National Bureau of Standards
Washington, DC 20234
Attention Dr. E. Passaglia

Battelle Memorial Institute
505 King Avenue
Columbus, OH 43201
Attention Mr. Stephan A. Rubin, Manager
Information Operations

IIT Research Institute
Metals Research Department
10 West 35th Street
Chicago, IL 60616
Attention Dr. N. Parikh

General Dynamics Convair Division
P. O. Box 80847
San Diego, CA 92138
Attention Mr. Jack Christian
Code 643-10

Kaman Aerospace Corporation
Old Windsor Road
Bloomfield, CT 06001
Attention Mr. M. L. White

Rockwell International
Columbus Division
Columbus, OH 43216
Attention Mr. P. Maynard
Dept. 75, Group 521

Rockwell International
Rocketdyne Division
Canoga Park, CA 91305
Attention Dr. Al Jacobs, Group Scient.
Materials Branch

Rockwell International
Los Angeles Division
International Airport
Los Angeles, CA 90009
Attention Gary Keller
Materials Applications

Lockheed Palo Alto Research Labs
Materials Science Laboratory
3251 Hanover Street
Palo Alto, CA 94303
Attention Dr. Frank A. Crossley
52-31/204

Lockheed-California Company
P. O. Box 551
Burbank, CA 91503
Attention Mr. J. M. VanOrden
Dept. 74-71, Bldg. 221,
Plant 2

Lycoming Division
AVCO Corporation
Stratford, CT 06497
Attention Mr. Barry Goldblatt

Lockheed-Georgia Company
Marietta, GA 30061
Attention E. Bateh

Lockheed Missile & Space Corporation
Box 504
Sunnyvale, CA 94088
(1 copy to each)
Attention Mr. G. P. Pinkerton
Bldg. 154, Dept. 8122
and Mr. C. D. McIntyre
Bldg. 182, Dept. 84-13

Douglas Aircraft Company
3855 Lakewood Boulevard
Long Beach, CA 90808
Attention Mr. Fred Mehe, C1-250

Sikorsky Aircraft
Division of United Aircraft Corporation
Stratford, CT 06497
Attention Materials Department

Boeing-Vertol Company
Boeing Center
P. O. Box 16858
Philadelphia, PA 19142
Attention Mr. J. M. Clark

The Boeing Company
Commercial Airplane
ORG. 6-8733, MS77-18
P. O. Box 3707
Seattle, WA 98124
Attention Mr. Cecil E. Parsons

Northrop Corporation
Aircraft Division
Department 3771-62
3901 West Broadway
Hawthorne, CA 90250
Attention Mr. Allen Freedman

Vought Corporation
P. O. Box 5907
Dallas, TX 75222
Attention Mr. A. Hohman

McDonnell Aircraft Company
St. Louis, MO 63166
Attention Mr. H. J. Siegel
Materials & Processes Dev.
General Engineering Div.

Detroit Diesel Allison Division
General Motors Corporation
Materials Laboratories
Indianapolis, IN 46206

AiResearch Manufacturing Co. of America
Sky Harbor Aircraft
402 South 36th Street
Phoenix, AZ 85034
Attention Mr. Jack D. Tree
Dept. 93-35-5M

General Electric Company
Aircraft Engine Group
Materials & Processes Tech. Labs
Evendale, OH 45215

Solar
2200 Pacific Highway
San Diego, CA 92112
Attention Dr. A. Metcalfe

Teledyne CAE
1330 Laskey Road
Toledo, OH 43601

Dr. Charles Gilmore
Tompkins Hall
George Washington University
Washington, DC 20006

Dr. Michael Hyatt
The Boeing Company
P. O. Box 707
Seattle, WA 98124

General Electric Company
Corporate Research & Development
P. O. Box 8
Schenectady, NY 12301
Attention Dr. D. Wood

Westinghouse Electric Company
Materials & Processing Labs
Beulah Road
Pittsburgh, PA 15235
Attention Don E. Harrison

Dr. John D. Wood
Associate Professor
Lehigh University
Bethlehem, PA 18015

General Dynamics Corporation
Convair Aerospace Division
Fort Worth Operation
P. O. Box 748
Fort Worth, TX 76101
Attention Tom Coyle

Dr. A. I. Mlavsky
Sr. Vice Pres. for Technology &
Dir. of Corporation Technology Center
Tyco Laboratories Inc.
16 Hickory Drive
Waltham, MA 02145

Martin Marietta Aluminum
19200 South Western Avenue
Torrance, CA 90509
Attention Mr. Paul E. Anderson
M/C 5401

Dr. Howard Bomberger
Reactive Metals Inc.
Niles, OH 44446

Mr. W. Spurr
The Boeing Company
12842 72nd Avenue, N.E.
Kirkland, WA 98033

Dr. John A. Schey
Department of Materials Engineering
University of Illinois at Chicago Circle
Box 4348
Chicago, IL 60680

Rockwell International
P. O. Box 1082
1027 Camino Dos Rios
Thousand Oaks, CA 91320

Pratt and Whitney Aircraft
Division of United Technologies
Florida Research & Development Center
P. O. Box 2691
West Palm Beach, FL 33402

P. R. Mallory & Company Inc.
3029 East Washington Street
Indianapolis, IN 46206
Attention Technical Librarian

Martin Marietta Corporation
P. O. Box 5837
Orland, FL 32805
Attention Dr. Richard C. Hall
Mail Point 275

Southwest Research Institute
8500 Culebra Road
P. O. Box 28510
San Antonio, TX 78284
Attention Dr. C. Gerald Gardner

Avco Space Systems Division
Lowell Industrial Park
Lowell, MA 01851

Brush Wellman Inc.
17876 St. Clair Avenue
Cleveland, OH 44110
Attention Mr. Bryce King

General Electric Company
Missile & Space Division
Materials Science Section
P. O. Box 8555
Philadelphia, PA 19901
Attention Technical Library

Kawecki Berylco Industries
P. O. Box 1462
Reading, PA 19603

Linde Company
Division of Union Carbide
P. O. Box 44
Tonawanda, NY 14152

Midwest Research Institute
425 Volker Boulevard
Kansas City, MO 64110

University of California
Lawrence Radiation Laboratory
P. O. Box 808
Livermore, CA 94550
Attention Mr. L. W. Roberts

ERDA Division of Reactor Dev. & Tech.
Washington, DC 20545
Attention Mr. J. M. Simmons, Chief
Metallurgy Section

Dr. W. C. Setzer, Director
Metallurgy & Surface Technology
Consolidated Aluminum Corporation
P. O. Box 14448
St. Louis, MO 63178

Kaiser Aluminum & Chemical Corporation
Aluminum Division Research Center for
Technology
P. O. Box 870
Pleasanton, CA 94566
Attention Mr. T. R. Pritchett

Reynolds Metals Company
Metallurgical Research Division
Fourth and Canal Streets
Richmond, VA 23261
Attention Mr. G. E. Spangler

The Dow Metal Products Company
Hopkins Building
Midland, MI 48640

Dr. F. N. Mandigo
Olin Metals Research Laboratories
91 Shelton Avenue
New Haven, CT 06515

General Electric Company
Corporate Research & Development
Building 36-441
Schenectady, NY 12345
Attention Dr. J. H. Westbrook, Manager
Materials Information Services

Dr. E. A. Starke Jr.
School of Chemical Engineering & Metallurgy
Georgia Institute of Technology
Atlanta, GA 30332

Dr. R. Balluffi, Chairman
Dept. of Materials Science & Engineering
Bard Hall
Cornell University
Ithaca, NY 14853

Dr. D. J. Duquette
Materials Engineering Department
RPI
Troy, NY 12181

United Technologies Research Labs
East Hartford, CT 06108
Attention Mr. Roy Fanti

Autonetics Division of Rockwell International
P. O. Box 4173
Anaheim, CA 92803
Attention Mr. A. G. Gross Jr.
Dept. 522-92